Cancer Imaging

Mukund Seshadri, DDS, PhD
Associate Professor of Oncology
Depts. of Pharmacology & Therapeutics
Oral Medicine/Head and Neck Surgery
Director, Translational Imaging Shared Resource (TISR)

Mukund.Seshadri@roswellpark.org
Ph: 716-845-1552

2/16/2016

What is an image?

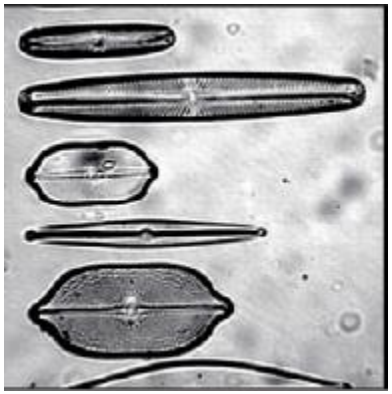

[1]Burger W and Burge MJ, Digital Image Processing, Springer

What is an image?

2D rectilinear array of pixels

www.roswellpark.org

Rows and columns of image points or picture elements (pixels)

What is a pixel?

Smallest constitutive element of a digital image

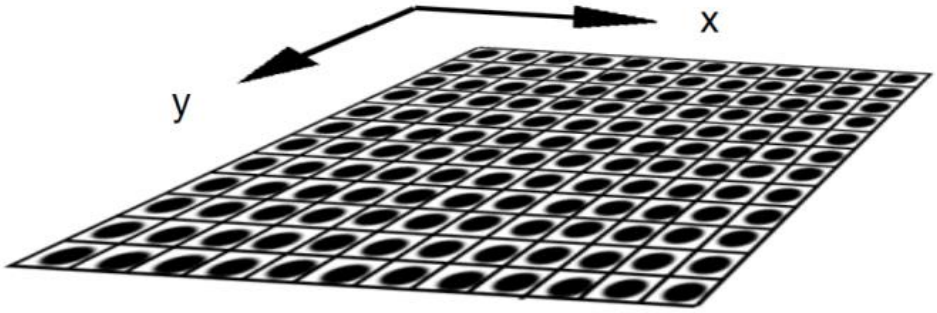

Pixel dimension

i.e. how many pixels does the image have horizontally and vertically (x, y)

Actual size of the image file

Resolution and Pixel dimension

Resolution

Specifies the spatial dimensions of the image
Often expressed as number of image elements per measurement (dpi or ppi)

Resolution = Pixel dimensions/physical dimensions
For example.
Image dimension = 10 x 7.5 inches
Pixel dimension = 720 x 540
Resolution = ___ dpi ?

Higher the DPI or PPI, the more detail (higher resolution)

Pixel dimensions

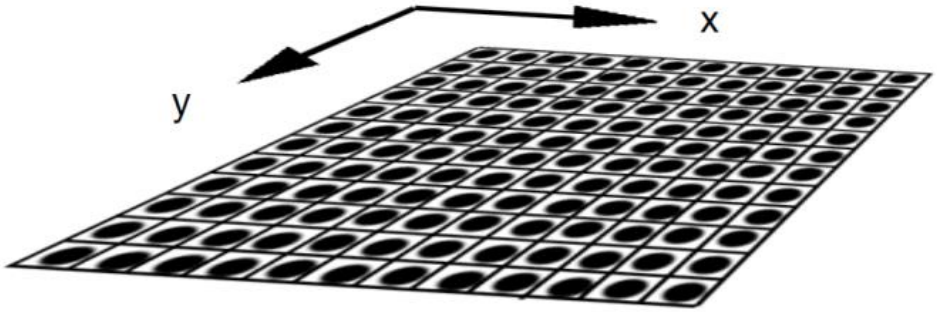

Pixels per inch (PPI) or Dots per inch (DPI)

- Output (printer)or display capabilities (monitor)
- # of pixels (or dots) in a printed inch (x or y)
- DPI: Multiple dots are needed to create a pixel (dithering)
- Images will require more DPI than PPI to show same degree of detail

Pixel dimensions

How many of you have smart phones?

Digital cameras – 2 MP → 16 MP

What does that mean?

Mega pixel (MP) = million pixels

# of Megapixels	Maximum 3:2 Print Size at 300 PPI:	at 200 PPI:
2	5.8" x 3.8"	8.7" x 5.8"
3	7.1" x 4.7"	10.6" x 7.1"
4	8.2" x 5.4"	12.2" x 8.2"
5	9.1" x 6.1"	13.7" x 9.1"
6	10.0" x 6.7"	15.0" x 10.0"
8	11.5" x 7.7"	17.3" x 11.5"
12	14.1" x 9.4"	21.2" x 14.1"
16	16.3" x 10.9"	24.5" x 16.3"
22	19.1" x 12.8"	28.7" x 19.1"

For a certain resolution (PPI), there is a maximum print size you can get for a given number of MPs.

e.g. iPhone 6 has a 8MP camera

@300 PPI: 8 MP camera → 11.5 x 7.7 (3:2 print size)

http://www.cambridgeincolour.com/tutorials/digital-camera-pixel.htm

Resolution

Vascular cast of a normal kidney showing a single glomerulus

512 X 512

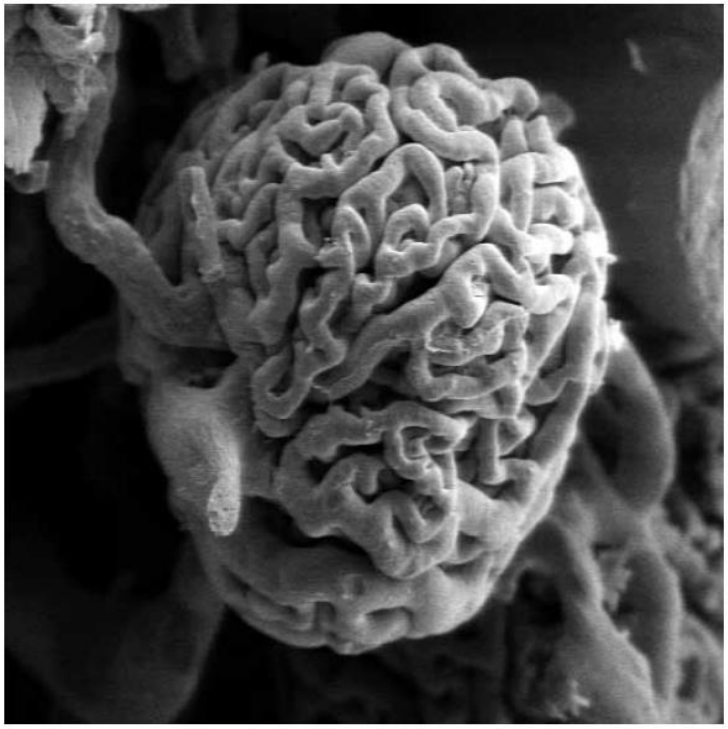

256 X 256

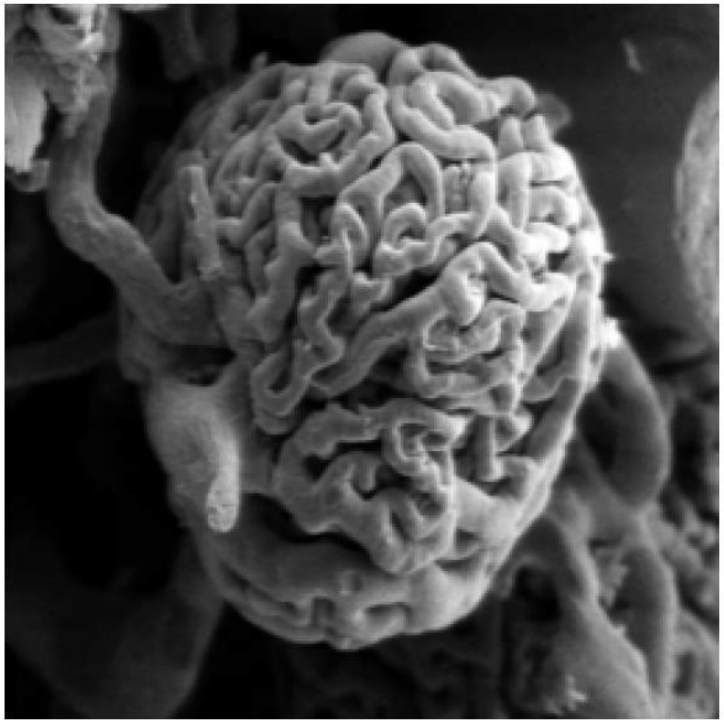

Resolution not magnification determines image quality

Images – courtesy of Dr. Arindam Sen

Resolution

Vascular cast of a normal kidney showing a single glomerulus

128 X 128

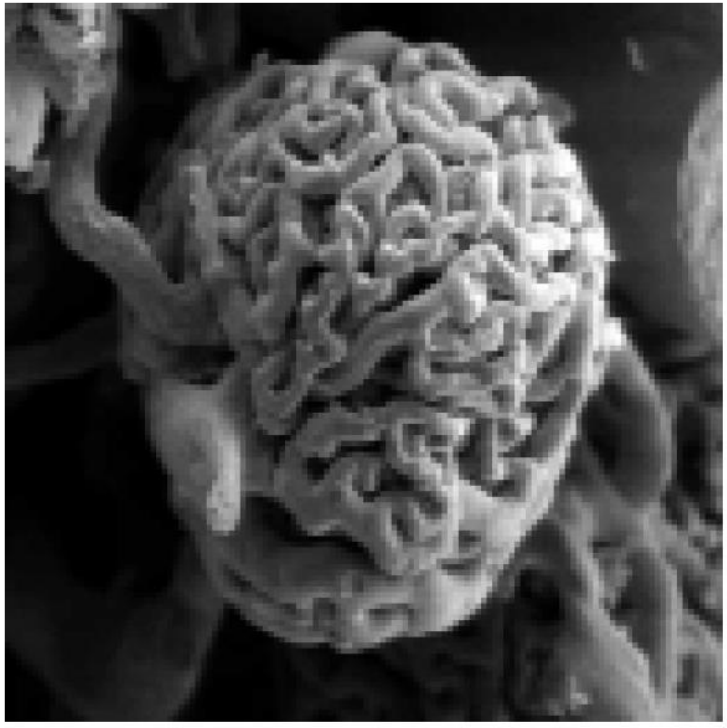

64 X 64

Resolution not magnification determines image quality

Images – courtesy of Dr. Arindam Sen

Resolution and Pixel dimension

Vascular cast of a normal kidney showing a single glomerulus

8 X 8 **4 X 4**

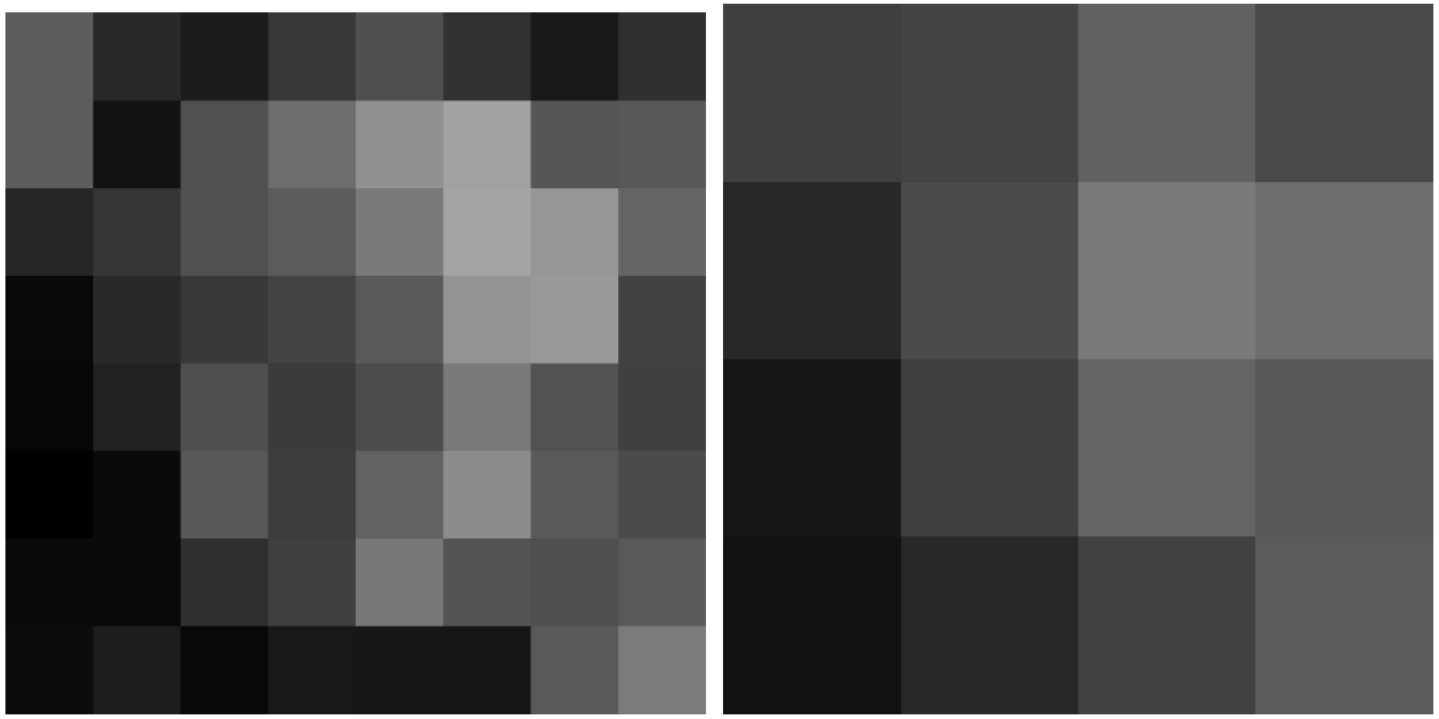

Resolution not magnification determines image quality

Images – courtesy of Dr. Arindam Sen

Do you recognize these images?

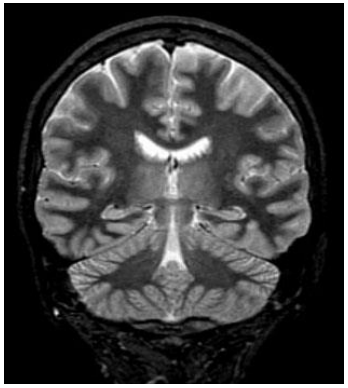

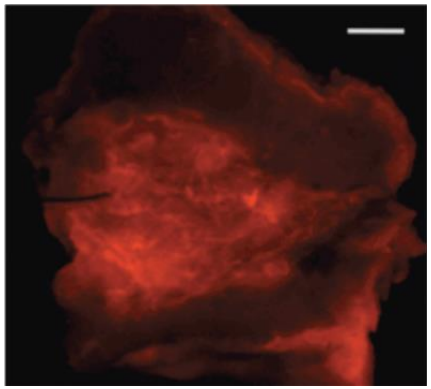

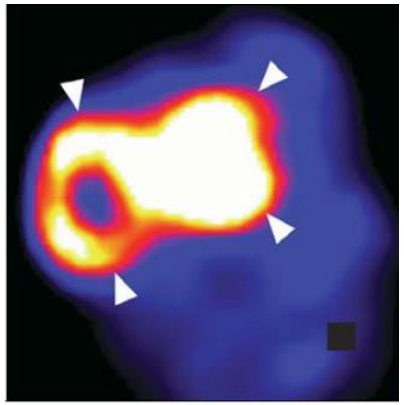

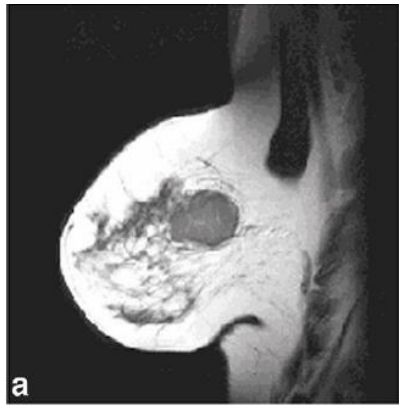

History of Imaging (Radiology)

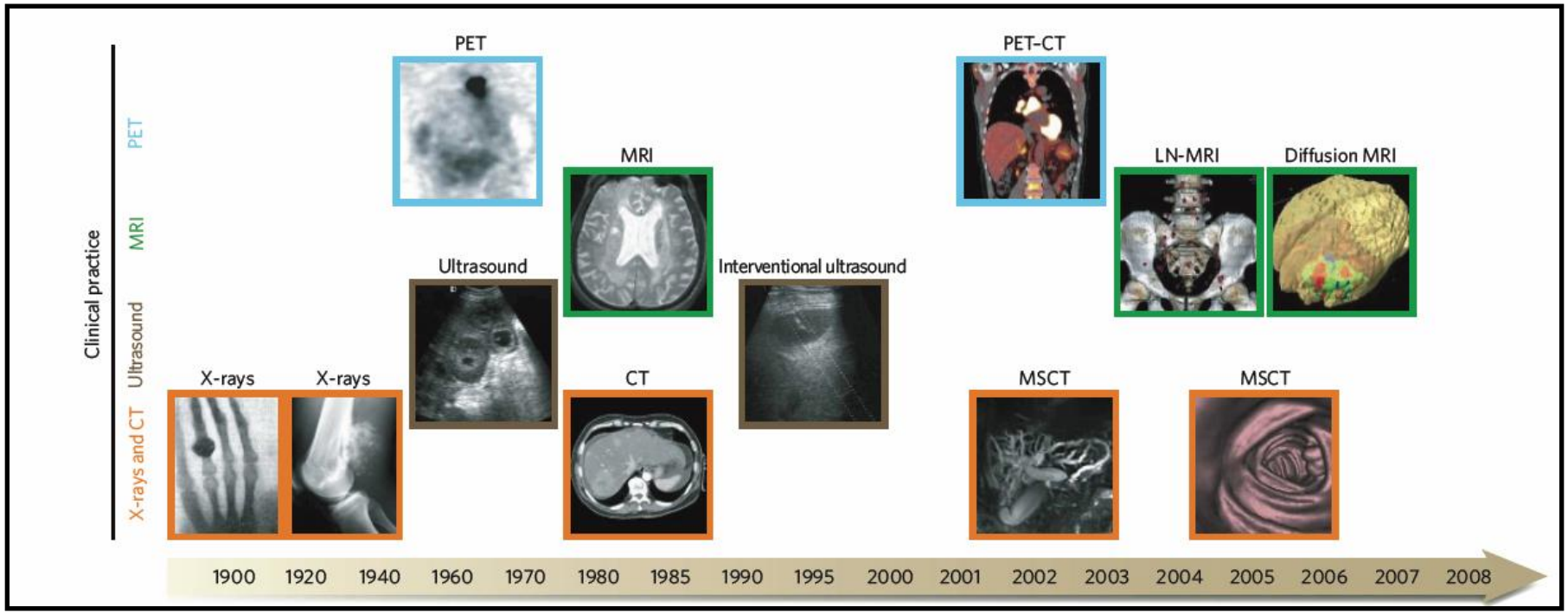

Weissleder & Pittet, Nature 2008

History of Imaging (Radiology)

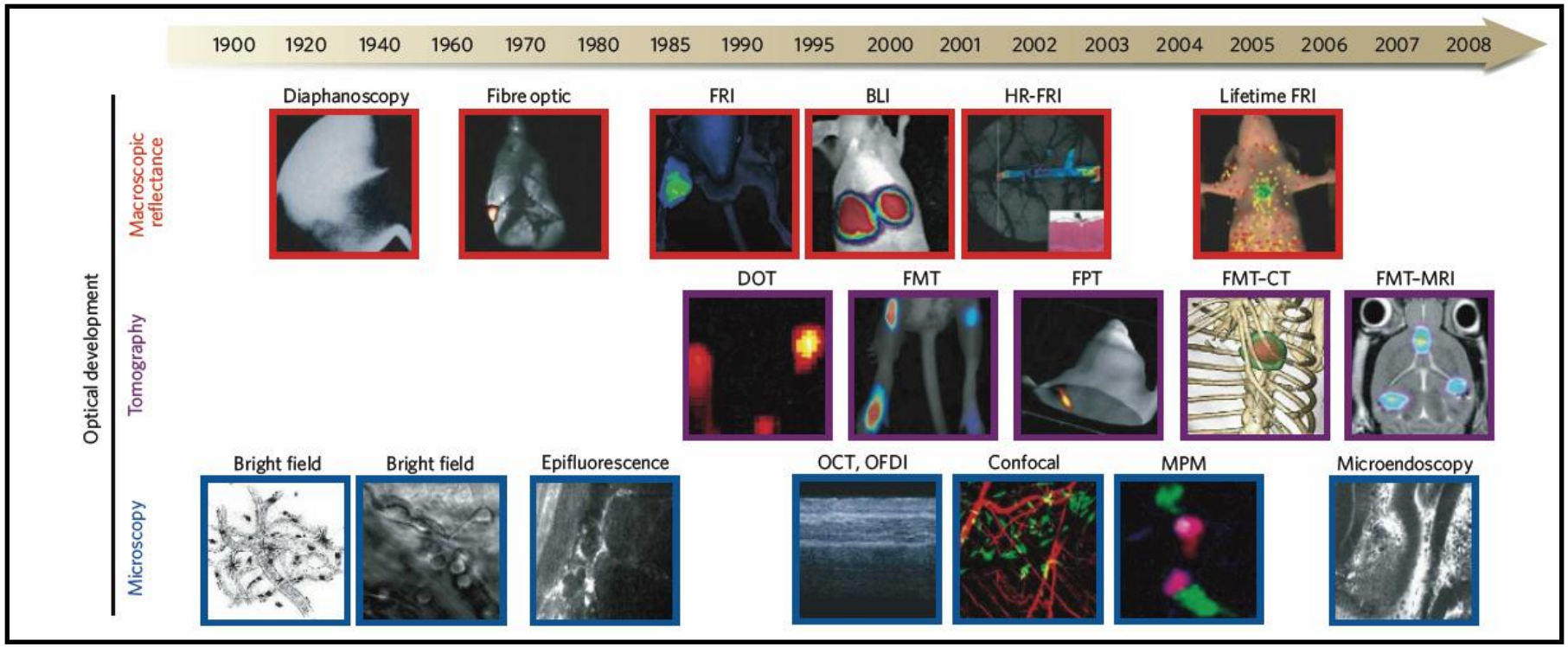

Weissleder & Pittet, Nature 2008

Radiologic Methods

Table 1. Characteristics of imaging modalities used in the clinic

Imaging modality	Spatial resolution	Limit for depth of imaging	Sensitivity estimates	Agent/probe used	Amount of agent[a]
PET	1–2 mm	No	10^{-11}–10^{-12} M	Radiolabel (e.g. ^{18}F)	Nanograms
SPECT	1–2 mm	No	10^{-10}–10^{-11} M	Radiolabel (e.g. ^{99m}Tc)	Micrograms
Optical/fluorescence	~1/10 of depth of imaging	Up to 10 cm[b]	10^{-9}–10^{-11} M	Fluorescence	Micrograms to milligrams
Ultrasound	50–500 μm	No?[c]	—[d]	Gas-filled bubbles	Micrograms to milligrams
MRI	25–100 μm	No	10^{-3}–10^{-5} M[e]	Paramagnetic or ferromagnetic	Milligrams to grams
CT	50–200 μm	No	10^{-2}–10^{-3} M[f]	Iodine[g]	Grams

[a]Estimates of the amounts needed to be injected into humans.
[b]Less than 1 cm for reflectance imaging; up to approximately 10 cm with fluorescence tomographic technique.
[c]Reduced signals from deep tissues, depending upon the frequency used.
[d]Depends very much on bubble size and structure, and the frequency used; single bubbles may be detected.
[e]Cells labeled with SPIO may have sensitivity close to SPECT.
[f]Not well characterized; less sensitive than MRI; not sensitive enough for MI.
[g]So far mostly iodine used; other heavy atoms can theoretically be used.

Radiology in Medicine (Oncology)

Presentation

Diagnosis/staging

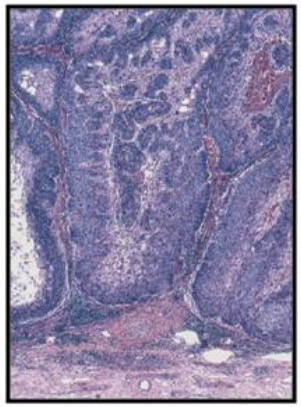

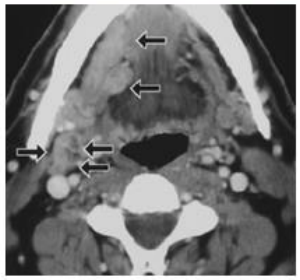

TNM classification of carcinomas of the oropharynx [1,2]

T – Primary tumour
- TX Primary tumour cannot be assessed
- T0 No evidence of primary tumour
- Tis Carcinoma in situ
- T1 Tumour 2 cm or less in greatest dimension
- T2 Tumour more than 2 cm but not more than 4 cm in greatest dimension
- T3 Tumour more than 4 cm in greatest dimension
- T4a Tumour invades any of the following: larynx, deep/extrinsic muscle of tongue (genioglossus, hyoglossus, palatoglossus, and styloglossus), medial pterygoid, hard palate, and mandible
- T4b Tumour invades any of the following: lateral pterygoid muscle, pterygoid plates, lateral nasopharynx, skull base, or encases the carotid artery

N – Regional lymph nodes##
- NX Regional lymph nodes cannot be assessed
- N0 No regional lymph node metastasis
- N1 Metastasis in a single ipsilateral lymph node, 3 cm or less in greatest dimension
- N2 Metastasis as specified in N2a, 2b, 2c below
- N2a Metastasis in a single ipsilateral lymph node, more than 3 cm but not more than 6 cm in greatest dimension
- N2b Metastasis in multiple ipsilateral lymph nodes, none more than 6 cm in greatest dimension
- N2c Metastasis in bilateral or contralateral lymph nodes, none more than 6 cm in greatest dimension
- N3 Metastasis in a lymph node more than 6 cm in greatest dimension

Note: Midline nodes are considered ipsilateral nodes.

M – Distant metastasis
- MX Distant metastasis cannot be assessed
- M0 No distant metastasis
- M1 Distant metastasis

Stage grouping

Stage 0	Tis	N0	M0
Stage I	T1	N0	M0
Stage II	T2	N0	M0
Stage III	T1, T2	N1	M0
	T3	N0, N1	M0
Stage IVA	T1,T2,T3	N2	M0
	T4a	N0, N1, N2	M0
Stage IVB	T4b	Any N	M0
	Any T	N3	M0
Stage IVC	Any T	Any N	M1

The regional lymph nodes are the cervical nodes.

Management

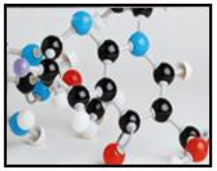

- Diagnosis/staging of disease at the time of presentation (“Diagnostic Radiology)
- Screening tool for clinically occult cancers

Radiology in Medicine (Oncology)

Radiation Oncology

- Identification of tumors to be irradiated
- Accurate delivery of radiation to the target (tumor)

Goals

Delineation of patient anatomy (desired radiation target) and organs at risk that should be spared from radiation dose.

Identified volumes are then used to compute an optimal radiation treatment strategy.

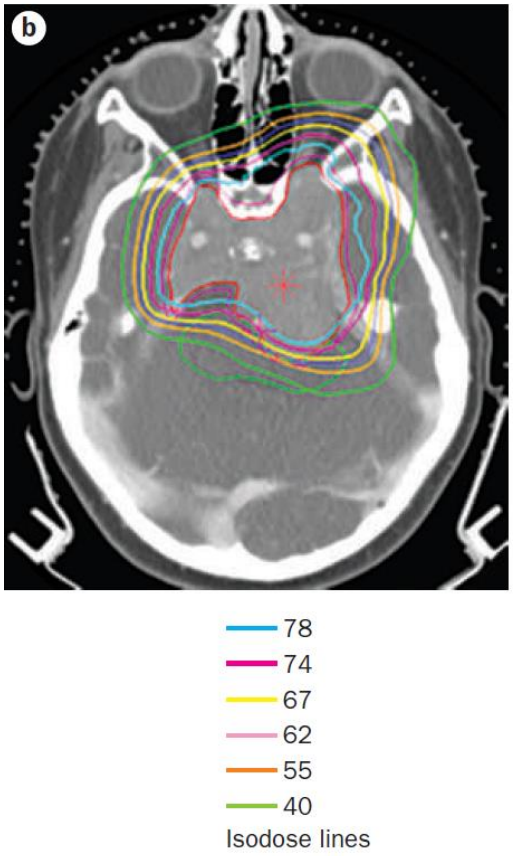

Durante & Loeffler, Nat Rev Clin Oncol

Radiology in Medicine (Oncology)

Drug Discovery and Development

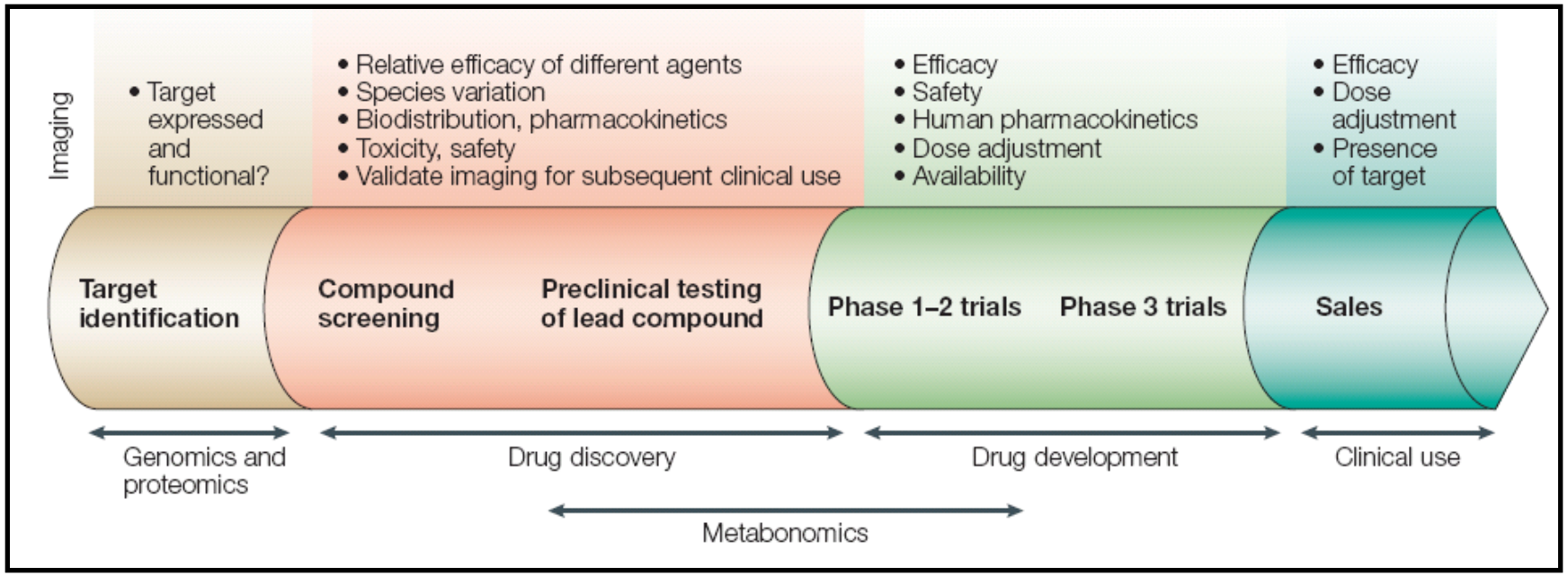

Rudin and Weissleder, Nature Rev 2003

Radiologic Assessment

RECIST: Response Evaluation Criteria In Solid Tumors

RECIST criteria are a voluntary, international standard, and are not an NCI standard. They are based on a simplification of former methods (WHO, ECOG) and based on measurable disease, i.e., the presence of at least one measurable lesion.

RECIST criteria offer a simplified, conservative, extraction of imaging data for wide application in clinical trials. They presume that linear measures are an adequate substitute for 2-D methods and registers four response categories:

- CR (complete response) = disappearance of all target lesions
- PR (partial response) = 30% decrease in the sum of the longest diameter of target lesions
- PD (progressive disease) = 20% increase in the sum of the longest diameter of target lesions
- SD (stable disease) = small changes that do not meet above criteria

✓ Simple ruler measurements

✓ Common language of efficacy

Great!! So what is the problem?

http://www.recist.com/recist-in-practice/19.html

The Changing Landscape of Medicine

Medicine has gone molecular…

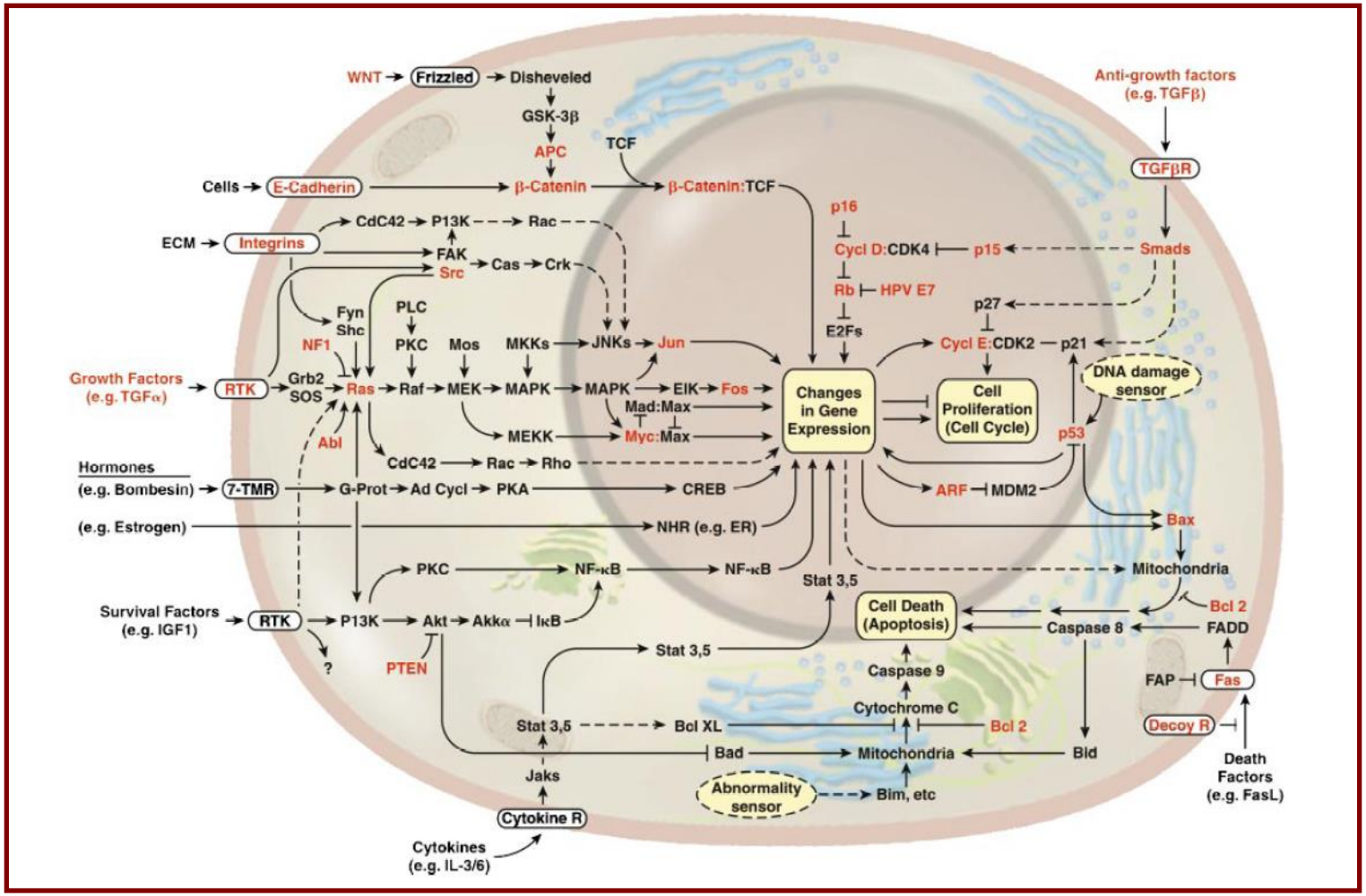

The Hallmarks of Cancer

Hanahan and Weinberg, Cell 2011

Molecular Cancer Therapeutics

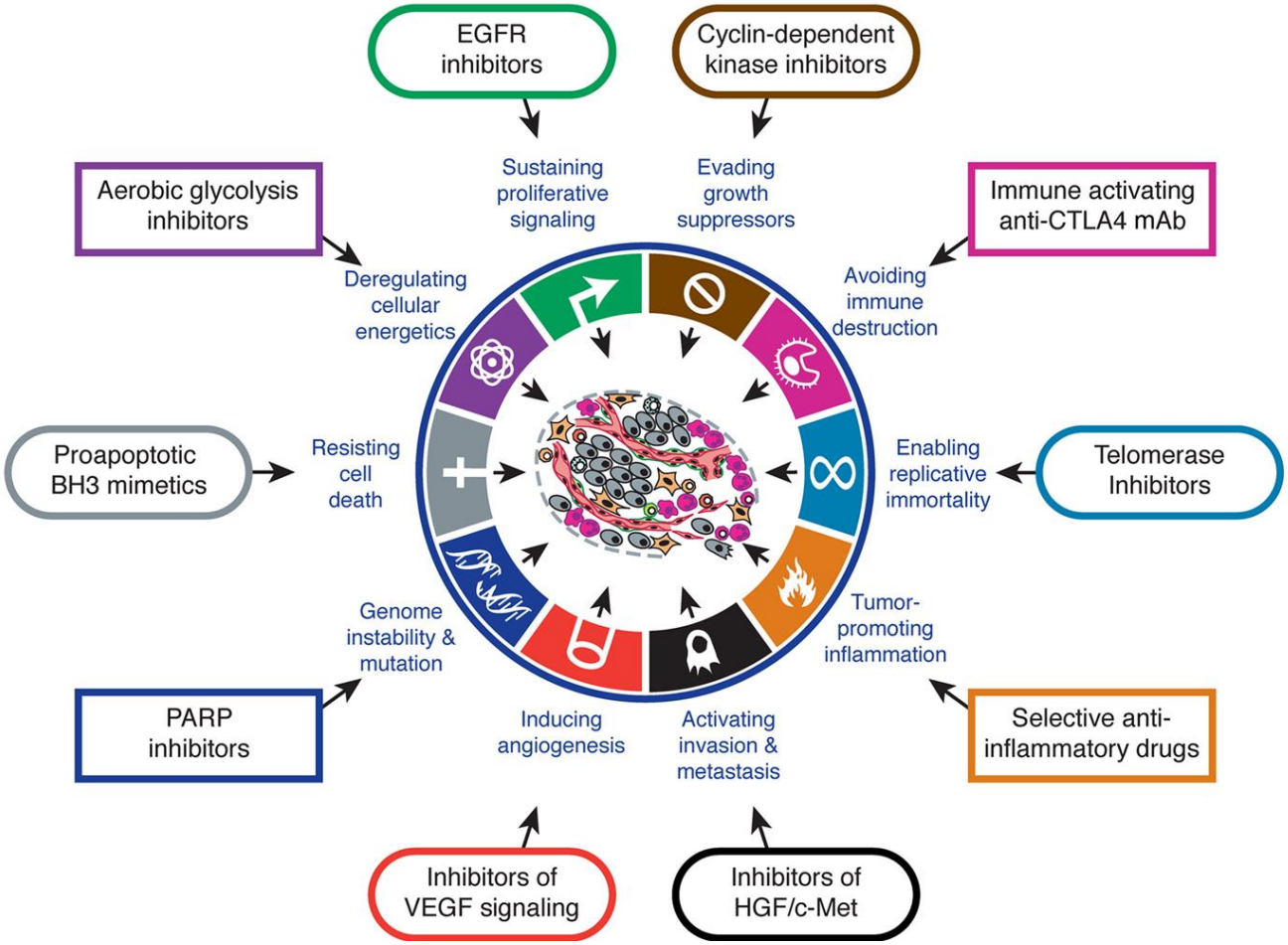

Problems: Patient selection, biological end point assessment

Hanahan and Weinberg, Cell 2011

Molecularly Targeted Therapies

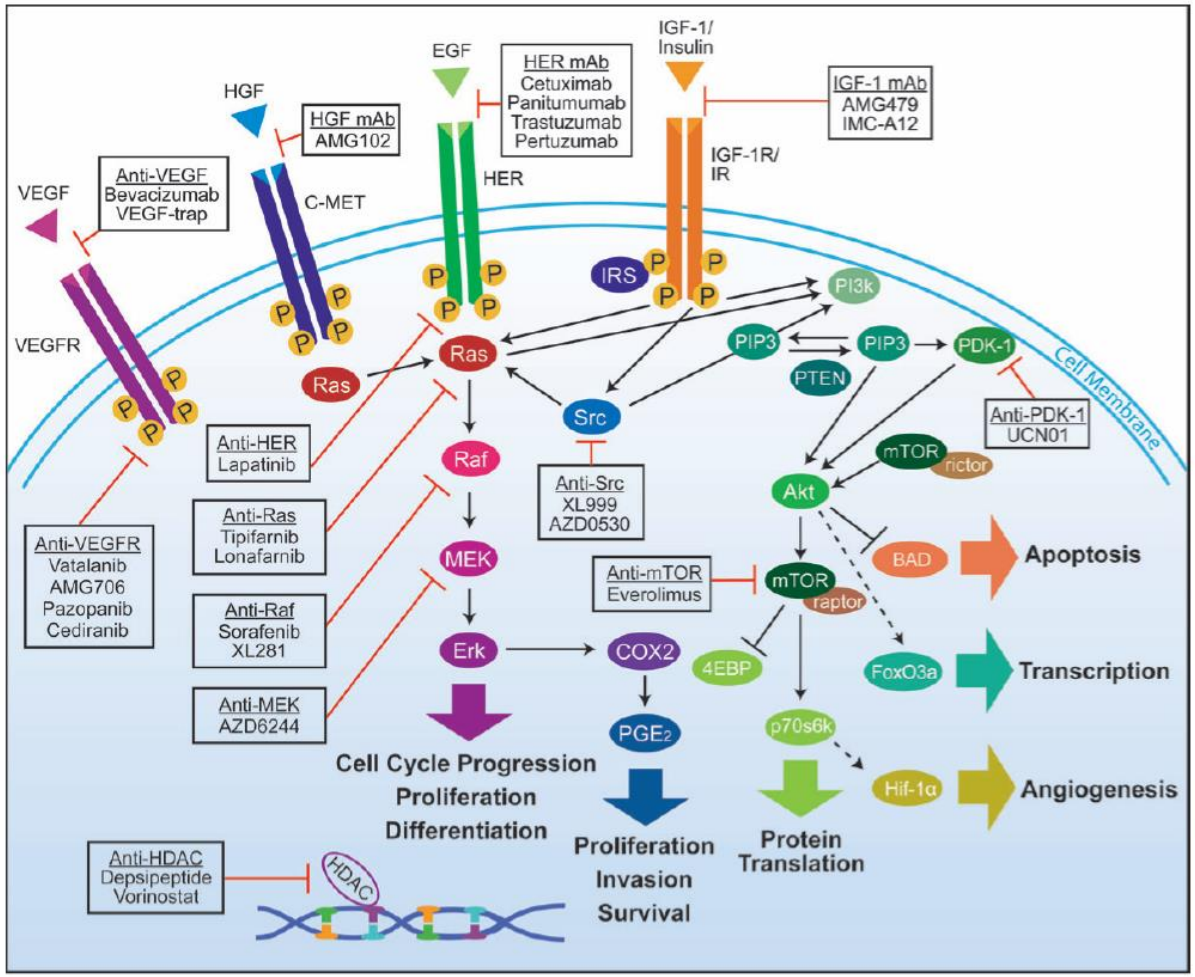

Problems:

Patient selection

Biological end point assessment

Siena et al., JNCI

Petrella et al., Radiology 2008

~~Diagnostic~~ Prognostic Radiology

Is RECIST good enough?

Traditional **cytotoxics** vs. modern **cytostatics**

Does not account for morphologic complexity; tumor heterogeneity

Tumor shrinkage alone may not be a sensitive measure of biological activity

Volumetric change is better – a late, non-specific end point

Clinical need: Early Response Indicators (Imaging Biomarkers)

The changing landscape of Radiology

Molecular Imaging

Visualization, characterization and measurement of biological processes at the molecular and cellular levels in humans and other living systems.
(includes 2D and 3D imaging and quantification over time)

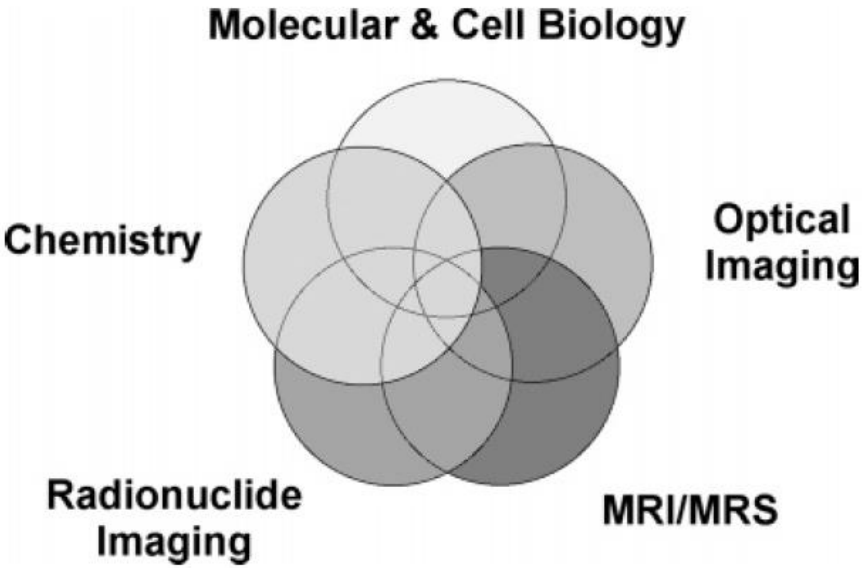

Molecular Imaging Definitions Task Force

Functional Molecular Imaging

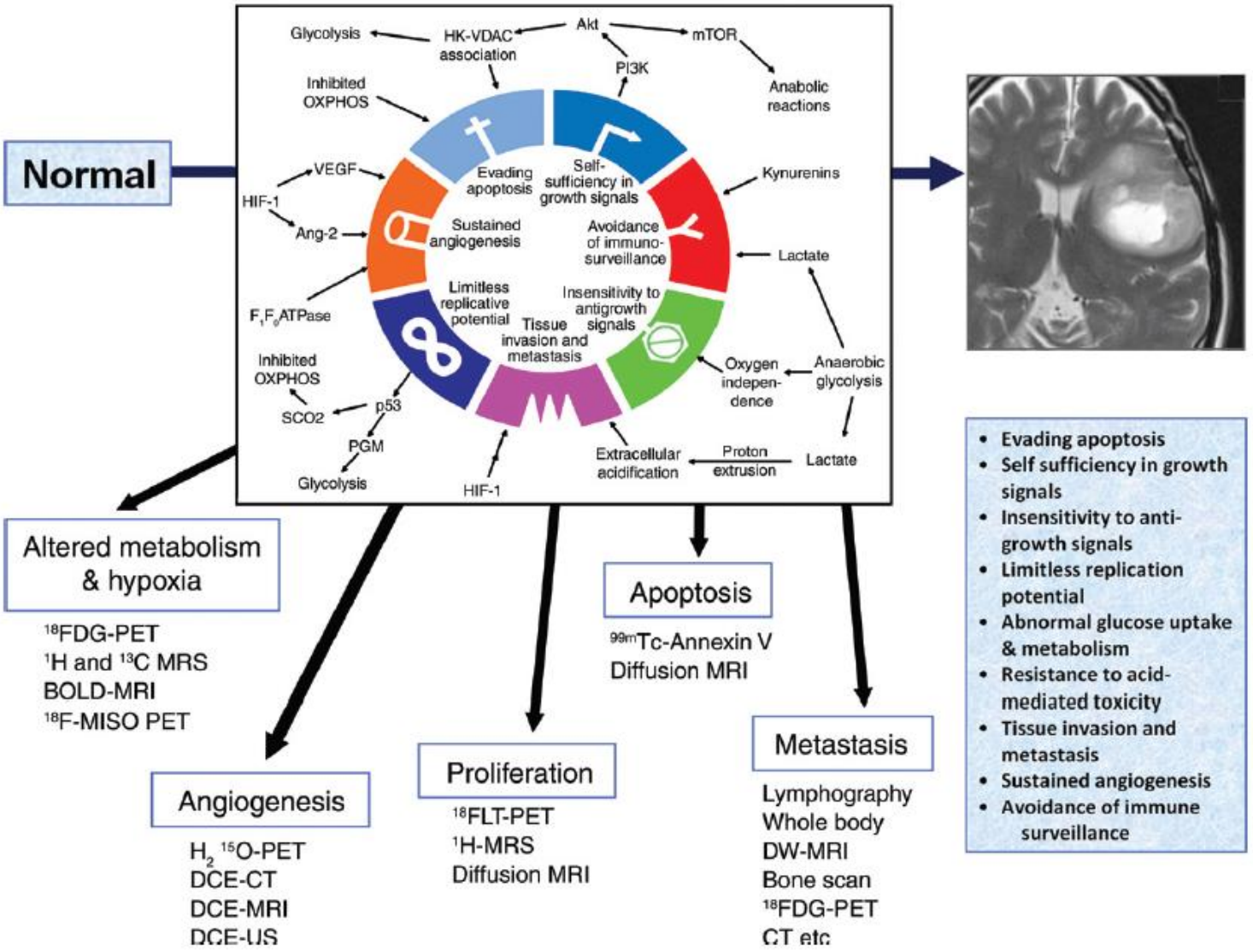

Padhani, Radiology 2010

Magnetic Resonance Imaging (MRI)

Basics of MRI

Nuclear spin – Hydrogen nuclei (protons)

Magnetization

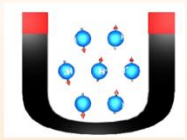

Radiofrequency

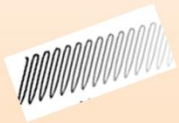

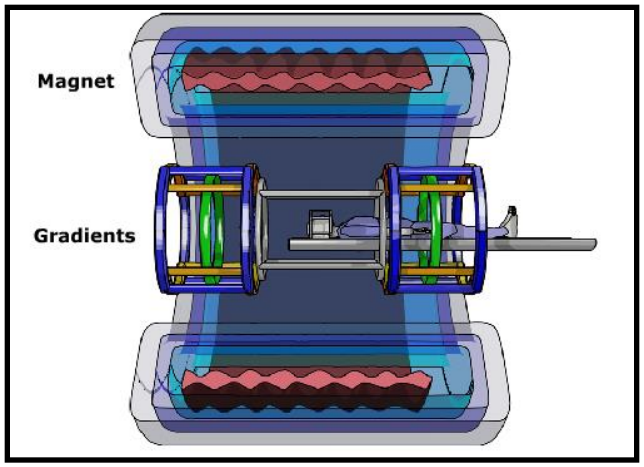

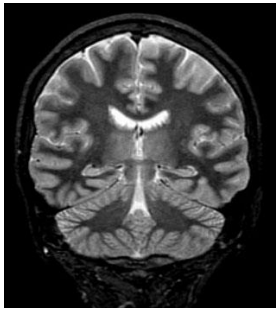

www.lahey.org/.../MRI_CommonTypes_Brain.asp

Basics of MRI

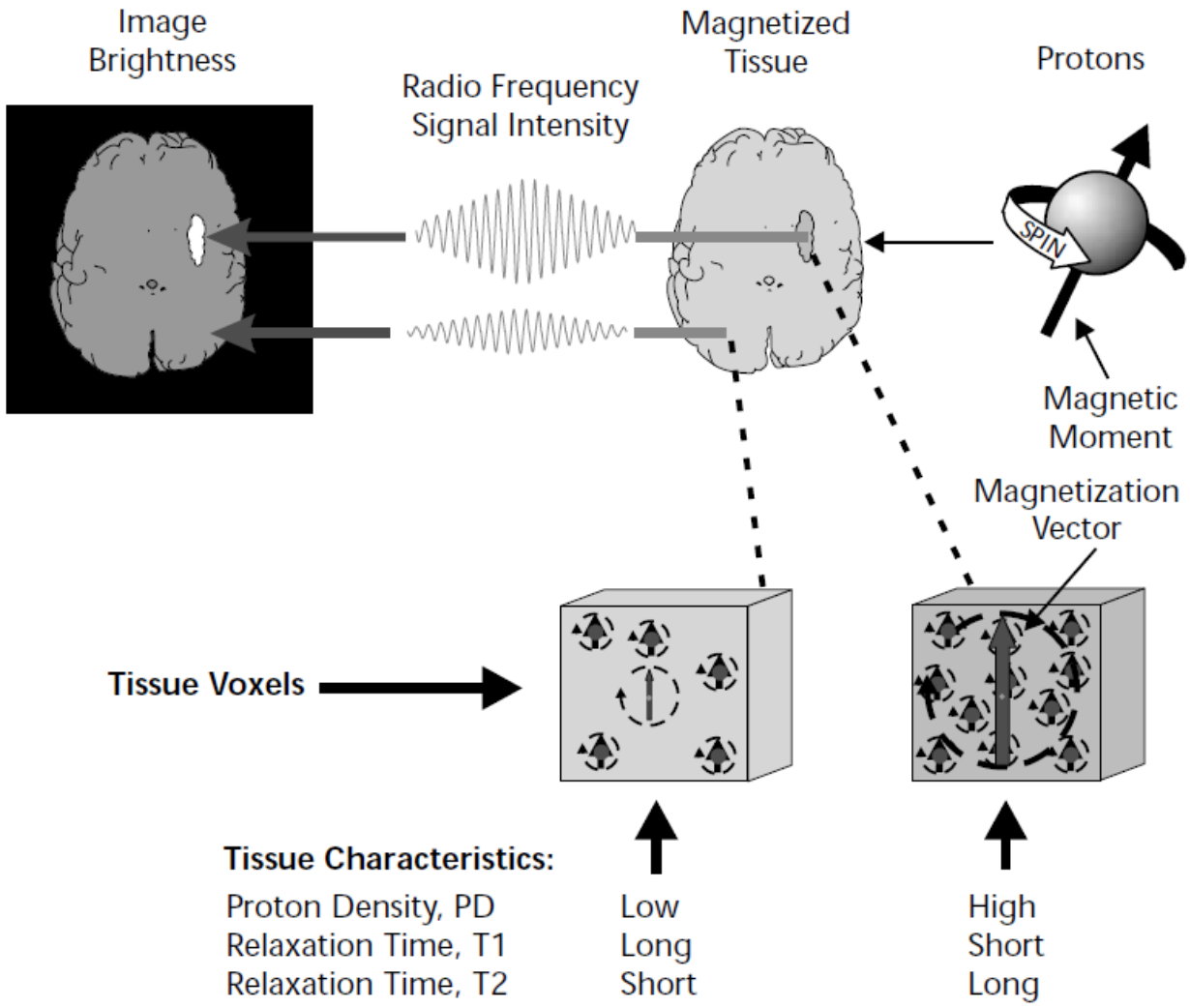

Sprawlsch, MRI basics

Image contrast in MRI

Contrast sensitivity

- Ability to produce an image that can distinguish different objects or tissues

Image contrast in MRI

Acquisition parameters (T1 or T2-weighted images)
Proton density
Physical/chemical environment of the protons (biological states of water)
*Contrast-enhancing agents: DCE-MRI

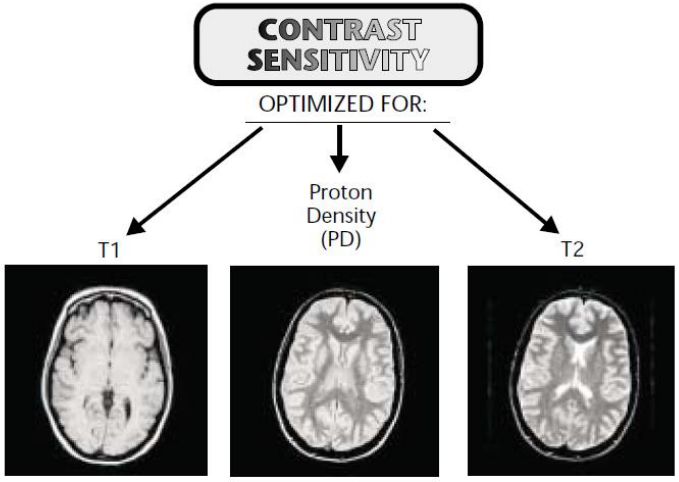

Figure 1-5. The images produced when the contrast sensitivity is optimized for each of the three specific tissue characteristics.

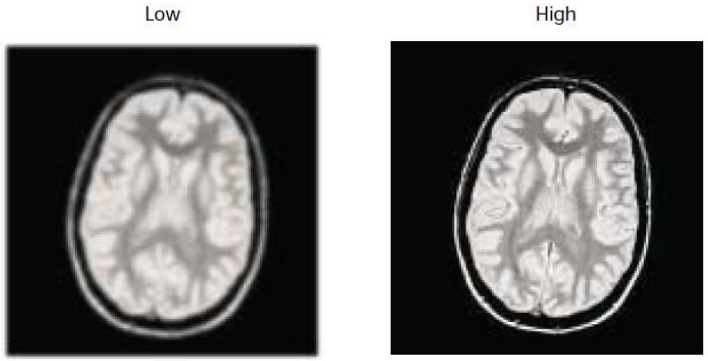

Applications of MRI

Anatomic Imaging

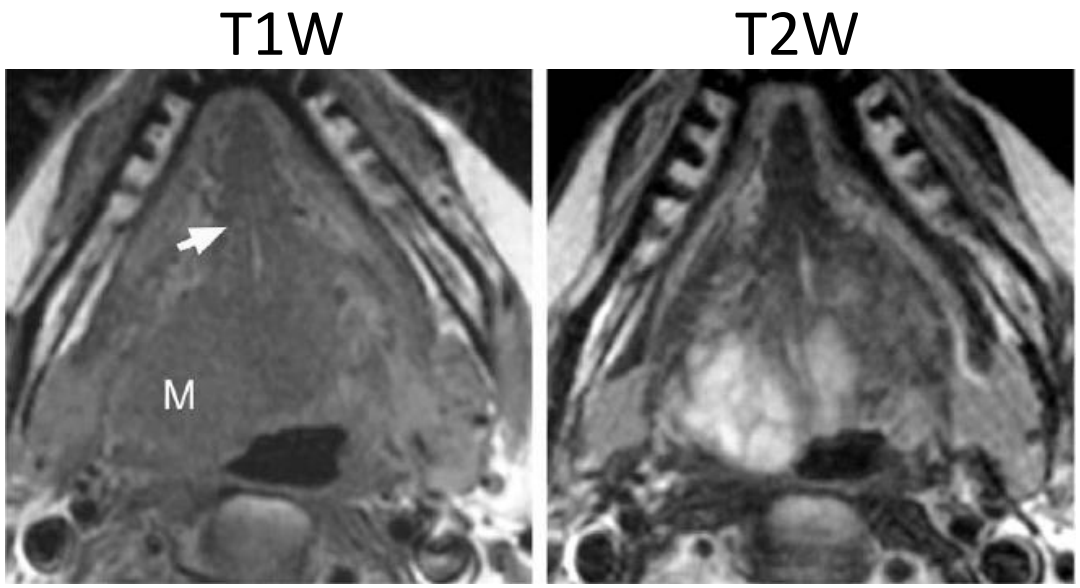

Ca - Floor of the Mouth (Axial) M – soft tissue mass; Arrow - genioglossus

- ✓Simple anatomic imaging
- ✓Extent of tumor (delineation of margins)

Rumboldt et al.,Oral Oncol 2006

Non-invasive imaging of Oral carcinogenesis

Cancer Prevention Research

Impact of Short-term 1,25-Dihydroxyvitamin D_3 on the Chemopreventive Efficacy of Erlotinib against Oral Cancer

Katelyn D. Bothwell[1], Tatiana Shaurova[1], Mihai Merzianu[2], Amritha Suresh[3], Moni A. Kuriakose[4], Candace S. Johnson[1], Pamela A. Hershberger[1], and Mukund Seshadri[1,3,4]

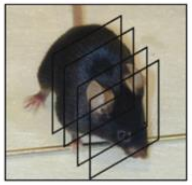

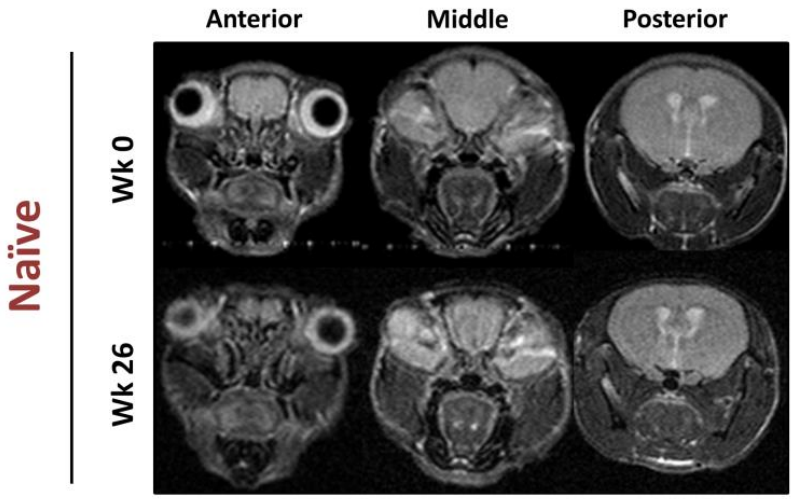

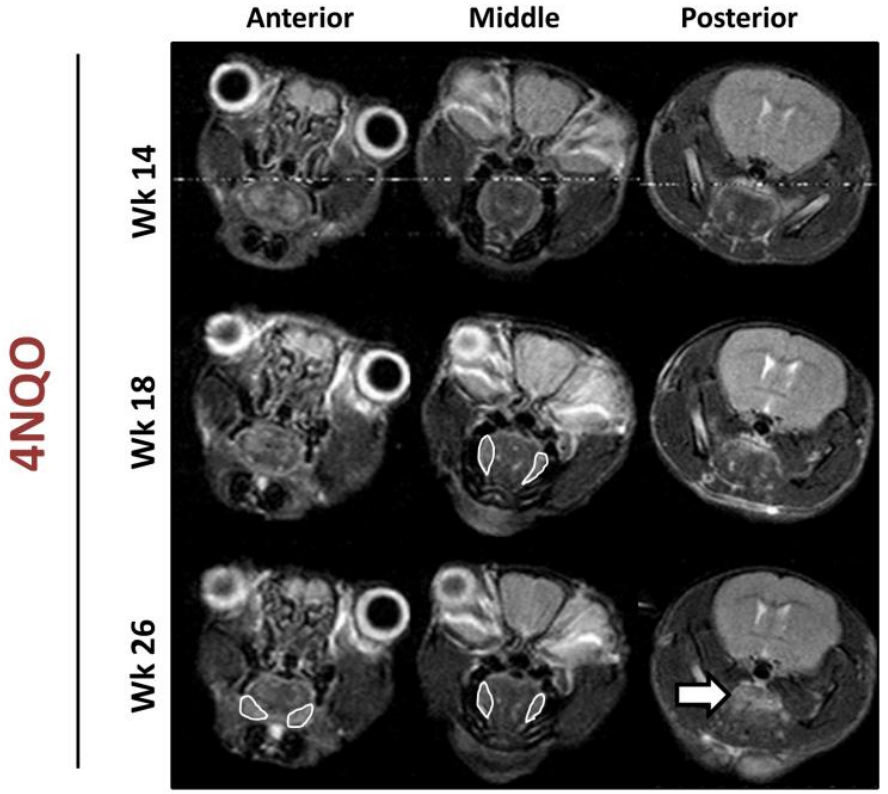

Bothwell et al., Cancer Prev Res. 2015

Non-invasive imaging of Oral carcinogenesis

Impact of Short-term 1,25-Dihydroxyvitamin D_3 on the Chemopreventive Efficacy of Erlotinib against Oral Cancer

Katelyn D. Bothwell[1], Tatiana Shaurova[1], Mihai Merzianu[2], Amritha Suresh[3], Moni A. Kuriakose[4], Candace S. Johnson[1], Pamela A. Hershberger[1], and Mukund Seshadri[1,3,4]

Cancer Prevention Research

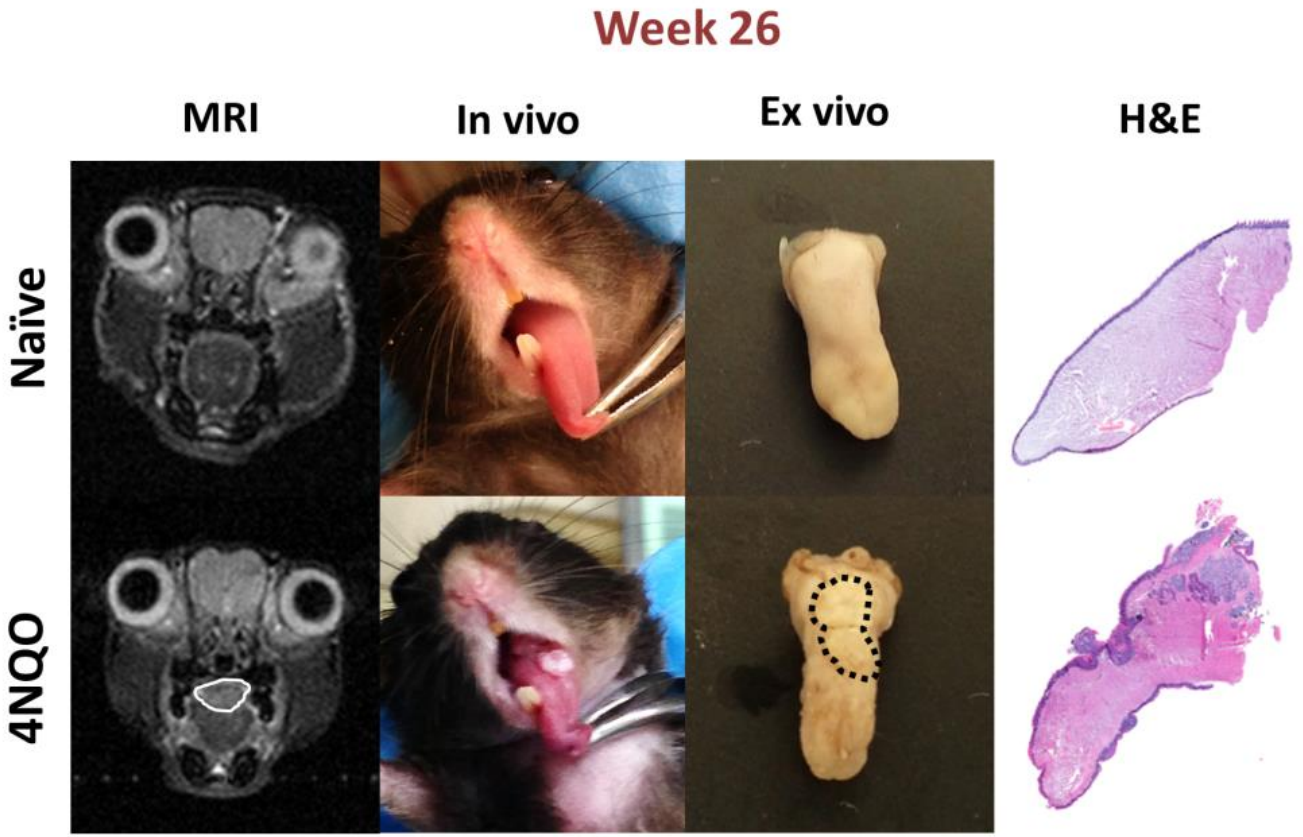

Bothwell et al., Cancer Prev Res. 2015

Dynamic contrast-enhanced MRI

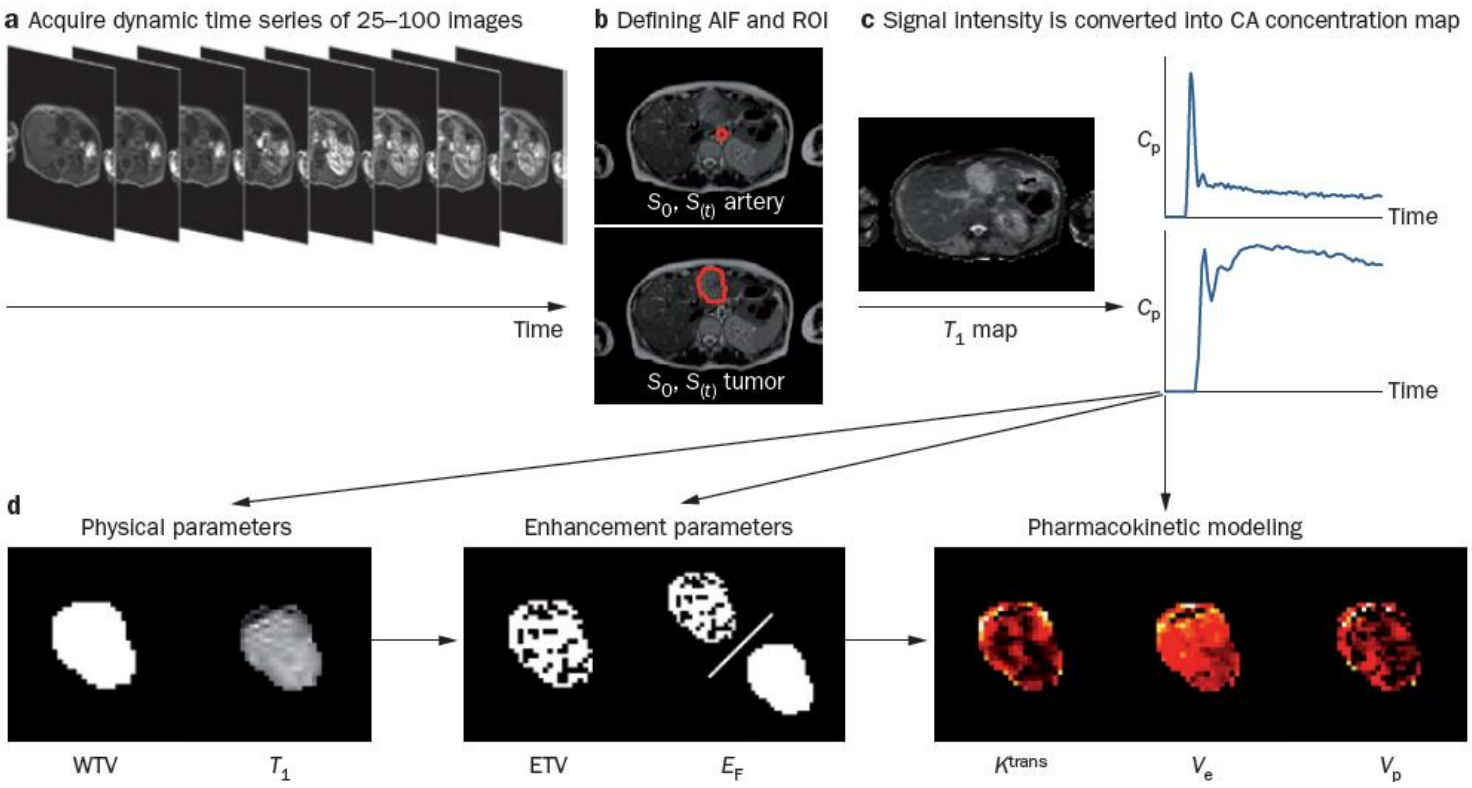

Typically involves repeated (dynamic) T1/T2-weighted imaging of tissues before and after administration of the contrast agent (contrast-enhanced).

Relates **enhancement pattern** of tissues to underlying physiological parameters (perfusion, permeability) by analyzing time-dependent tracer concentration.

O'Connor et al, NR Clin Prac Oncol

DCE-MRI of Breast Cancer

Maximum increase in signal intensity normalized to baseline signal intensity

$$E = \left[\frac{S_t - S_0}{S_0} \right]_{\max,}$$

S_t – signal intensity at time *t*, S_0 – baseline signal intensity

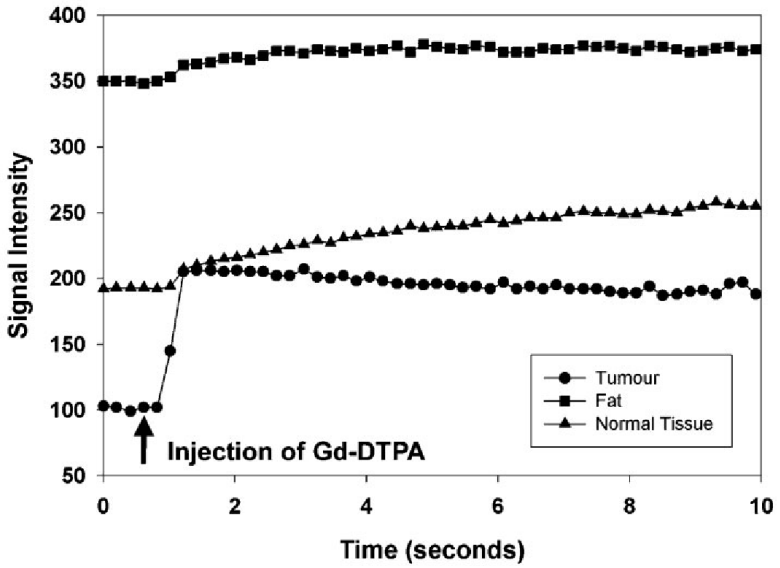

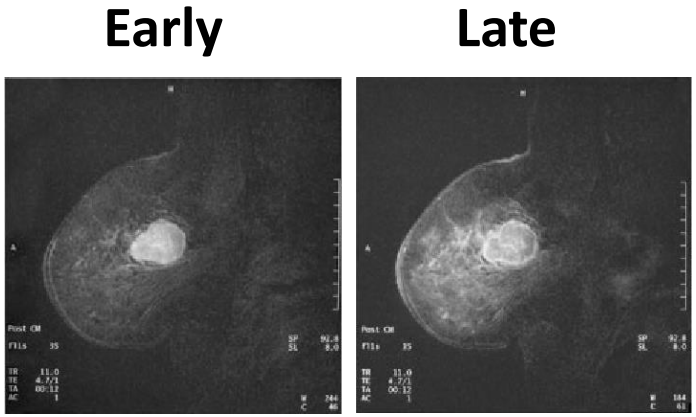

Padhani, BJR 2003

DCE-MRI of Breast Cancer

PK modeling of CA kinetics

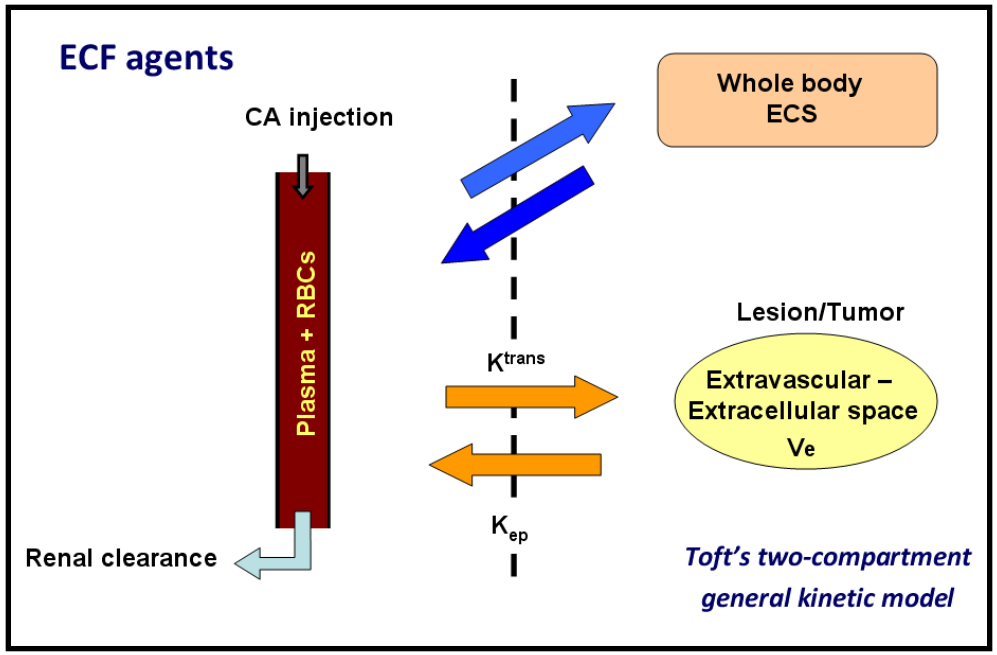

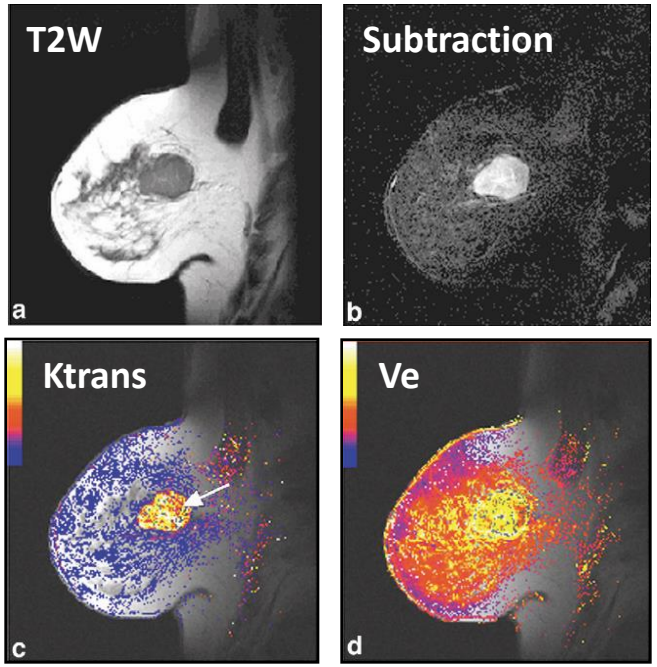

Kinetics of low MW CAs in tissues is determined by **3 factors**

1. Blood perfusion
2. Transendothelial transport (across the vessel wall)
3. Diffusion of the CA into the interstitial space

Padhani, JMRI 2002

DCE-MRI of Nodal Metastases

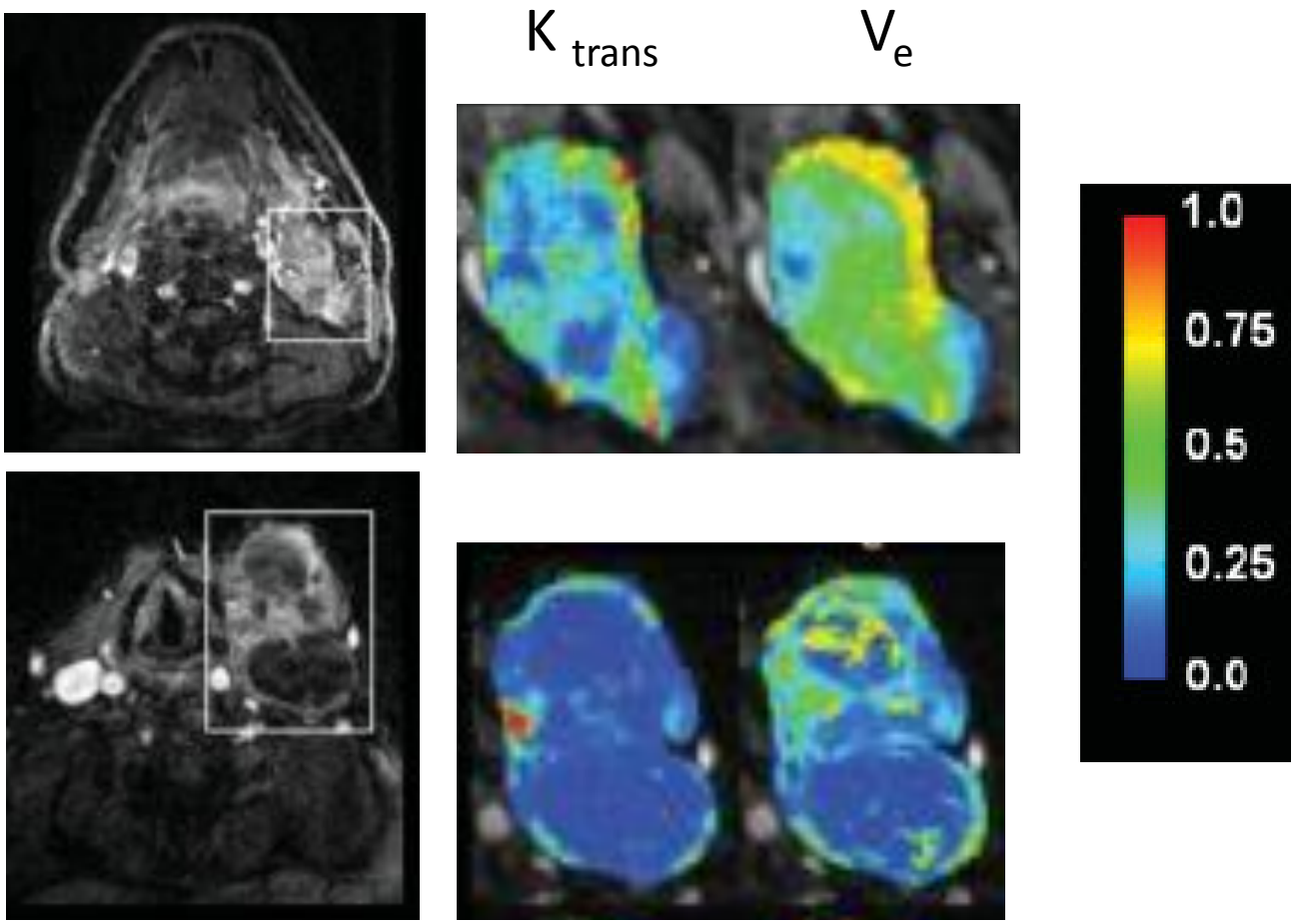

Ktrans – permeability constant; Ve – volume fraction of EES
Top – solid composition; Bottom – cystic or necrotic

Kim et al., JMRI 2007

MRI-guided Photodynamic Therapy

Image-guidance interstitial PDT

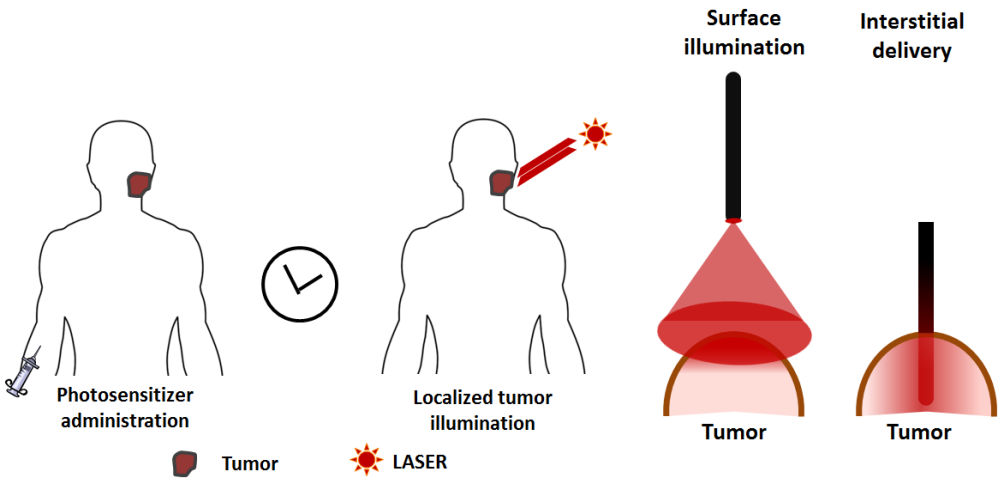

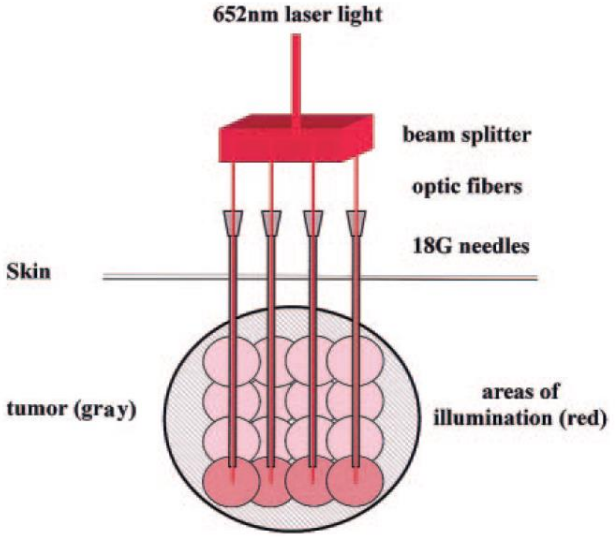

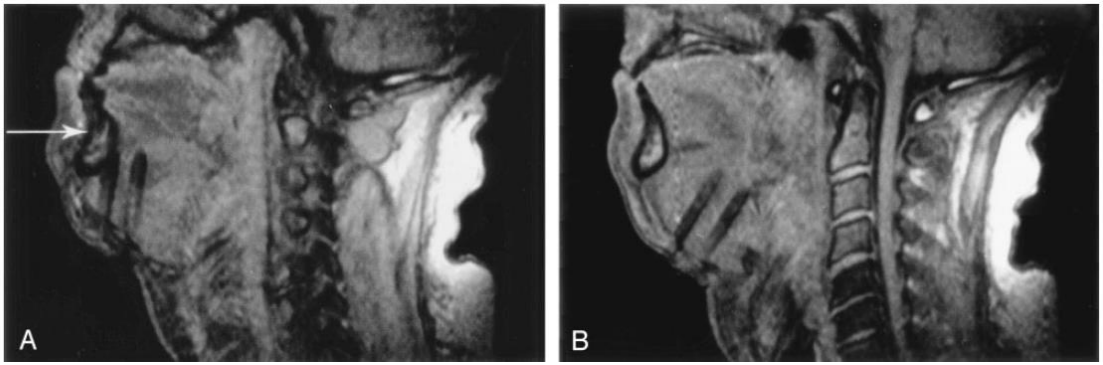

Sajisevi et al., 2016+ In press

Jerges et al.,2008

MRI-guided Photodynamic Therapy

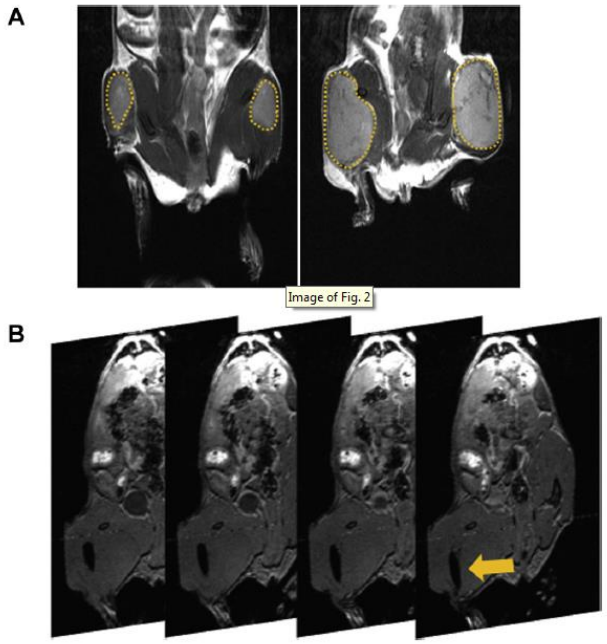

Fig. 2. Image-guided interstitial PDT of SCC tumors. (A) Coronal T2-weighted MRI was performed at different times (days 5–10) post implantation for serial monitoring of the growth of intramuscular SCCVII tumors (*dotted outline*). (B) Contiguous slices from a 3D spoiled-gradient echo scan of a mouse bearing intramuscular SCCVII tumor with the visible trace of the fiber placed in the tumor interstitium (*arrow*).

Original Research

Image-guided interstitial photodynamic therapy for squamous cell carcinomas: Preclinical investigation

Mirabelle Sajisevi[a], Nestor R. Rigual[a,b], David A. Bellnier[b], Mukund Seshadri[a,c,d,*]

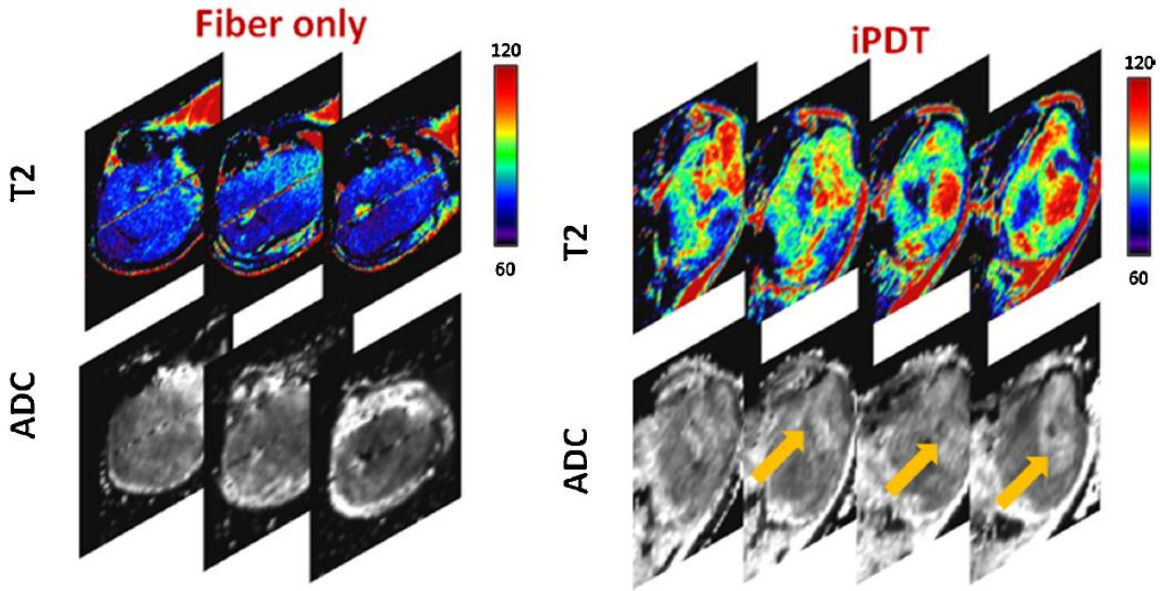

Utility of MRI as a non-invasive tool to guide fiber placement and map early tissue response to PDT.

Sajisevi et al., J Oral Max Surg Med Pathol 2015

Imaging-based monitoring of PDT efficacy

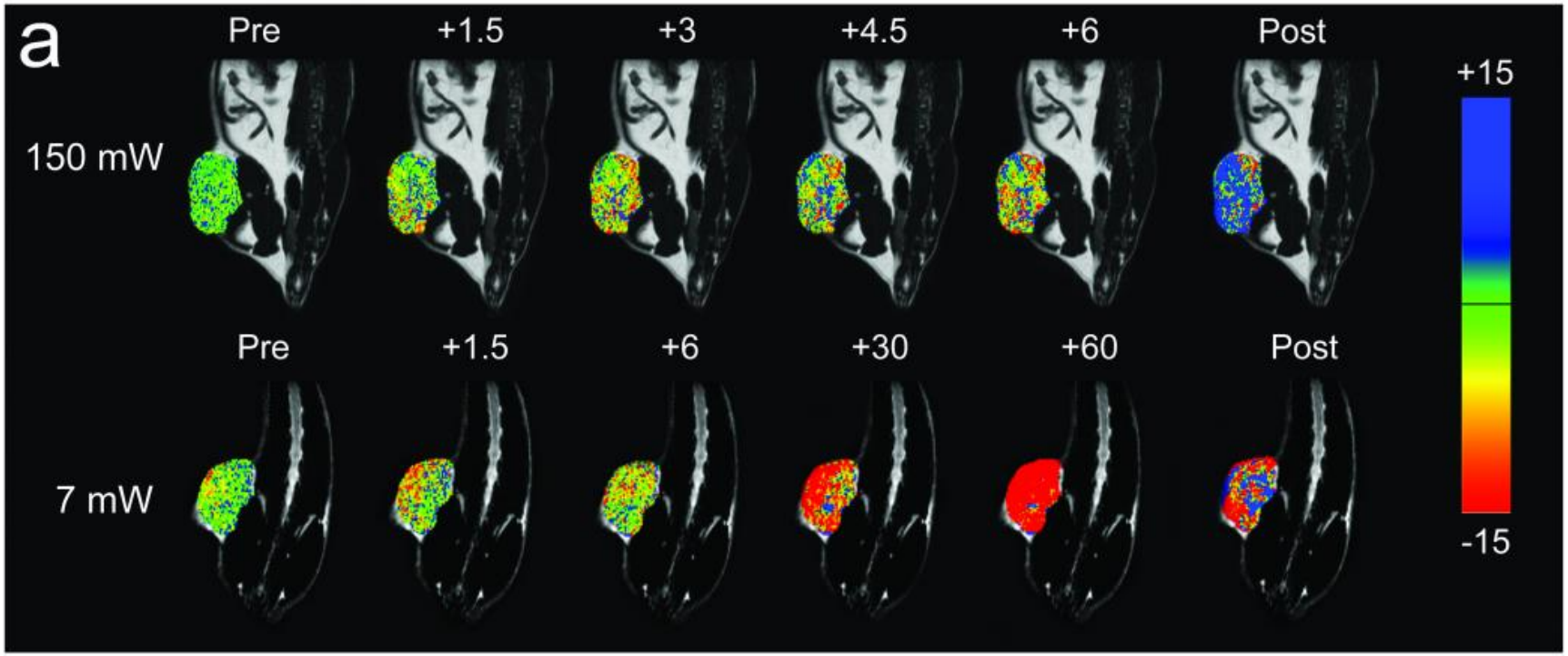

Real-time monitoring of PDT efficacy using blood oxygenation level dependent MRI

Seshadri et al.,Clin Cancer Res 2008

Positron Emission Tomography

Basics of PET

A compound labeled with a positron-emitting radionuclide is introduced into the body, usually by intravenous injection.

When one of the radionuclide atoms decays, a positron is emitted, travels a very short distance in tissue (typically 0^{-1}-10^{0} mm for radionuclides of interest), and annihilates with an electron in the tissue.

The mass of the two particles is converted into energy, which is emitted in the form of two back-to-back 511 keV gamma rays

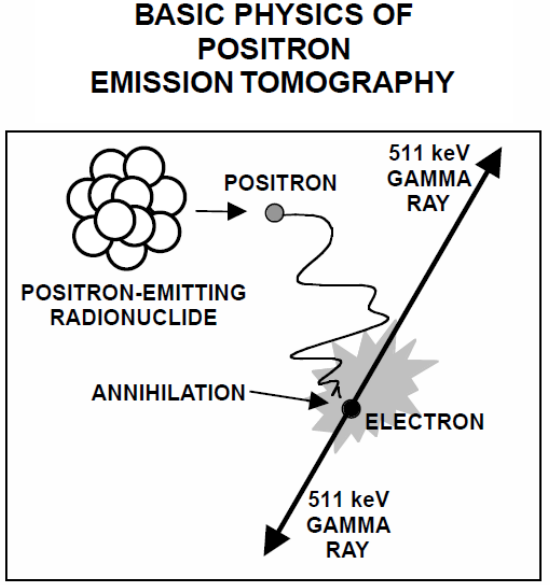

Basics of PET

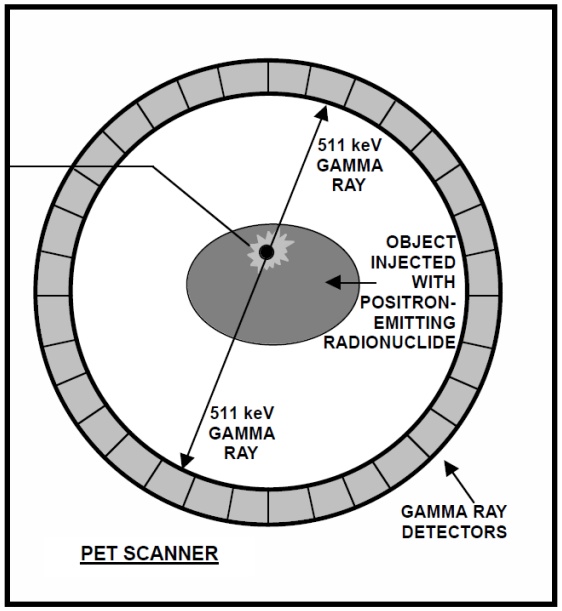

Table 1 Positron-emitting radionuclides of interest for biomedical studies

Radionuclide	Half-life	Production
^{11}C	20.3 min	Cyclotron
^{13}N	9.97 min	Cyclotron
^{15}O	122 sec	Cyclotron
^{18}F	109.8 min	Cyclotron
^{62}Cu	9.74 min	$^{62}Zn/^{62}Cu$ generator
^{64}Cu	12.7 hr	Reactor, cyclotron
^{68}Ga	68.1 min	$^{68}Ge/^{68}Ga$ generator
^{76}Br	16.1 hr	Reactor, cyclotron
^{124}I	4.17 days	Reactor, cyclotron

A positron emission tomography scanner consists of a ring, or multiple rings, of gamma ray detectors that register simultaneous gamma ray hits and their location, thus defining the line along which the positron-emission took place. By collecting large numbers of gamma-ray pair events (typically 10^6 to 10^7) and using computed tomography methods, cross-sectional images reflecting the concentration of the positron-emitting radionuclide can be generated.

Cherry and Gambhir, ILAR 2001

Basics of PET

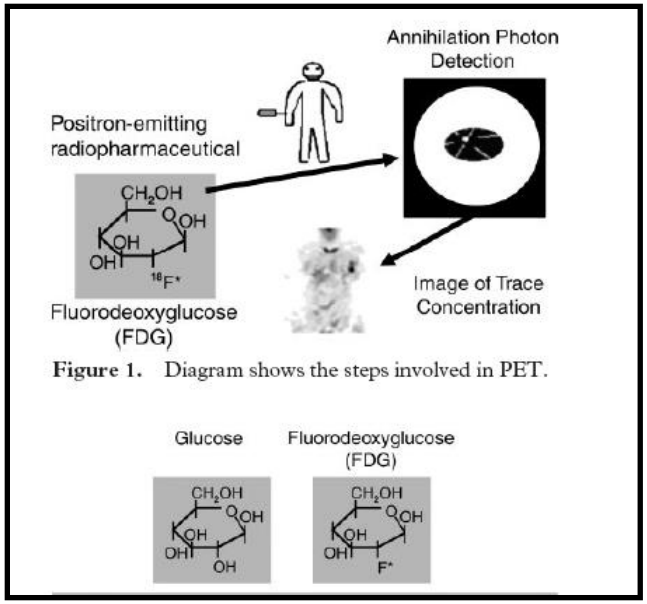

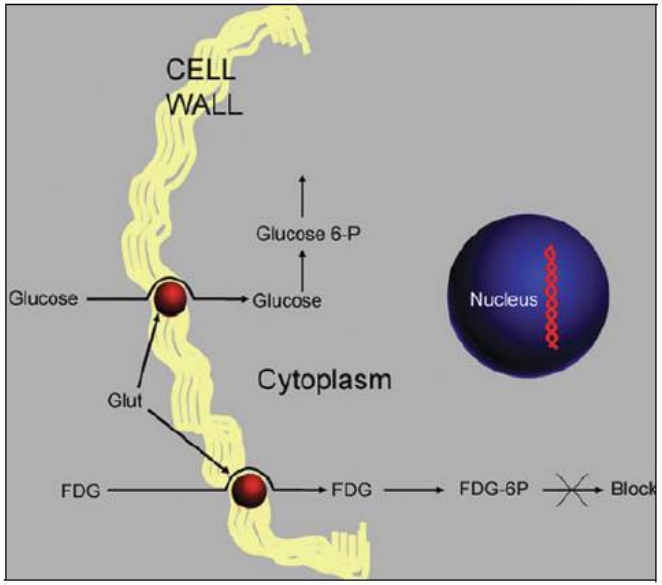

^{18}FDG is taken up in facilitated transport by metabolically active cells via glucose transporters (Glut) in cell membrane. In cell cytoplasm, 18FFDG undergoes phosphorylation to form FDG-6-phosphate (FDG-6-P) that, unlike glucose, cannot undergo further metabolism and becomes trapped in cell with only negligible amount of FDG-6P diffusing from cells.

Rosen et al.,Radiographics

Kapoor et al AJR 2005

Basics of PET

TABLE 15.1 Positron Emission Tomography Radiotracers Used to Image Cancer

Radiotracer	Label	Half-life (hours)	Application
Choline	^{11}C	0.34	Choline metabolism
Acetate	^{11}C	0.34	Fatty acid/sterol metabolism
Tyrosine	^{11}C	0.34	Amino acid metabolism
Methionine	^{11}C	0.34	Amino acid metabolism
Ammonia	^{13}N	0.17	Vascular perfusion
Water	^{15}O	0.03	Vascular perfusion
FDG	^{18}F	1.83	Glucose metabolism
FLT	^{18}F	1.83	Cellular proliferation
FHBG	^{18}F	1.83	Gene expression
FIAU	^{18}F	1.83	Gene expression
Galacto-RGD	^{18}F	1.83	Angiogenesis
Dimeric-RGD	^{18}F	1.83	Angiogenesis
FMISO	^{18}F	1.83	Hypoxia
FAZA	^{18}F	1.83	Hypoxia
EF5	^{18}F	1.83	Hypoxia
Cu-ATSM	^{64}Cu	12.70	Hypoxia
Cu-PTSM	^{64}Cu	12.70	Vascular perfusion

FDG, [^{18}F]fluoro-2-deoxyglucose; FLT, [^{18}F]fluorothymidine; FHBG, ^{18}F-9-[4-fluoro-3-(hydroxymethyl)butyl]guanine; FIAU, ^{131}I-2′-fluoro-2′-deoxy-1-ß-D-arabinofuranosyl-5-iodouracil ; RGD, arginine-glycine-aspartic acid; FMISO, [^{18}F]fluoromisonidazole; FAZA, [^{18}F]fluoroazomycin-arabinoside; EF5, 2-(2-nitro-1*H*-imidazol-1-yl)-N-(2,2,3,3,3-[^{18}F] pentafluoropropyl)-acetamide; Cu-ATSM: Cu(II)-diacetyl-bis(N(4)-methylthiosemicarbazone); Cu-PTSM: Cu(II)-pyruvaldehyde-bis(N(4)-methylthiosemicarbazone).

Cherry and Gambhir, ILAR 2001

PET in Clinical Oncology

^{18F}FDG PET/CT of Head and Neck Cancers

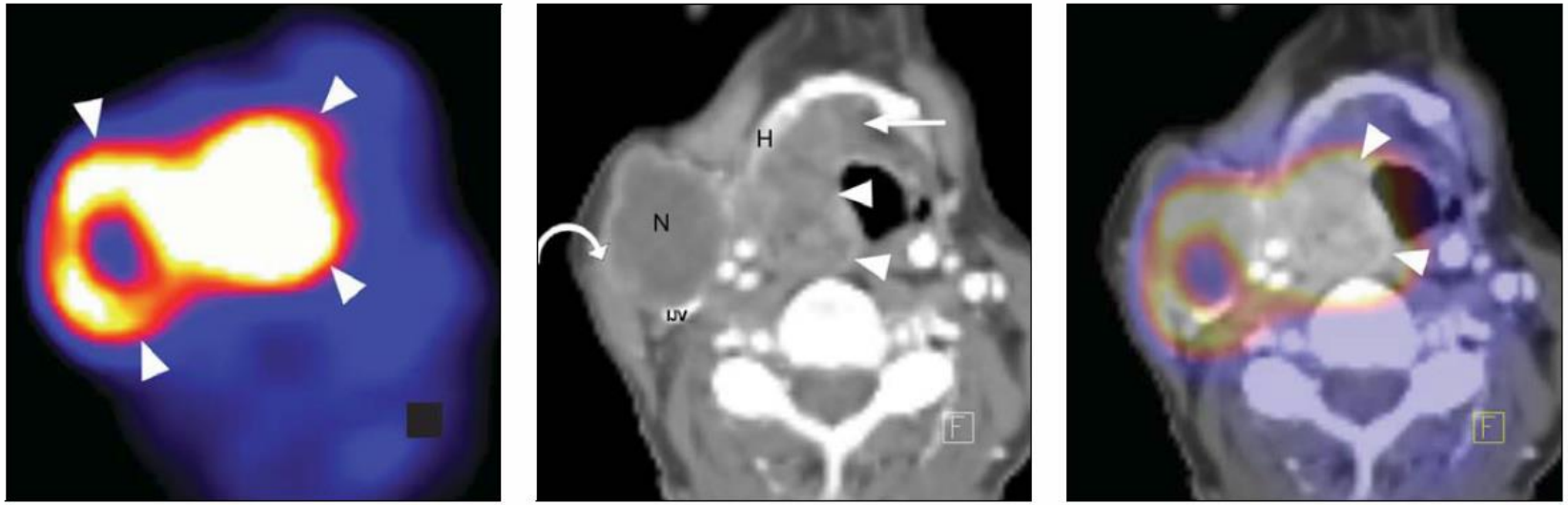

Fig. 8.—59-year-old man with poorly differentiated laryngeal carcinoma evaluated on ^{18F}FDG PET/CT for local and nodal extent of disease.
A, Axial image from ^{18F}FDG PET portion of examination shows intense hypermetabolism (*arrowheads*) at site of primary tumor and right neck, consistent with malignancy. However, local extent of primary tumor cannot be evaluated on PET alone.
B and **C**, Axial contrast-enhanced CT (**B**) and fused ^{18F}FDG PET/CT (**C**) images show large laryngeal mass (*arrowheads,* **B** and **C**) invading adjacent structures—hyoid bone (H, **B**) and ipsilateral pyriform sinus—and crossing midline (*straight arrow,* **B**). Large metastatic level 2a-III jugulodigastric lymph node (N, **B**) is also seen at same level as extracapsular spread (*curved arrow,* **B**) and necrotic center (focal central area of less intense ^{18F}FDG uptake, **C**), compressing adjacent internal jugular vein (IJV, **B**).

Kapoor et al AJR 2005

PET imaging of receptor expression

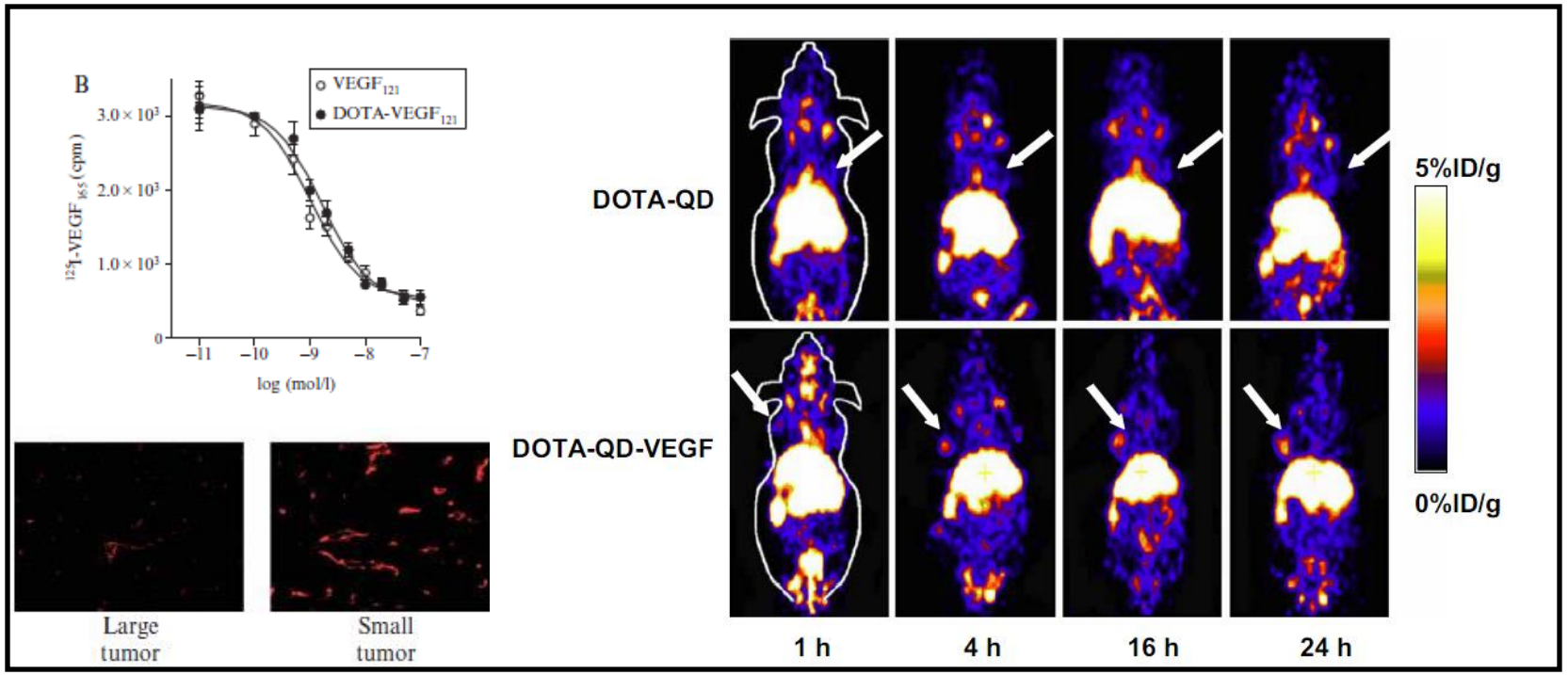

Dual-modality optical and positron emission tomography imaging of vascular endothelial growth factor receptor on tumor vasculature using quantum dots

Chen et al., Eur J Nuc Med 2008

PET imaging of AR occupancy

18 F-16*b*-Fluoro-5*a*-Dihydrotestosterone

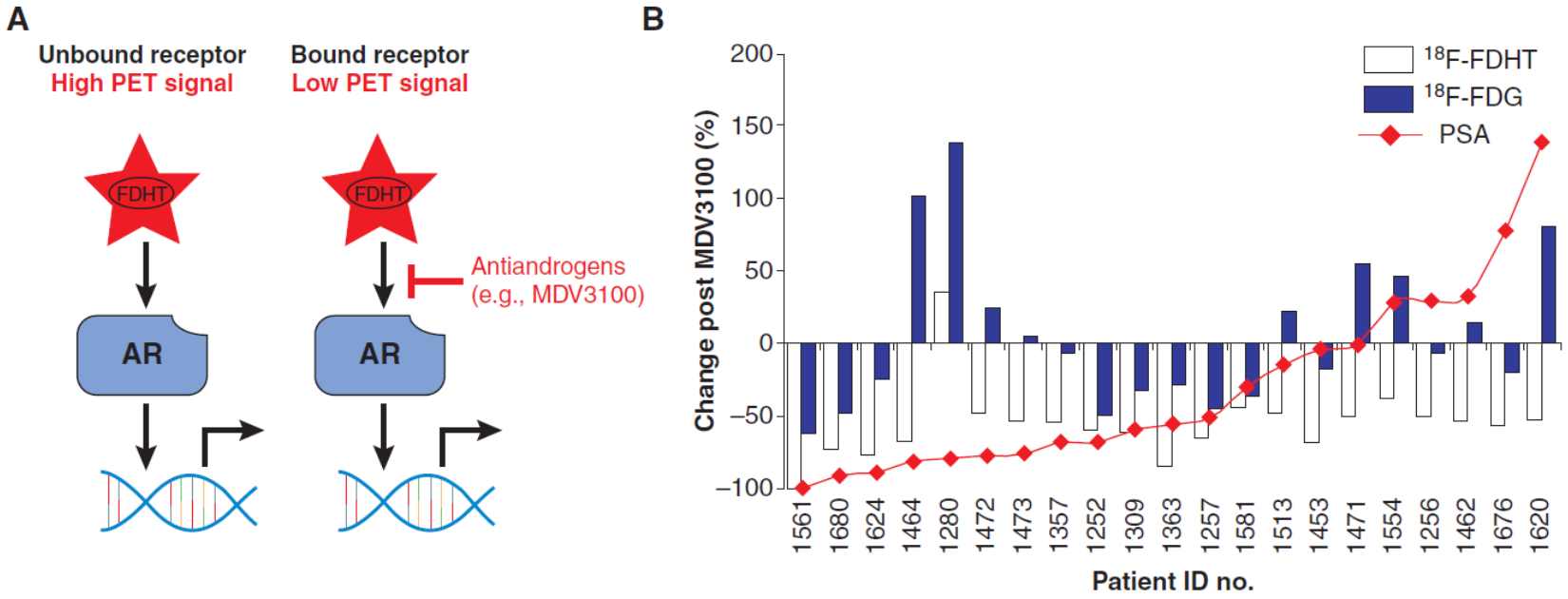

Figure 2. Monitoring the pharmacodynamics of antiandrogen therapies with the radioligand ^{18}F-FDHT. **A,** a schematic representation of how the radioligand ^{18}F-FDHT is applied in man to assess AR expression levels and receptor occupancy by drug. In the context of CRPC, pathologic activation of AR often occurs despite low circulating levels of androgens, allowing the radiotracer ^{18}F-FDHT to bind AR in prostate cancer lesions. When applied post-antiandrogen therapy, the absence of ^{18}F-FDHT binding can indicate that AR is effectively engaged by drug. **B,** a pilot study showing that ^{18}F-FDHT can be used to interpret dose selection of antiandrogens in man. Patients were scanned with ^{18}F-FDHT before enrolling in the phase I/II trial, and after 4 weeks of therapy, were scanned again to assess receptor blockade by MDV3100. Although ^{18}F-FDG SUV_{max} values almost uniformly declined in this cohort—pointing to effective engagement of AR by MDV3100—percent changes in serum PSA or ^{18}F-FDG SUV_{max} values did not overlay in an interpretable fashion with these ^{18}F-FDHT "responses," further pointing to a need for imaging agents that measure AR pathway signaling output directly.

PET imaging of Androgen Signaling

Prostate-specific membrane antigen (PSMA)

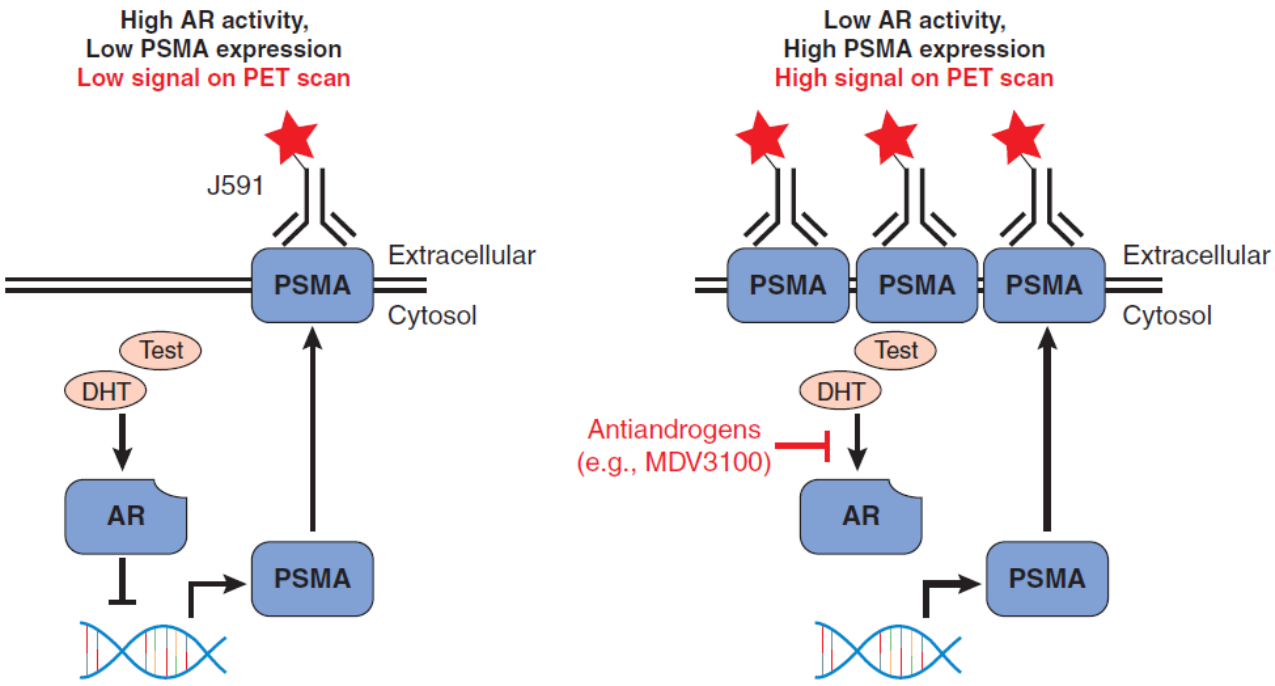

Figure 3. Noninvasively measuring AR signaling pathway output with a radiotracer targeting PSMA. A schematic representation of the relationship between AR activity and PSMA expression and the strategy to exploit this relationship for PET imaging. Several reports have shown that the gene encoding PSMA (*FOLH1*) is an androgen-repressed gene and that AR inhibition elevates PSMA expression. Chromatin immunoprecipitation sequencing data have shown AR to bind this gene, advancing the putative mechanism outlined in this figure.

Androgens repress PSMA expression in multiple prostate cancer models, whereas anti-androgens upregulate expression

Evans, Cancer Discovery 2012

Optical Imaging

Optical Imaging

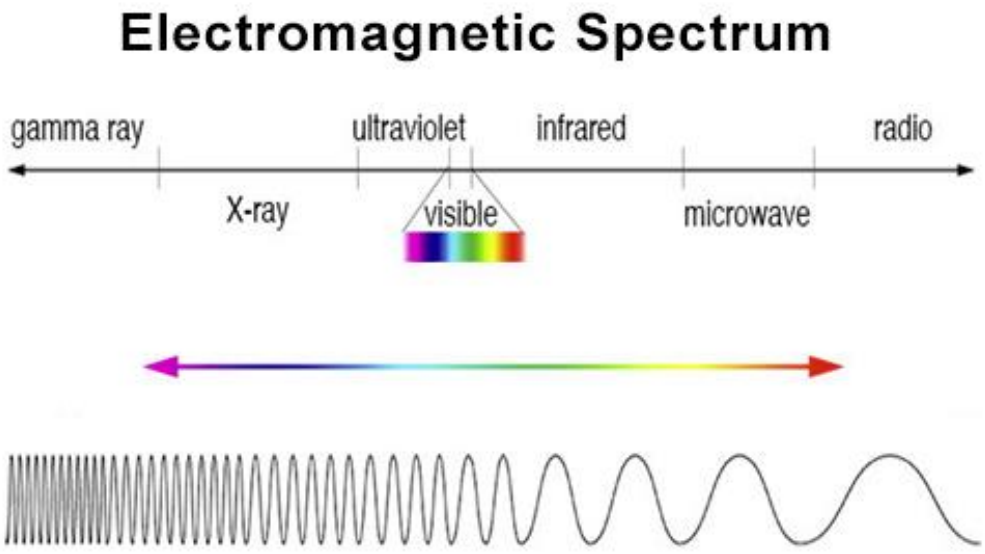

Strengths:

Uses non-ionizing radiation (visible, UV, IR) – safer for patients

Can provide detailed images of organs and tissues (contrast)

Quantitative

Faster acquisition times (short procedures, repeatable)

Optical Imaging

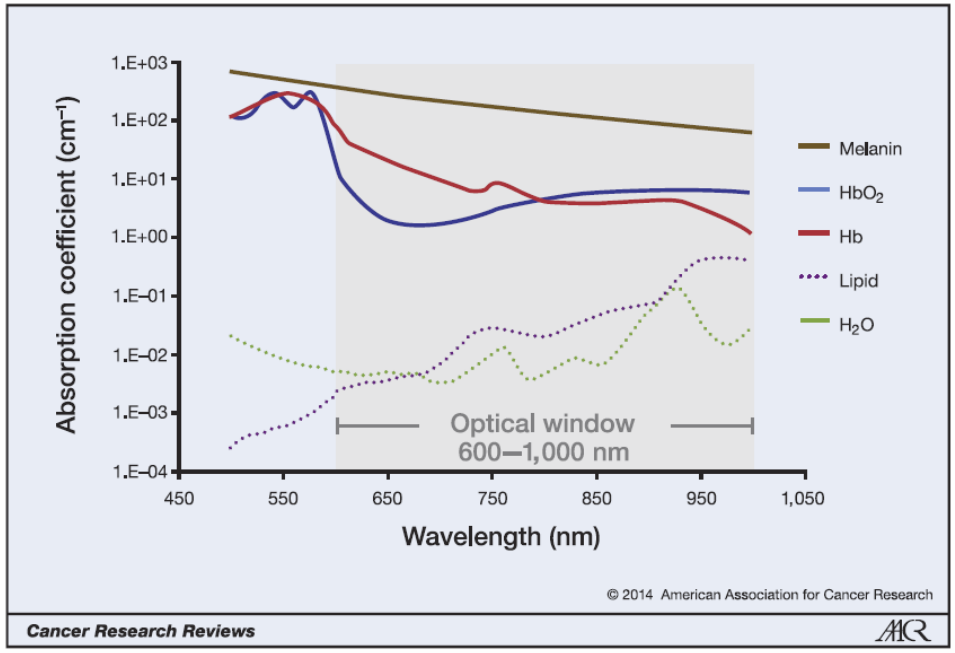

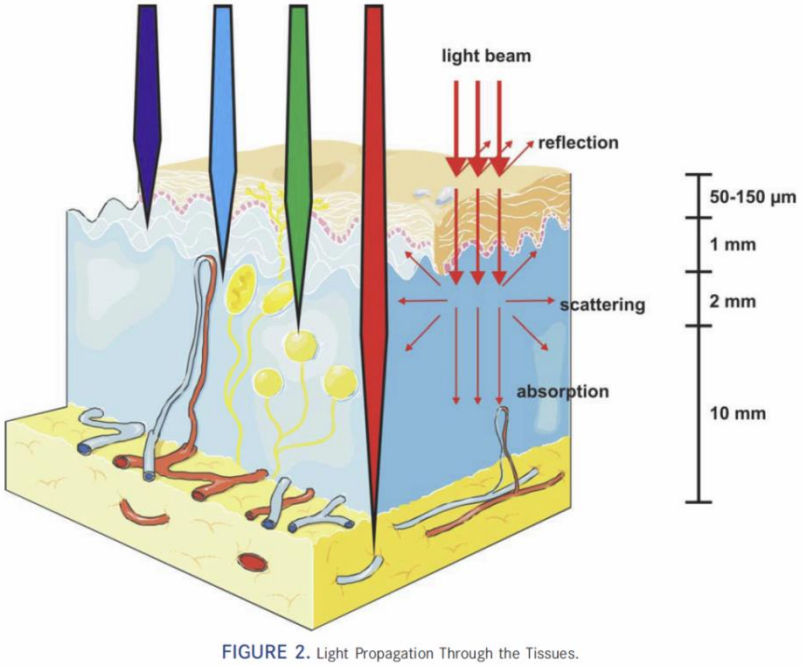

FIGURE 2. Light Propagation Through the Tissues.

Blue light vs. NIR

Weaknesses:

Tissue scattering/absorption (endogenous molecules – melanin, Hb)

Signal intensity is dependent on depth (light attenuation)

Zackrisson and Gambhir, Cancer Res 2014

Agostinis et al., CA Cancer J Clin 2011

Optical Imaging

Fluorescence imaging **Bioluminescence imaging**

Based on light emission
Use a charged coupled device (CCD) camera to collect photons

But there are differences in sensitivity and specificity

Image acquisition is generally performed in 2D
(Advances in hardware have made 3D tomography possible)

Both methods have advantages and limitations

Gheysens and Mottaghy, 2009

Optical Imaging Reporter Systems

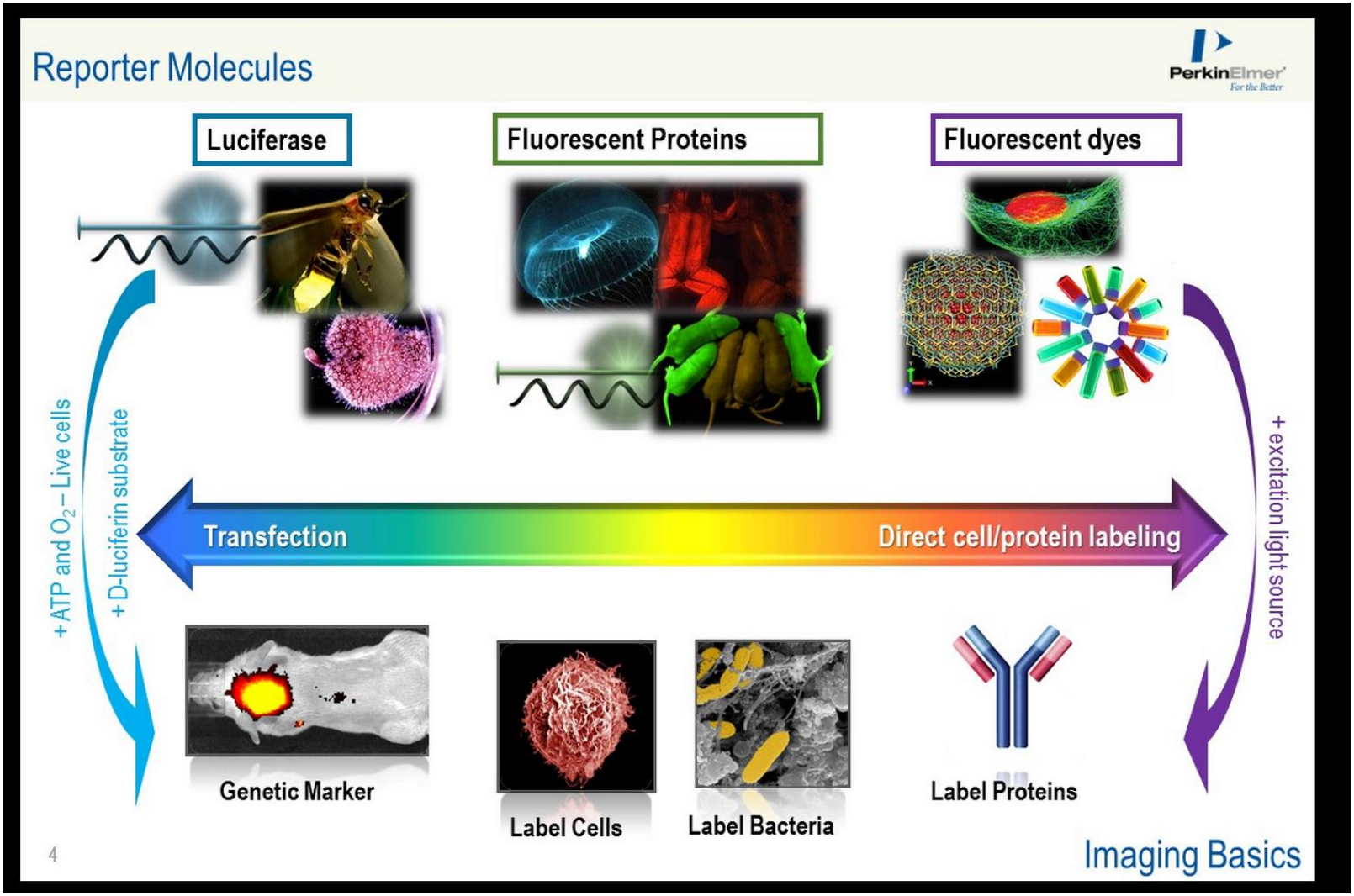

Kevin Francis, PhD – Perkin Elmer

Bioluminescence Imaging

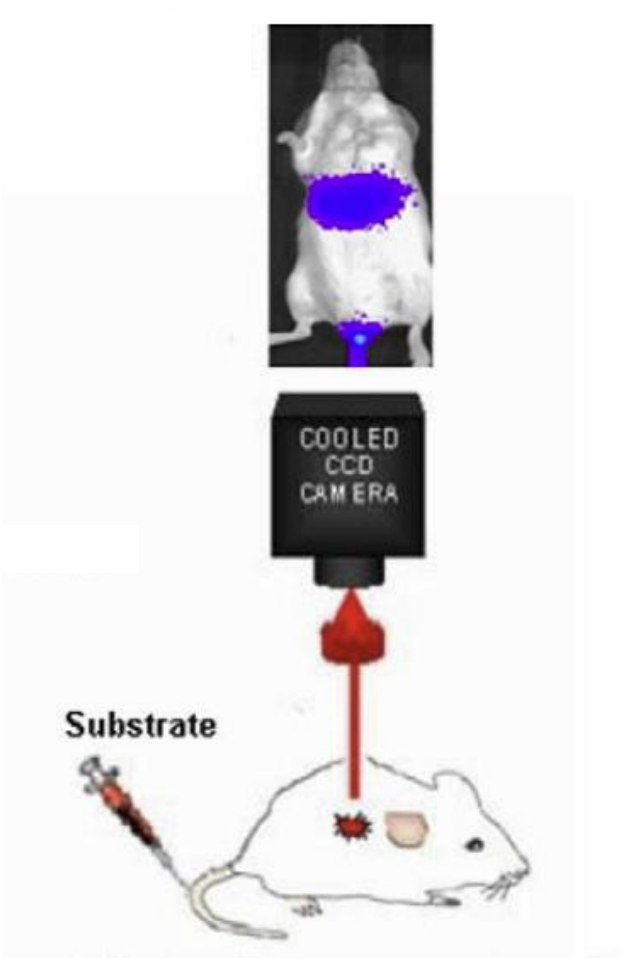

Does not require an external light source for excitation

Based on a biochemical interaction that produces light via a chemiluminescence reaction

Light is produced when the systemically delivered substrate undergoes enzymatic reaction

Advantages: Easy to use, high sensitivity, short acquisition times, high-throughput

Gheysens and Mottaghy, 2009

Bioluminescence reaction

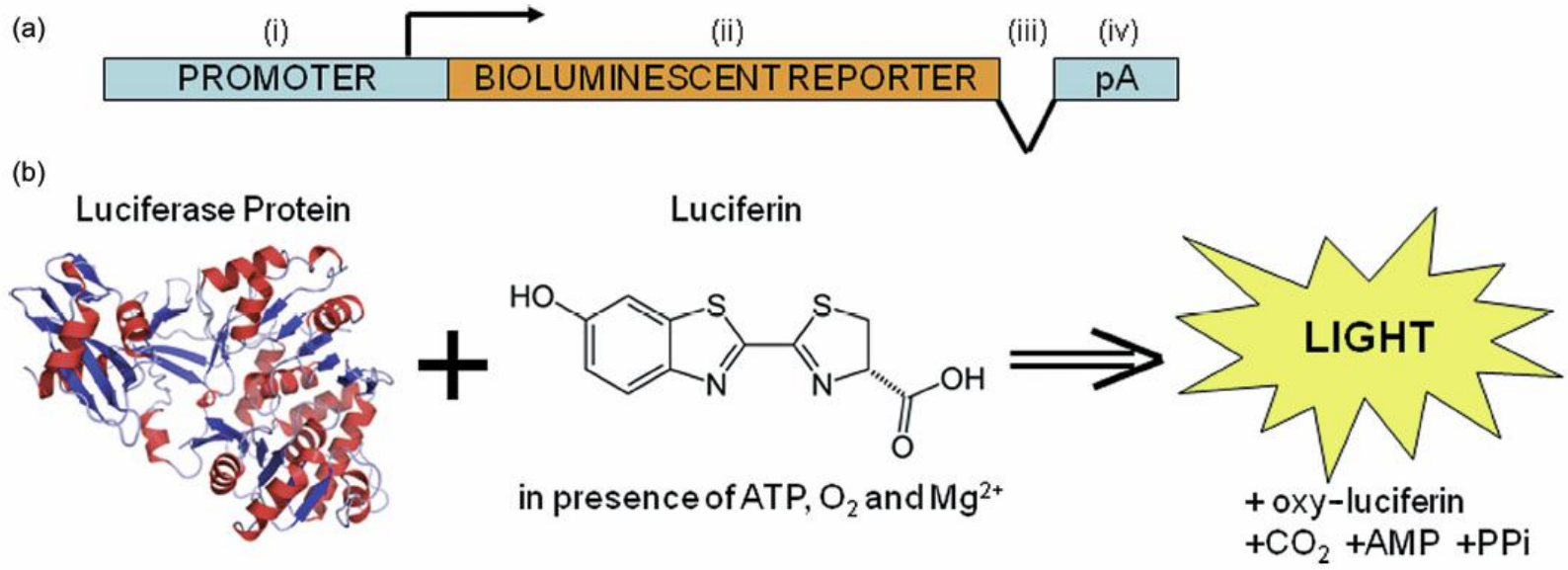

Figure 1. Panel A depicts the typical architecture of a bioluminescent reporter transgene. (i) The promoter sequence used to drive the expression of the transgene. This is most commonly a constitutive promoter (eg CMV) capable of driving ubiquitous and high-level transgene expression in the majority of mammalian cell types. Alternatively, it could be a tissue-specific or context-specific (eg only at S-phase of the cell cycle) promoter. (ii) The bioluminescent reporter, typically encoding either a luciferin or a coelenterazine oxidizing enzyme (eg firefly or *Renilla* luciferase, respectively). (iii) A synthetic intron; although not requisite, splicing of the transgenic transcript can enhance transgene expression. (iv) The poly-A signal sequence to enhance the stability of the transgenic mRNA, thus enhancing expression. Panel B illustrates the firefly luciferase–luciferin reaction that results in the production of light

Neill et al., 2010

Bioluminescence Imaging

IVIS Spectrum Imaging System

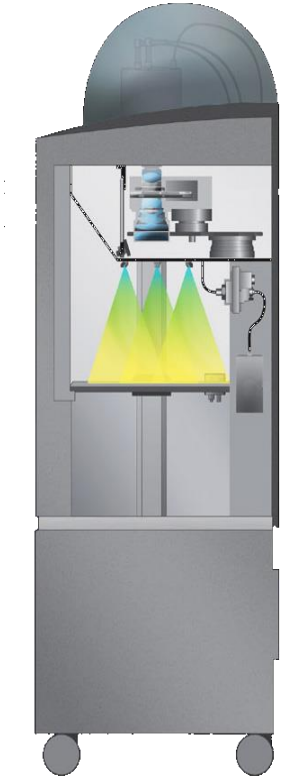

10 excitation filters

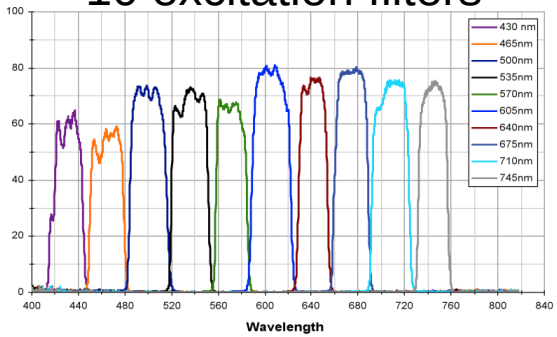

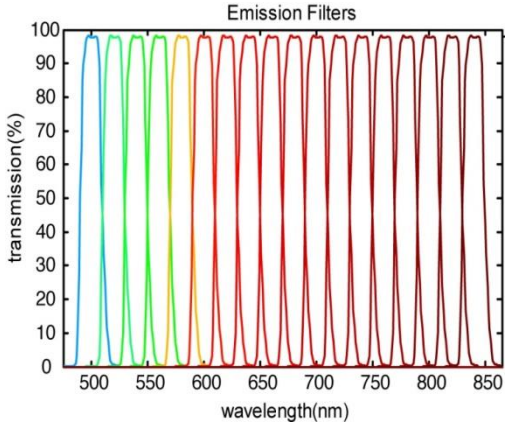

18 emission filters

Perkin Elmer Corporation

BLI in Preclinical Oncology

Application	Example
• Animal models	Xenograft, orthotopic, and GEM models of human cancer have been developed which express luciferase
• Drug development	BLI allows therapeutic efficacy of cancer drugs to be established
• Monitoring of genes	Luciferase-labelled cells may be used to monitor gene delivery and gene expression *in vivo* Genetic screening has also been performed using BLI, allowing identification of specific oncogenes
• Tumour development	BLI may be used to study processes such as angiogenesis, apoptosis, and adhesion in cancer cells
• Metastasis	High sensitivity of BLI allows the imaging of metastasis and minimal residual disease states in cancer models
• Protein interactions	BLI has been used to image protein–protein interactions *in vivo*

Byrne et al., 2013

Labeling cells for BLI

Bioware Ultra Cell lines

PerkinElmer
For the Better

- Labeled with luciferase or dual labeled with luciferase and GFP or tdTomato
- Ideal for non-invasive detection/quantification of tumors in whole animals
- Extensively used in orthotopic, metastatic and murine tumor models. Quantify tumor burden in the whole mouse, identify micrometastases and track residual disease
- Bioware lines are derived from breast, liver, colon, lung, prostate, melanoma, ovarian among others
- Dual labeled Cell lines ideal for *in vivo* imaging using luciferase and *ex vivo* analysis using the fluorescent protein
- All cell lines confirmed pathogen free

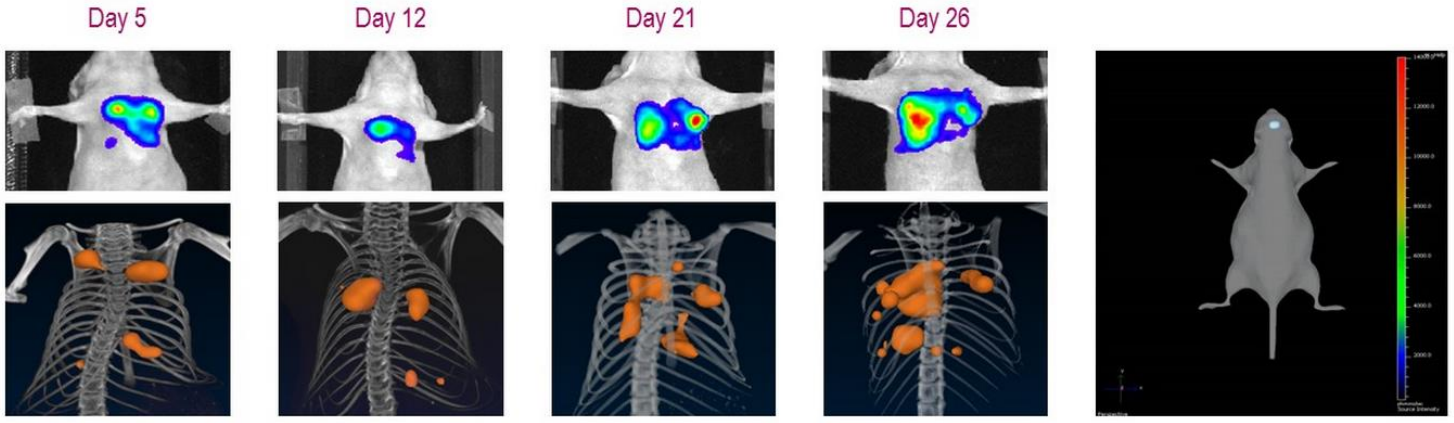

NCI-H460 orhtotopic Lung tumor model (left) and U87-MG-luc2 Brain tumor model

Caliper LifeSciences

BLI of Hematologic Malignancy

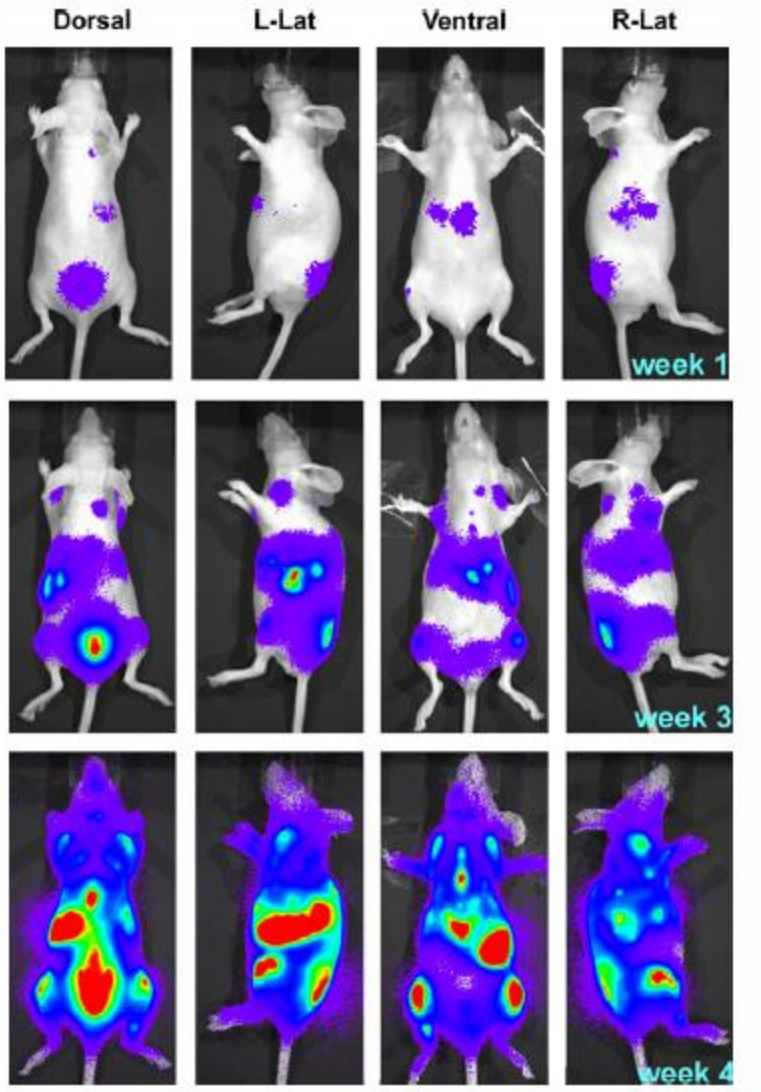

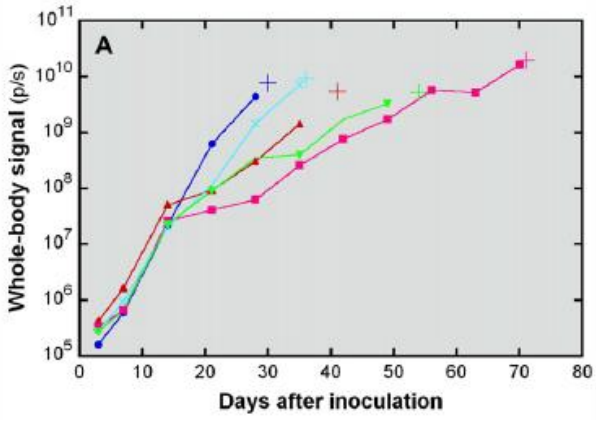

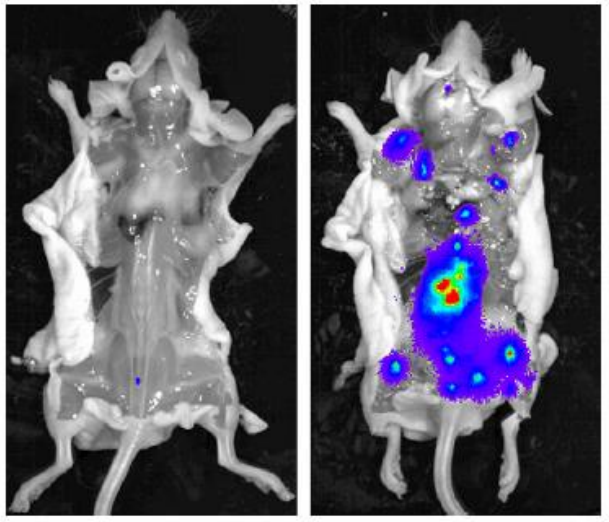

Inoue et al., 2007

Bioluminescence Imaging

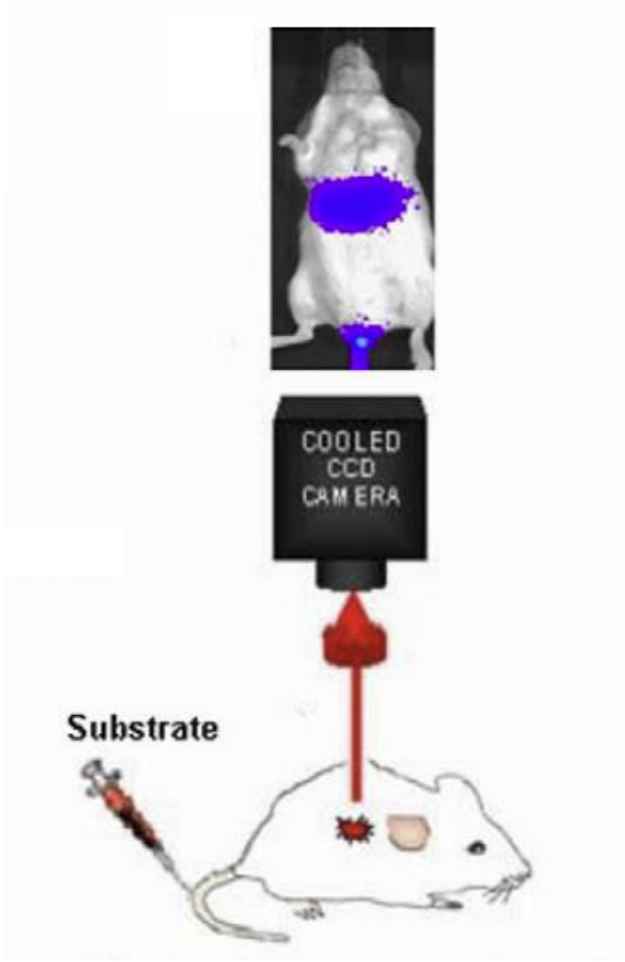

Caveats

Serum stability of luciferases
(several mutations have been screened to identify luciferases with high light output and stability)

Route of administration influences substrate availability and therefore the signal detected

Timing of administration is critical for longitudinal experiments

Sites – heart can obscure signal from the liver

Gheysens and Mottaghy, 2009

Bioluminescence Imaging

I. V. S.C. I.P.

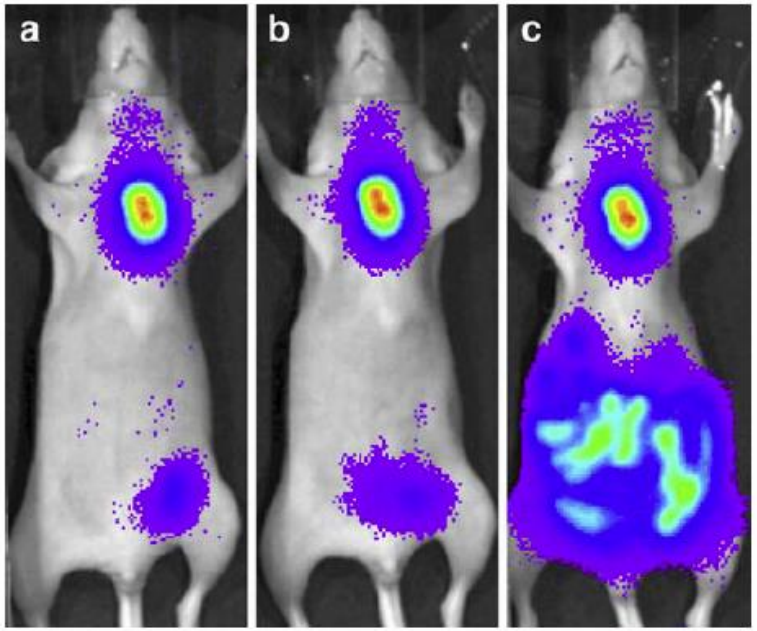

Fig. 4 Ventral BLI images obtained after IV (a), SC (b) or IP (c) injection of D-luciferin. The mouse was inoculated with HCT116-Luc cells subcutaneously near the upper border of the sternum and intraperitoneally. The pseudocolour luminescent images (blue, green, yellow, and red from least to most intense) are overlaid on the grey-scale photographic images. The upper level of the colour scale was adjusted for each panel so as to similarly display the SC tumour, and the lower level was set at 0.5% of the upper level

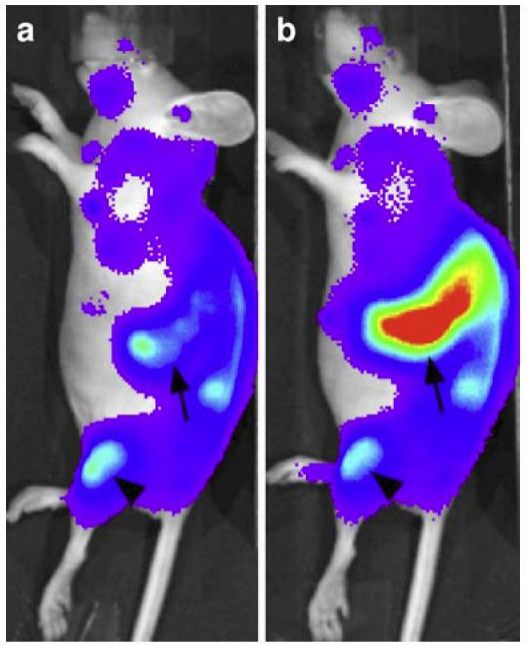

Fig. 6 Left-lateral BLI images obtained after SC (a) or IP (b) injection of D-luciferin. The mouse was inoculated intravenously with Ba/F3-Luc/Wt cells. BLI signals suggestive of cell proliferation in the spleen (*arrows*) and bone marrow, including the left knee (*arrowheads*) are observed, and the splenic signal is more evident after IP injection. The upper level of the colour scale was adjusted for each panel so as to similarly display the bone marrow lesions, and the lower level was set at 2% of the upper level

Route of administration, location of tumor influences BLI signal

Inoue et al., 2009

Bioluminescence Imaging

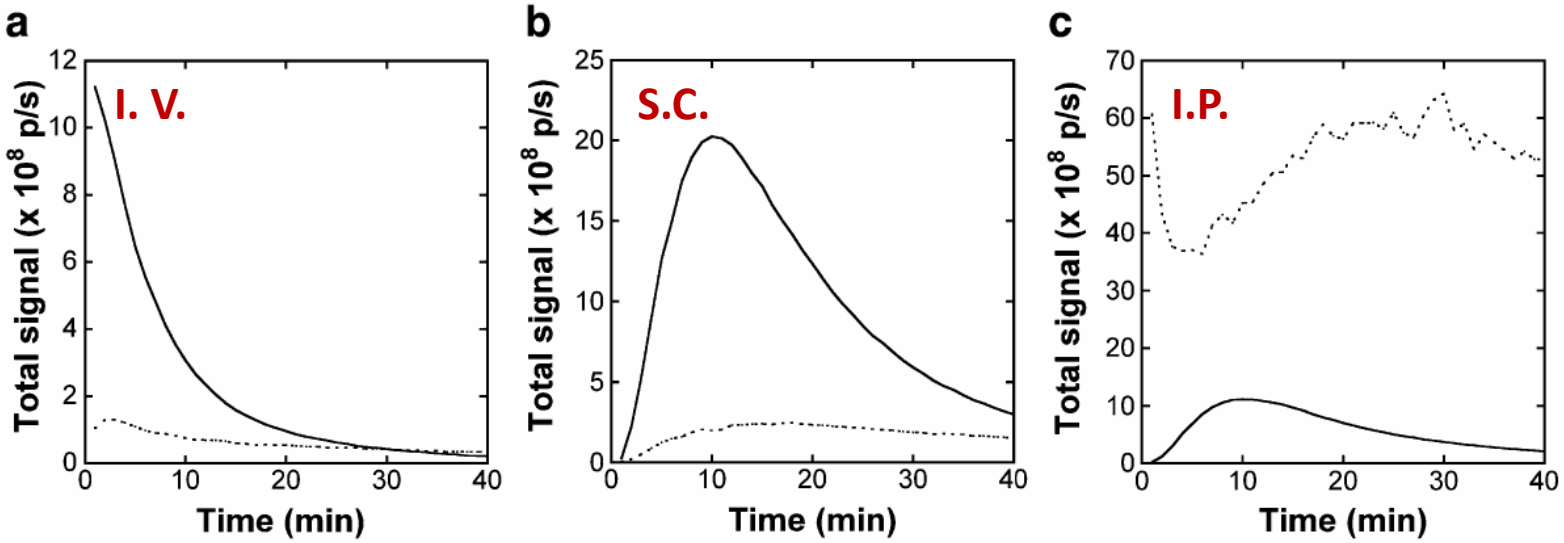

Fig. 5 Examples of the time–intensity curves determined after IV (**a**), SC (**b**) or IP (**c**) injection of D-luciferin in a mouse bearing both SC and IP tumours (the same mouse as that presented in Fig. 4). The *solid* and *broken lines* are curves for the SC and IP tumours, respectively

In SC tumors, the peak time was slightly shorter and the peak signal was greater using SC injection than using IP injection.

Signals from IP tumors relative to those from SC tumors were much greater using IP injection than using IV or SC injection.

Inoue et al., 2009

Fluorescence Imaging

‘Fluorescence’ – introduced by Sir George Gabriel Stokes (Physicist and Professor of Mathematics)

Stokes used a prism to disperse the solar spectrum and illuminate a solution of quinine. He noted that there was no effect until the solution was placed in the ultraviolet region of the spectrum.

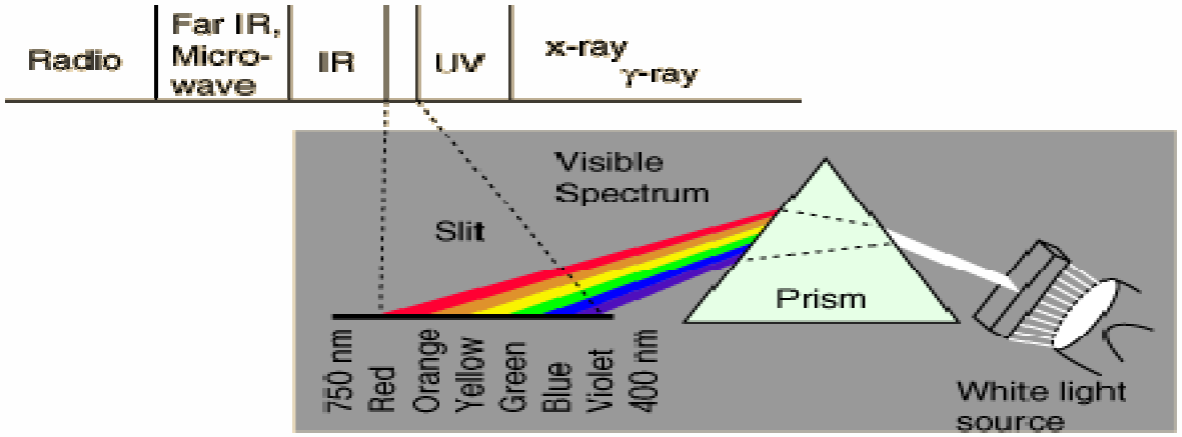

www.fluorescence-foundation.org

Re-emission (fluorescence) is of longer wavelength photons (lower frequency or energy) by a molecule that has absorbed photons of shorter wavelengths (higher frequency or energy) – This displacement is **the Stokes Shift**

Fluorescence Imaging

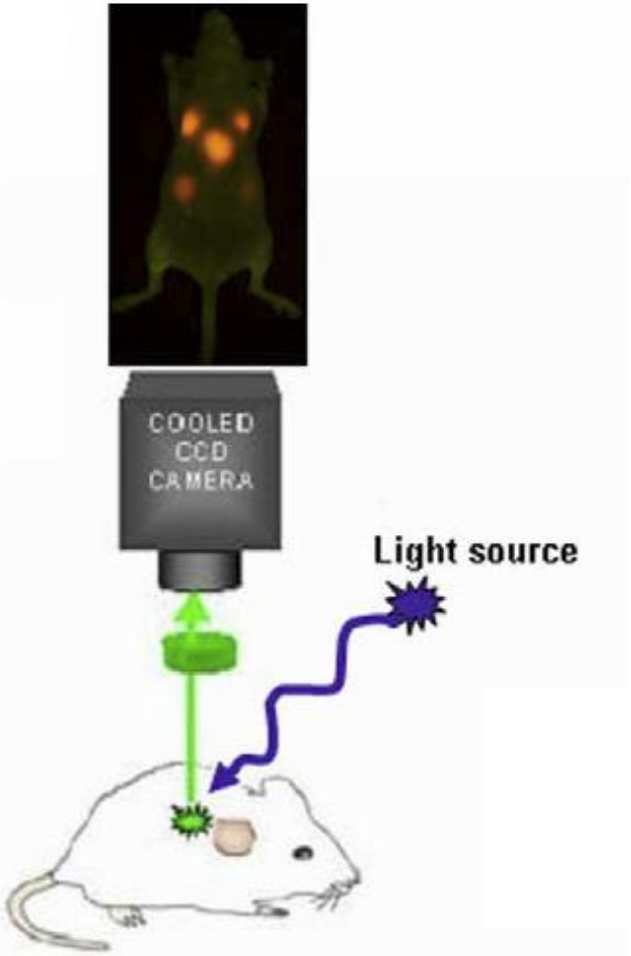

Involves excitation of an injected fluorophore (dye)

The fluorophore returns to the ground state through different pathways

Fluorescent light is emitted upon spontaneous emission of a photon

Light emission is detected by a CCD camera using the appropriate emission filters

Gheysens and Mottaghy, 2009

Fluorescence Imaging

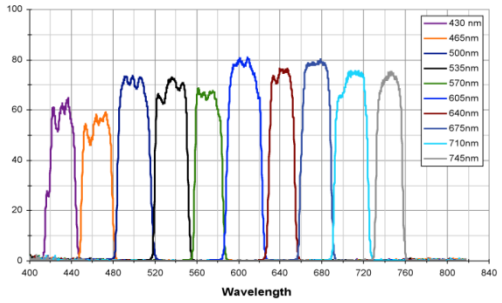

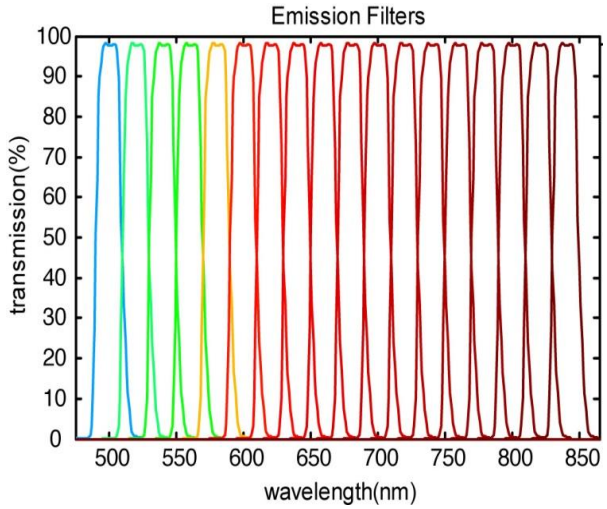

Limitations

Background autofluorescence

Need to distinguish signal from endogenous molecules (Hb; 400-600) vs. exogenous agents.

Often overlapping absorption spectra

Solutions

Near-infrared fluorophores (minimal autofluorescence)

Multispectral imaging – enables simultaneous imaging of multiple fluorophores (multiplexing)

Kevin Francis, PhD – Perkin Elmer

Gheysens and Mottaghy, 2009

Fluorescence Microscopy

Fluorescence imaging of tumor vessels

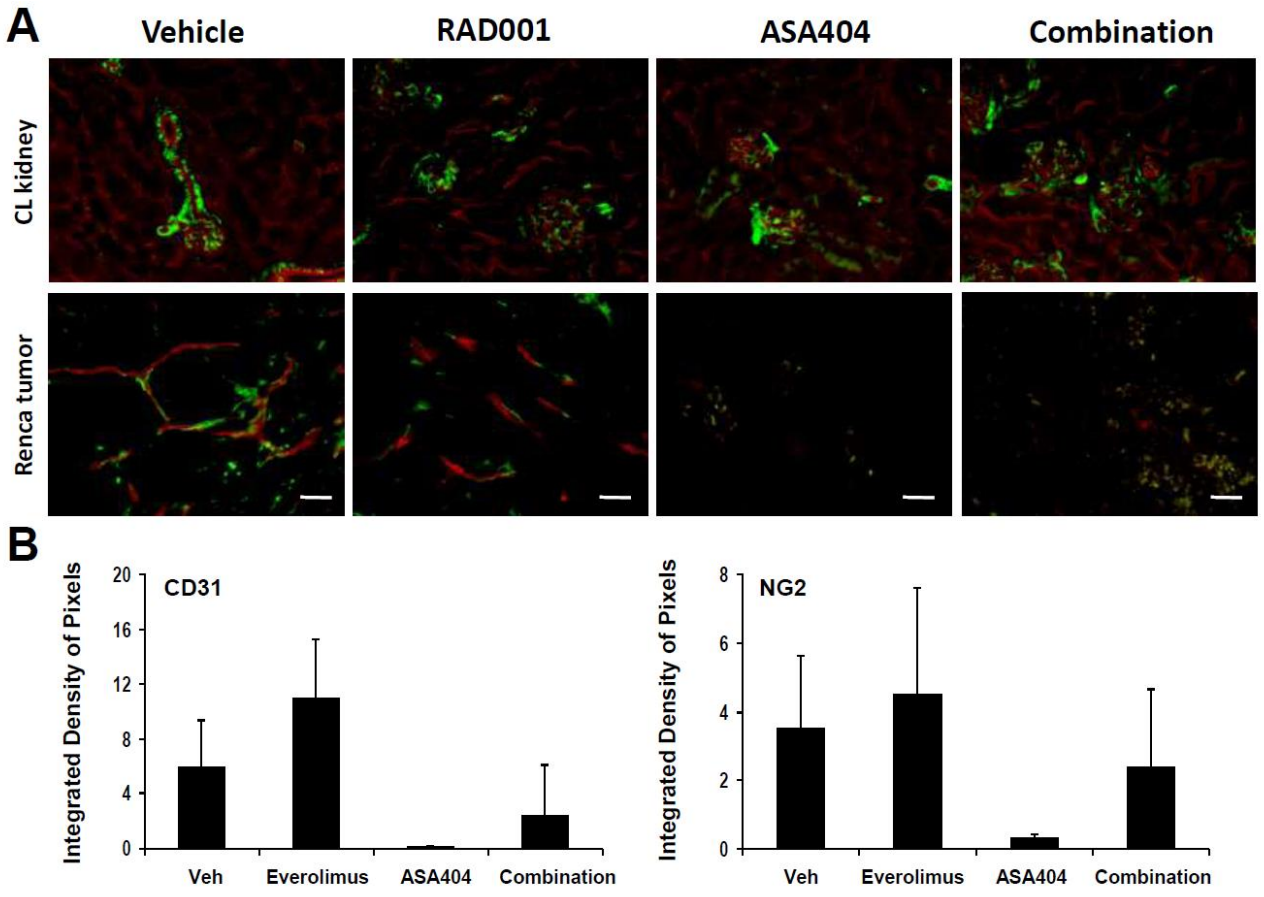

Quantification of pixels density (in tissue sections stained with two fluorescent dyes)

Ellis et al., Mol Cancer Therapeutics 2012

Fluorescence Microscopy

Fluorescence imaging of drug delivery

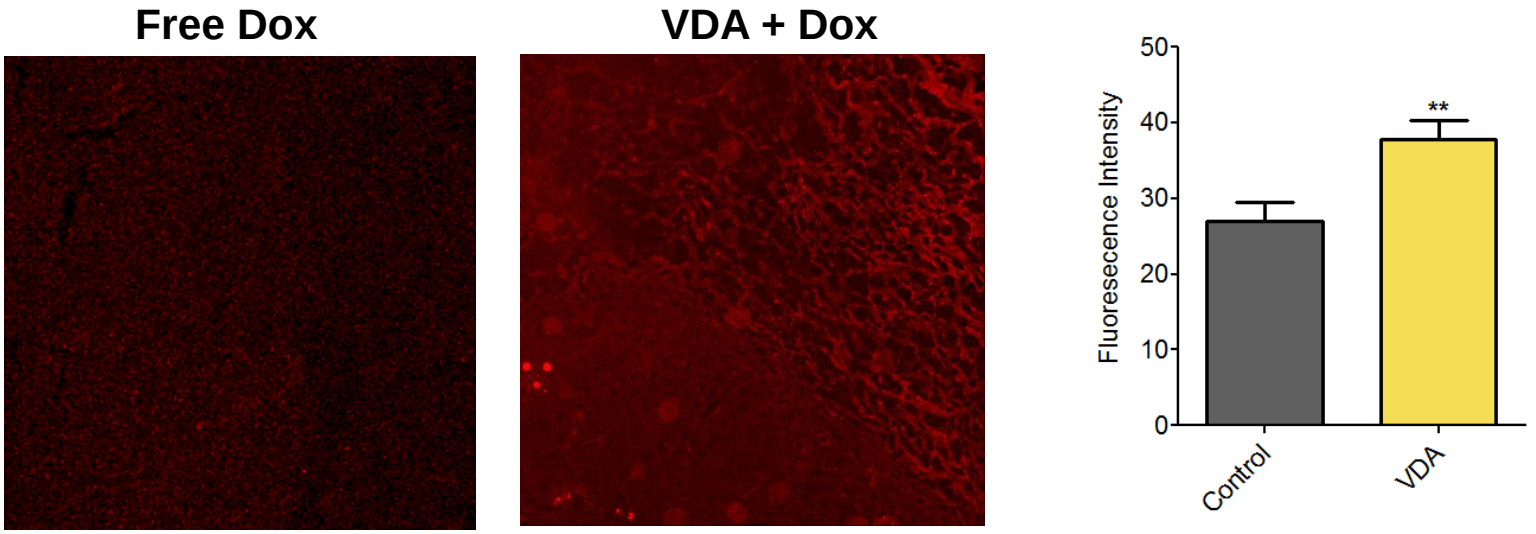

Exploits the autofluorescence properties of the drug Doxorubicin (Dox)

Quantification of total fluorescence intensity in specimens exposed to different therapies

Folaron et al., 2013 Oral Oncology

Fluorescence Microscopy

Vascular maturation and Drug delivery

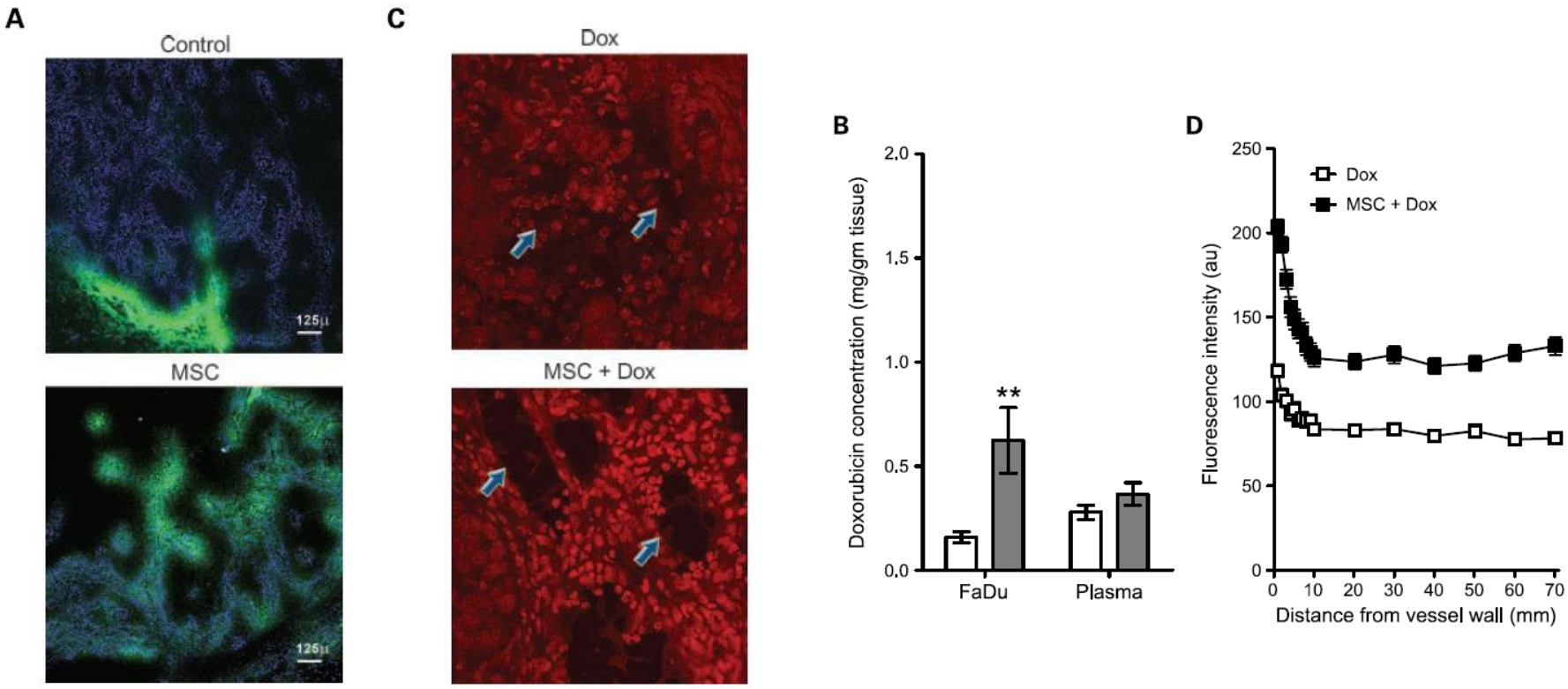

Fluorescence microscopy of tumor vessels (A) and drug (C) using two different dyes varying absorption and emission spectra

Folaron et al., 2013 Oral Oncology

Multispectral Fluorescence Imaging

Spectral unmixing

- Images acquired at multiple wavelengths
- Pixels mapped and grouped based on peak
- Pick emission filters centered around component peaks

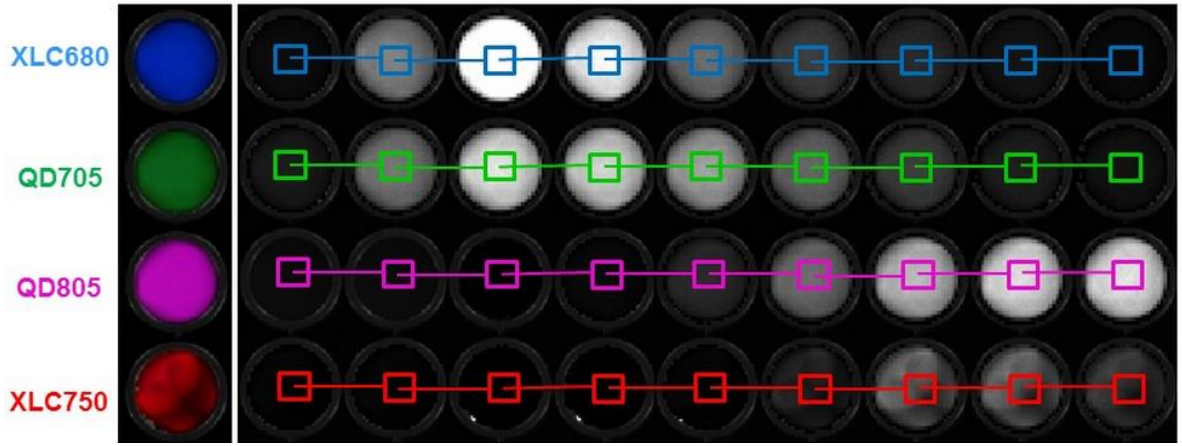

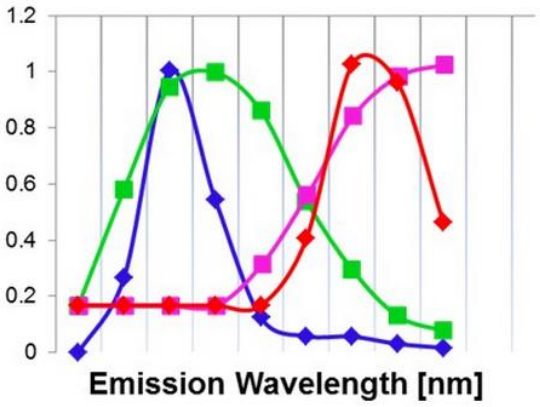

In vivo Fluorescence Imaging

GFP/RFP

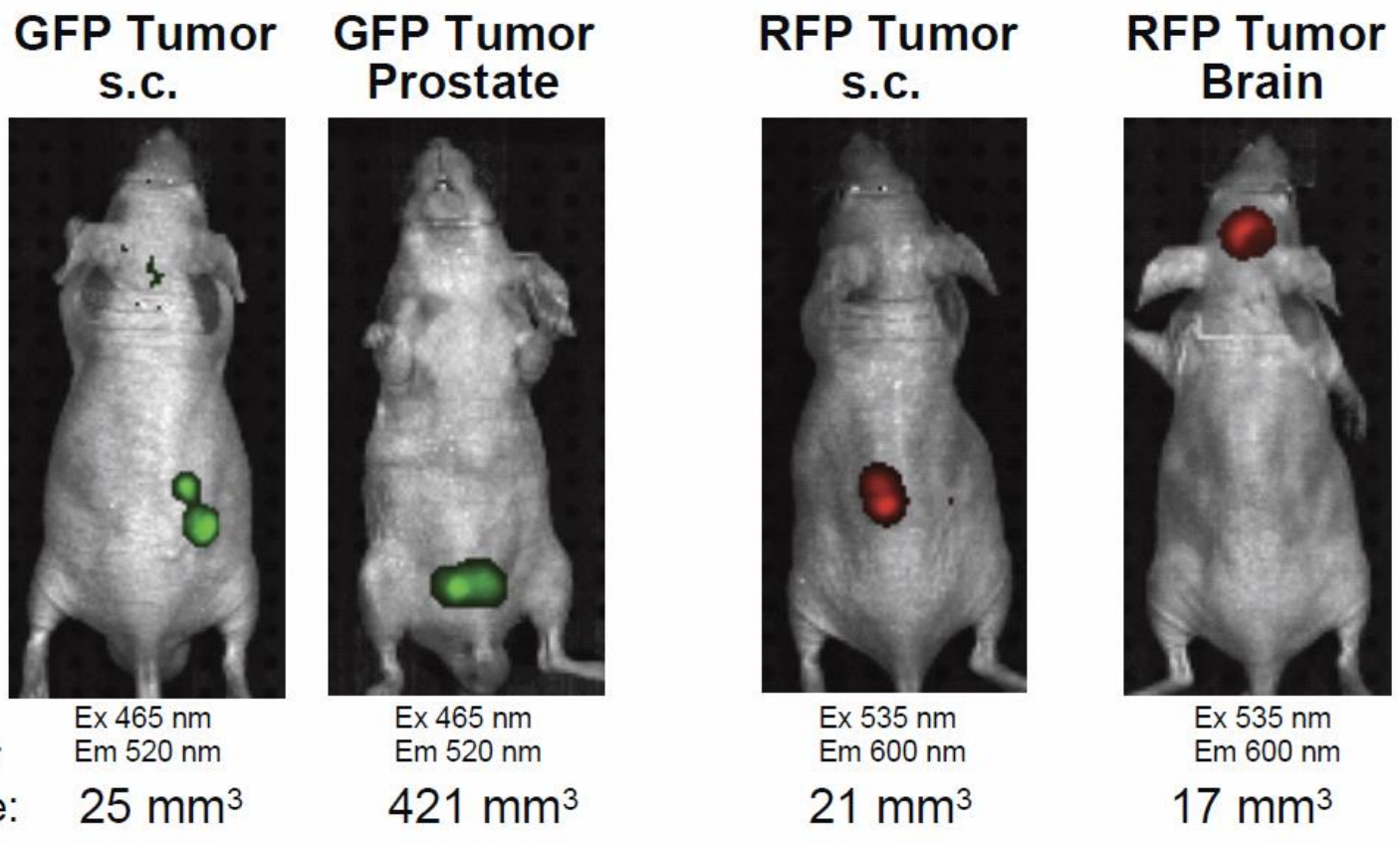

Caliper LifeSciences

Zhang et al., FLI-BLI-poster

Molecular Imaging Reporter Systems

Fluorescent Imaging Agents and Tags

PerkinElmer
For the Better

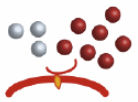

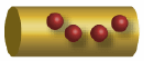

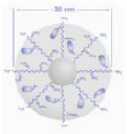

Activatable	MMPSense™ 680 MMPSense™ 750 FAST ProSense® 680/750 ProSense® 750 FAST™ ProSense® Control 680/750 Cat K 680 FAST™ Cat B 680/750 FAST™ Neutrophil Elastase 680 FAST™ ReninSense 680 FAST™
Targeted	OsteoSense® 680/750/800 IntegriSense™ 680/750 Annexin-Vivo 750
Vascular	GastroeSense™ 750 Genhance™ 680/750 (1 mg) Genhance™ 680/750 (5 mg) Superhance™ 680 AngioSense®-IVM 680/750 AngioSense® 680/750 AngioSPARK® 680/750
Labeling	VivoTag® 645/680/800 (1 mg) VivoTag® 645/680/800 (5 mg) VivoTag®-S 680/750 (1 mg) VivoTag®-S 680/750 (5 mg) VivoTag® 680/800 XL (1 mg) VivoTag® 680/800 XL (5 mg) AminoSPARK® 680/750

Enabling translational biomarker readouts of disease progression and therapeutic response

- Arthritis
- Bone Remodeling
- Cardiology
- CNS Disorders
- Fibrosis
- Infectious Disease
- Inflammation
- Metabolic Disease
- NIR Labeled Dyes & Agents
- Oncology
- Pulmonary Disease
- Vascularity
- Vascular Biology

4

Kevin Francis, PhD – Perkin Elmer

Multispectral Fluorescence Imaging

Multiplex imaging of Quantum Dots

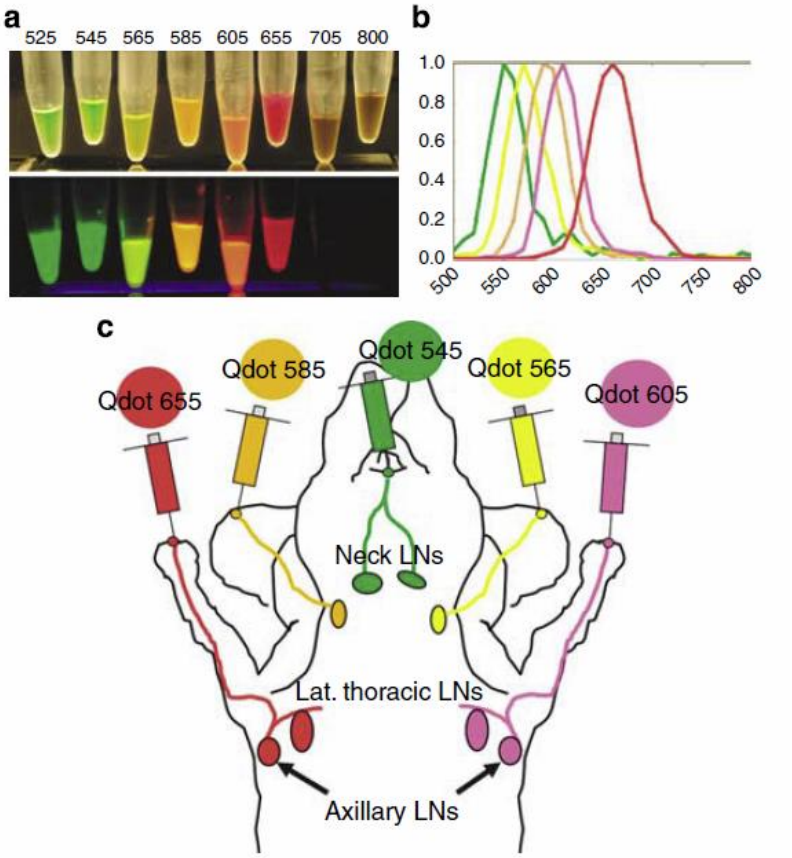

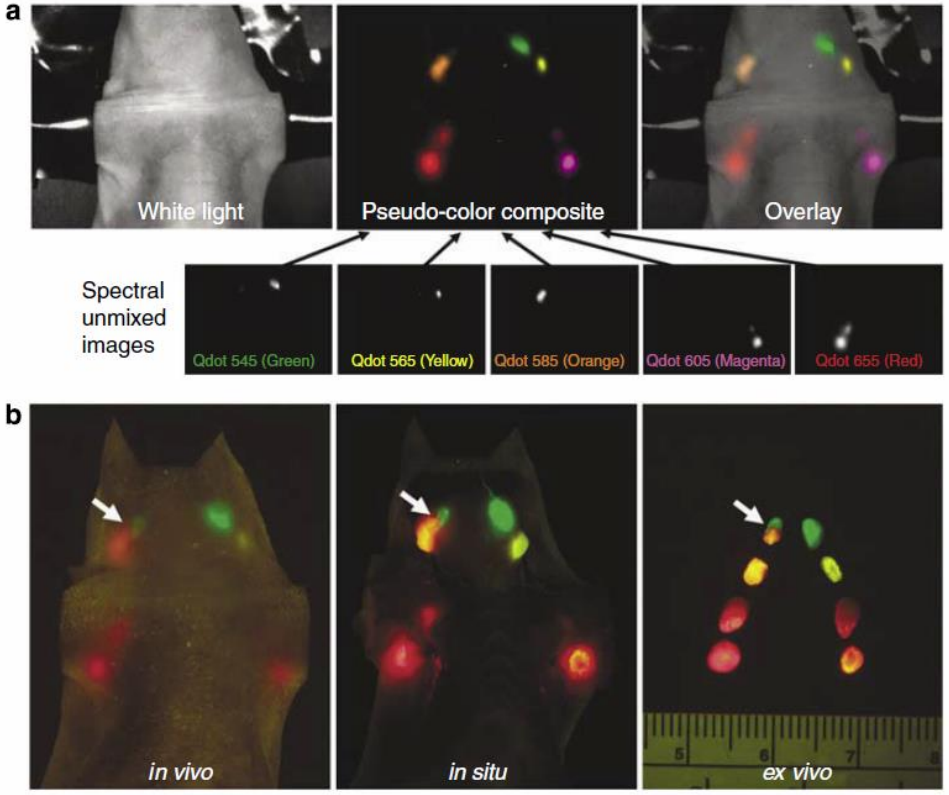

Kosaka et al., 2009

Combined FI + BLI

Combined Imaging of Angiogenesis and Metabolism

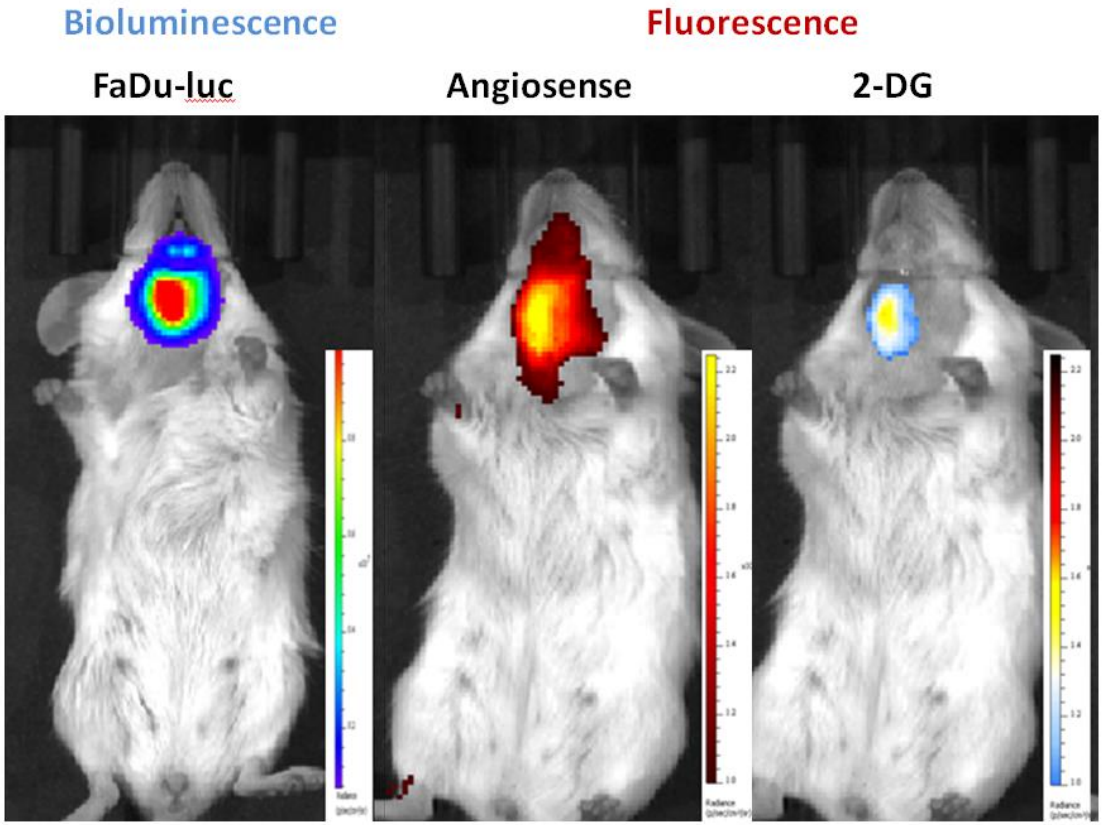

Seshadri lab, unpublished data

Optical Imaging of Tumor Response to Rx

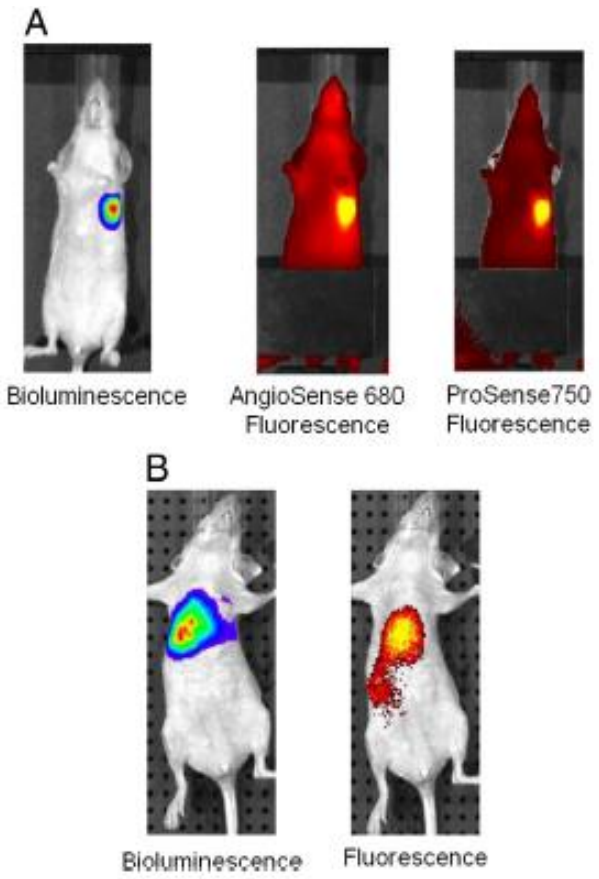

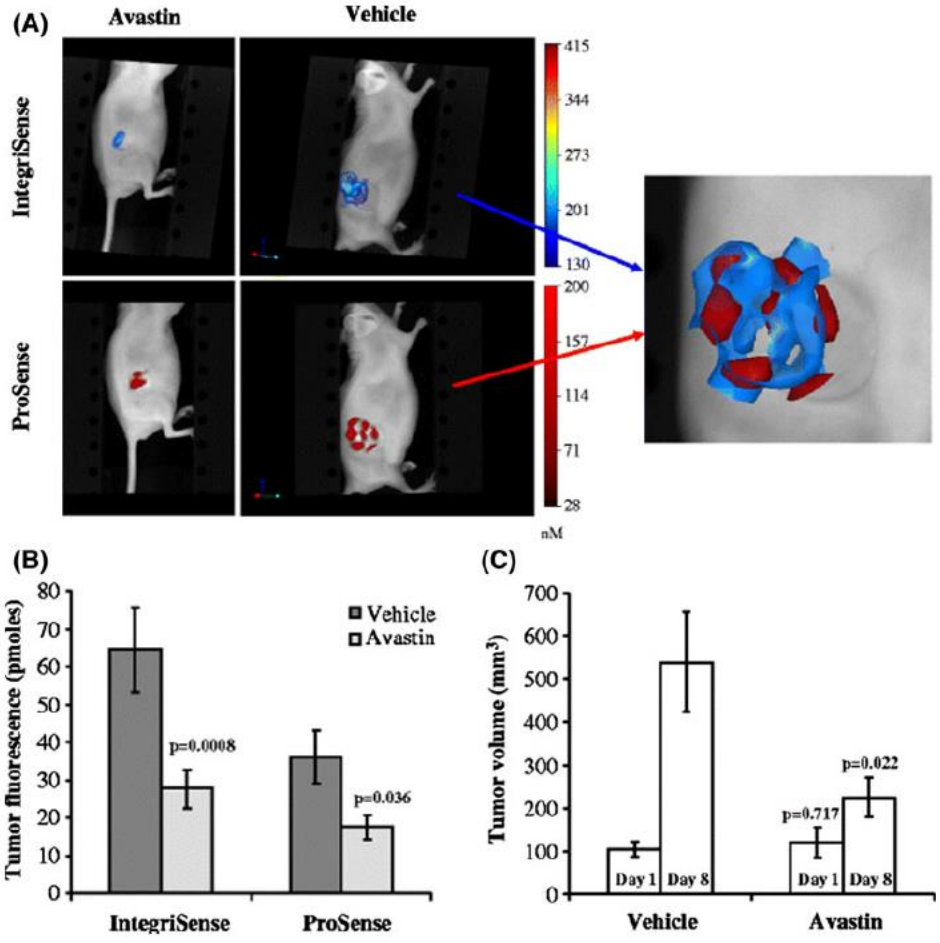

Kossodo et al., Perkin Elmer Corporation

Optical Imaging-guided surgery

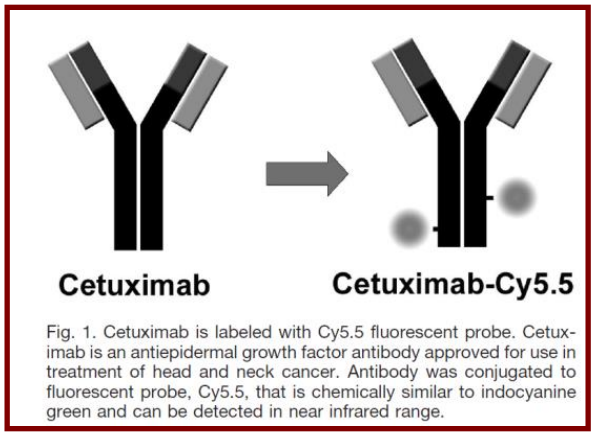

Fig. 1. Cetuximab is labeled with Cy5.5 fluorescent probe. Cetuximab is an antiepidermal growth factor antibody approved for use in treatment of head and neck cancer. Antibody was conjugated to fluorescent probe, Cy5.5, that is chemically similar to indocyanine green and can be detected in near infrared range.

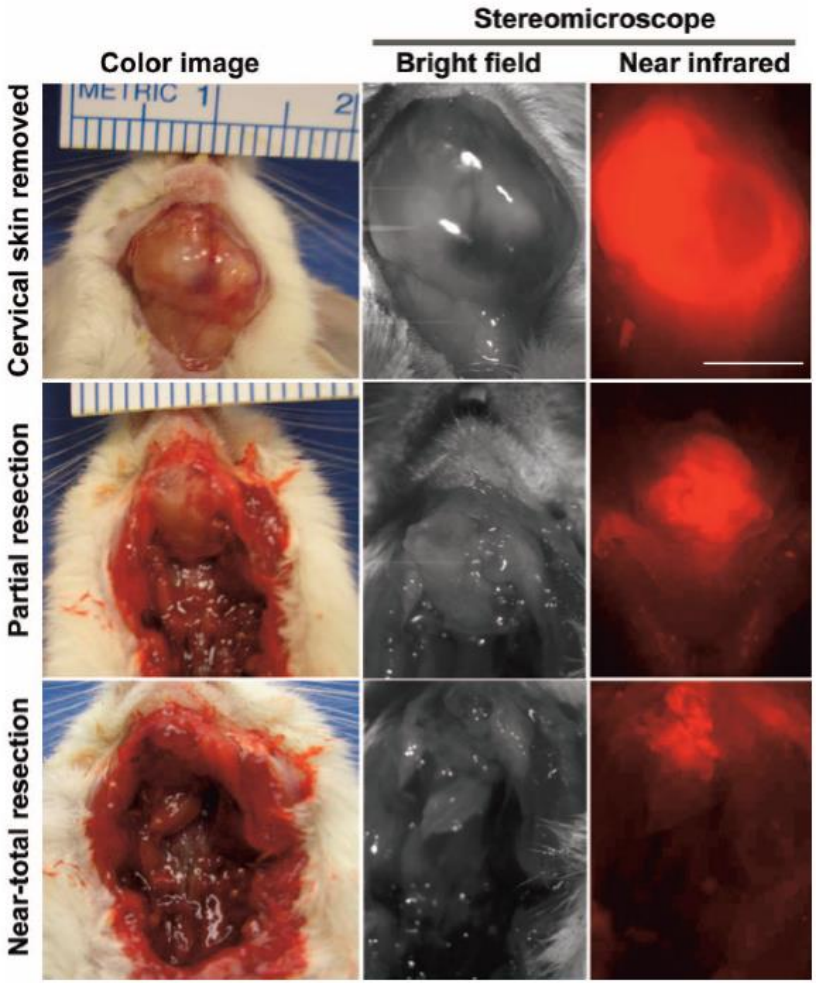

Rosenthal et al., 2006

Optical Imaging-guided surgery

Safety and Tumor-specificity of Cetuximab-IRDye800 for Surgical Navigation in Head and Neck Cancer

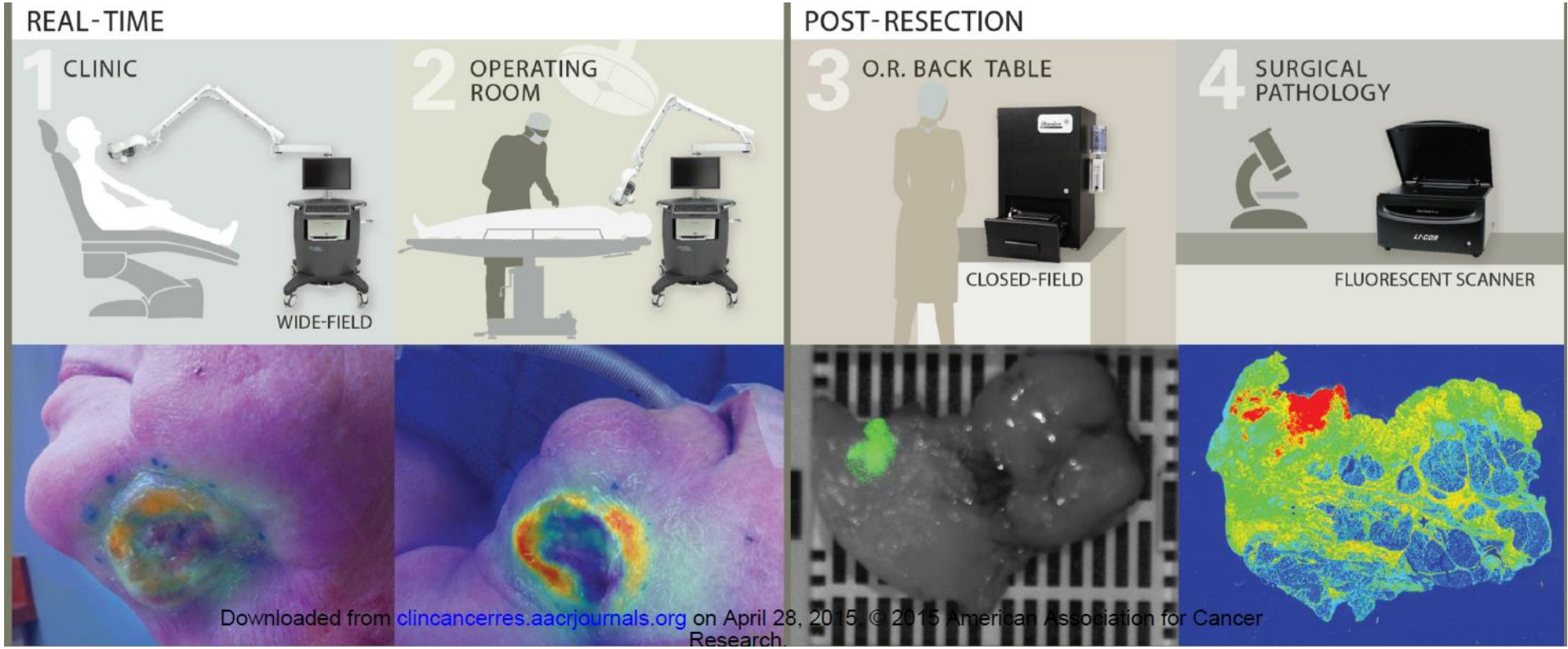

Rosenthal et al., Clin Cancer Res. 2015

Optical Imaging-guided surgery

Intraoperative

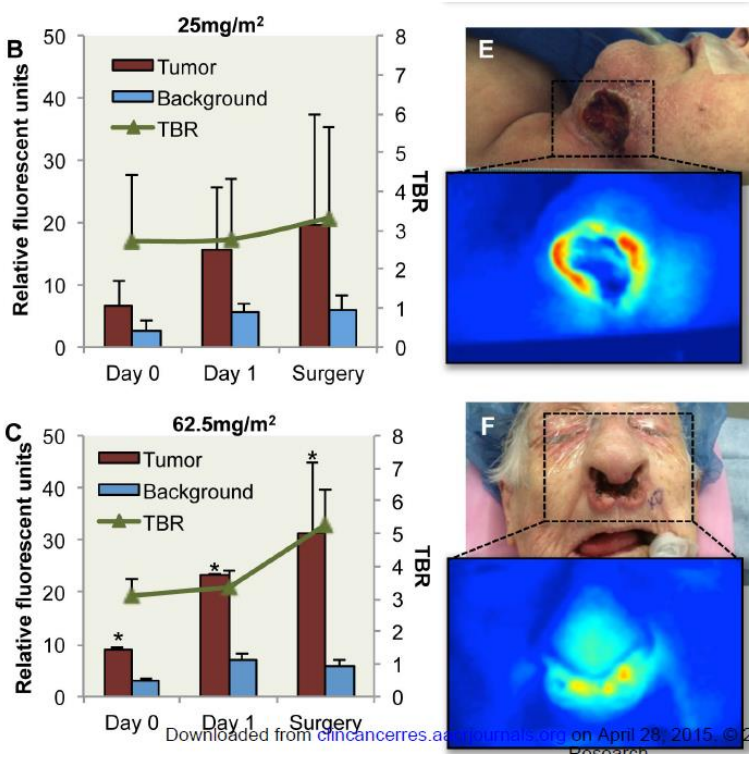

Ex-vivo

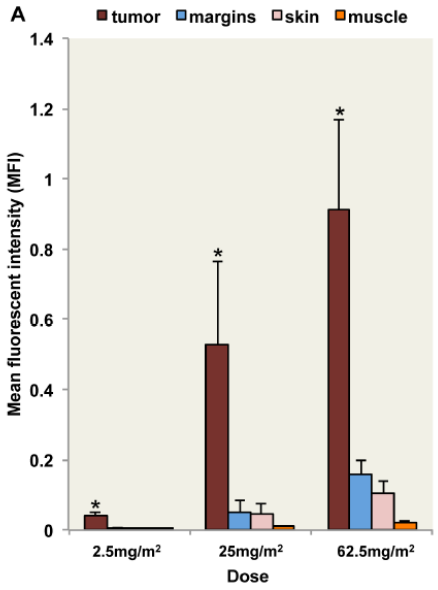

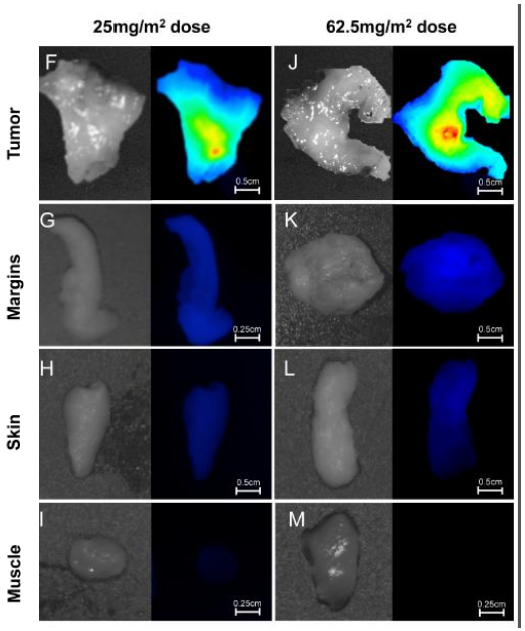

"Fluorescence imaging with an intraoperative, wide-field device successfully differentiated tumor from normal tissue during resection with an average tumor-to-background ratio of 5.2 in the highest dose range".

Rosenthal et al., Clin Cancer Res. 2015

Ultrasound

Ultrasound 101

- Ultrasound (US) – refers to oscillating sound pressure waves greater than the limit detectable by the human ear [20-20,000 cycles/sec (Hz)]
- Bats can detect beyond 100 kHz (echolocation)
- SONAR (Sound navigation and ranging)

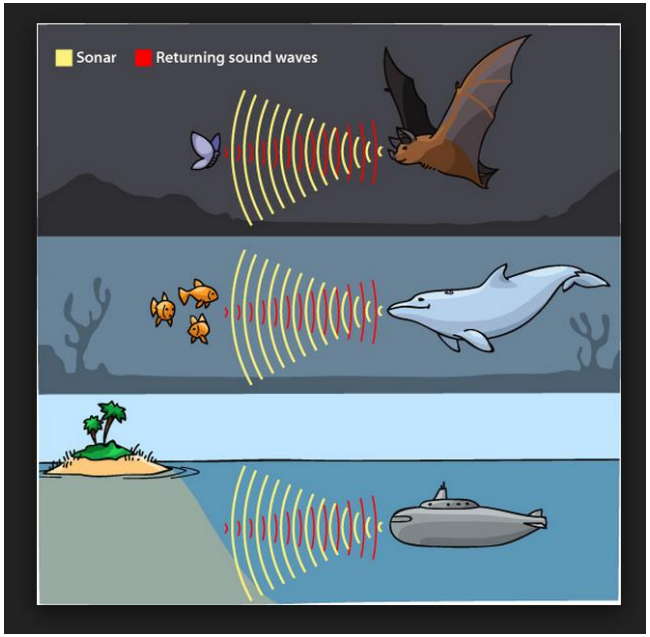

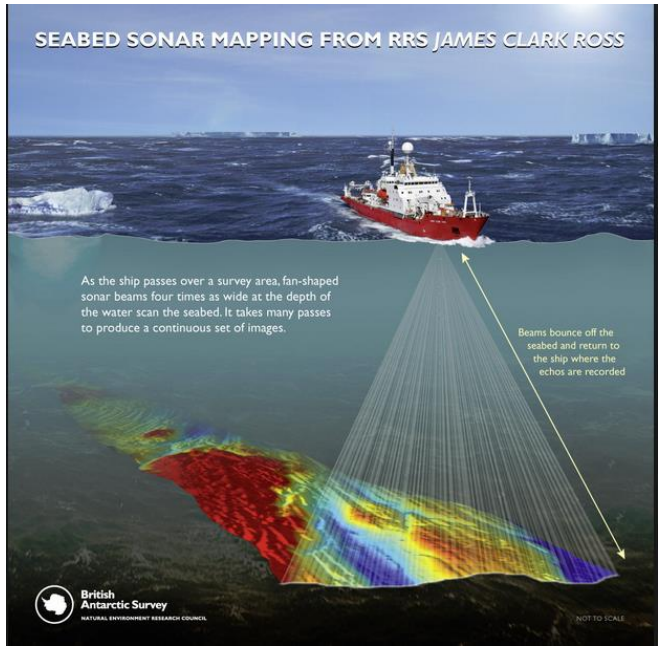

British Antarctic Survey

Ultrasound Imaging

- US imaging utilizes interaction of sound waves with living tissue
- Non-invasive tool that can provide structural and functional information
- Variety of medical applications

Source: Terese Winslow

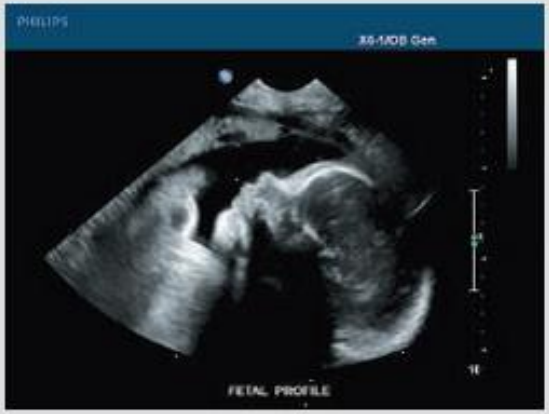

Cross-section ultrasound image of a fetus
Source: Courtesy of Phillips Health Care-iu22xMATRIX system

NIH National Institute of Biomedical Imaging and Bioengineering
www.nibib.nih.gov

Coatney, ILAR 2001

Ultrasound Imaging Systems

Vevo 2100 Micro-Ultrasound Imaging System

Siemens.com

Basic Components

1. CPU
2. Transducer (transmits and receives signal)
3. Image storage unit

VisualSonics Corporation (FUJIFILM)

Ultrasound Imaging Systems

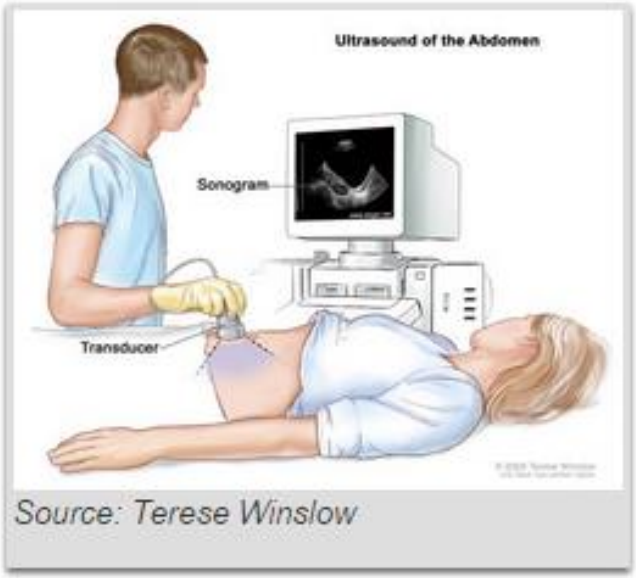

Source: Terese Winslow

The transducer produces the US beam as a slice
Beam profile (~1 mm thick)

User controls displayed depth

Direction of the beam is controlled by the operator (aimed at the target)

The vibrational energy of the mechanical oscillations (transducer) is directed into the scanned object and swept back and forth
The reflected signal from tissue interfaces (echoes) are detected by the transducer and transformed into electrical signals that are processed by a receiver to create an image.
The return of an echo depends mainly on the type of scanned object/tissue and penetration depth.

Biophysical Basis for US Imaging

Transmission of sound waves through a tissue is related to its acoustic impedance of each tissue (product of transmission velocity and tissue density).

However, transmission velocity in most soft tissues and blood is relatively uniform (1540 m/s; Merritt, 1998).

Therefore, the major determinant of acoustic impedance is tissue density.

Differences in tissue densities causes differences in the sound waves reflected and received by the transducer

Biophysical Basis for US Imaging

Tissue homogeneity also interaction of sound waves

Bone (4080 m/s) --- Tissue (1540 m/s) – Gas (330m/s)

The greater the acoustic mismatch or difference in tissue densities, the more sound waves are reflected and returned to the transducer.

Largest acoustic impedance mismatch -> Bone-Gas (majority of sound waves to be reflected – decreases penetration/causes artifacts)

Carina Li, http://www.usgraweb.hk

Coatney, ILAR 2001

Spatial Resolution in US

- Diagnostic US (2-15 MHz)

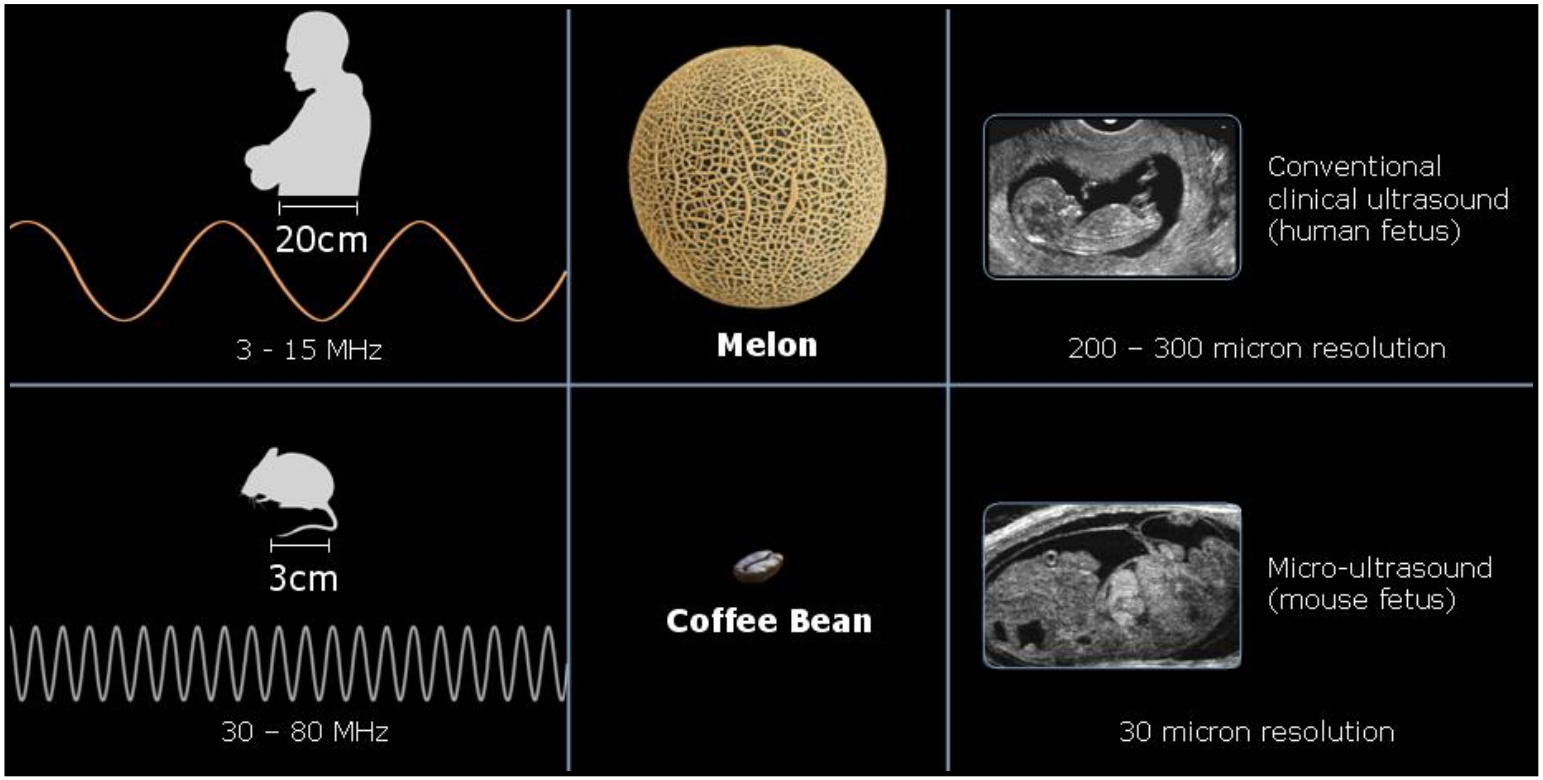

VisualSonics Corporation (FUJIFILM)

Biophysical Basis for US Imaging

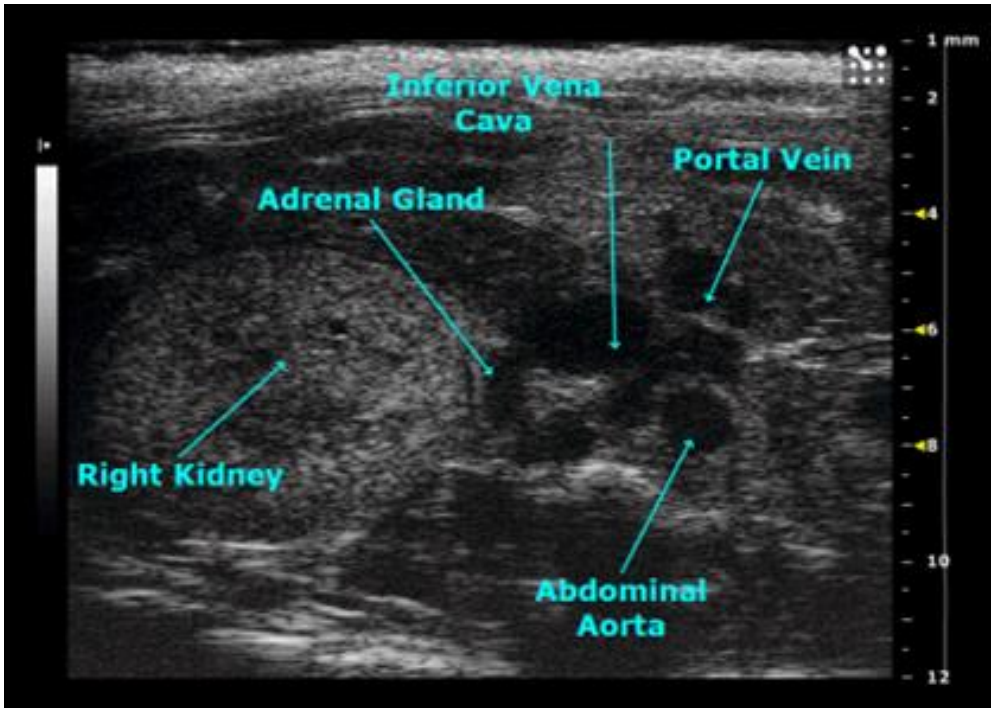

Strong reflections (hyperintense) – brighter (bone/diaphragm)

No reflection – dark/black dots (fluid/blood)

Ultrasound imaging is best suited for soft tissue imaging

Coatney, ILAR 2001

Applications of US Imaging

Anatomic Imaging

- Tumor volume
- Image-guided interventions

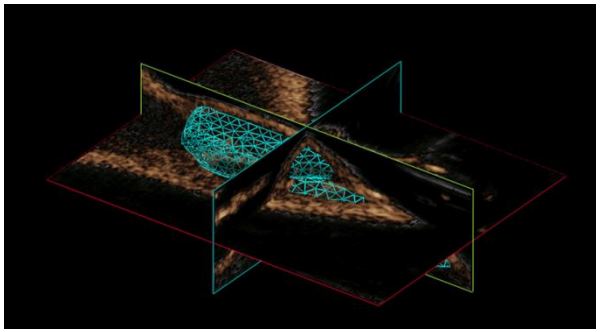

Functional Imaging

- Tumor vascularity
- Perfusion/oxygenation

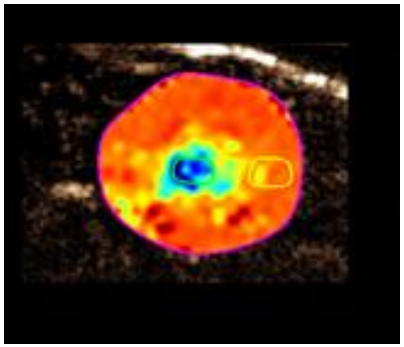

Molecular Imaging

- Targeted contrast agents
- Biomarkers of response

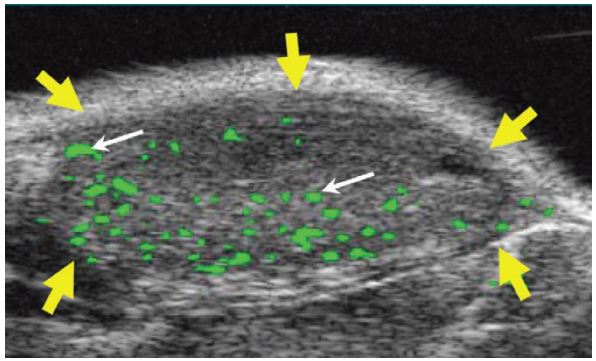

VisualSonics Corporation (FUJIFILM)

3D US of Prostate Cancer

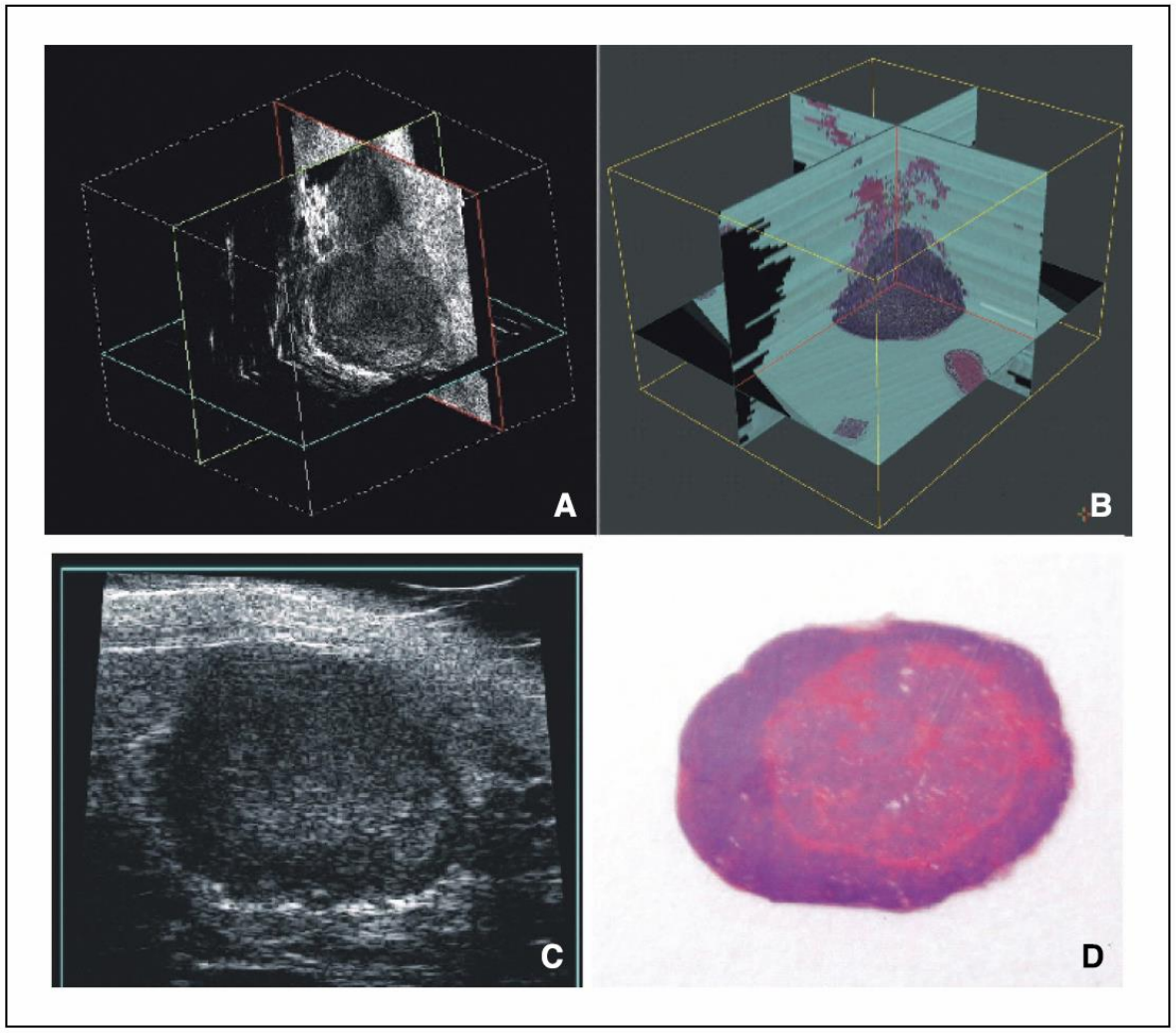

Figure 1. Three-dimensional ultrasound image of a genetically engineered mouse prostate cancer tumor confirmed by three-dimensionally reconstructed serial histology slides. *A,* three-dimensional image of a ventral prostate tumor mass displayed using three orthogonal planes through the ultrasound image volume. A movie showing user manipulation of the three-dimensional ultrasound image is available as Supplementary Data from the Journal Web site. *B,* orthogonal planes through a three-dimensional reconstruction of the serial H&E-stained histology slides from the same tumor. *C,* transverse two-dimensional ultrasound image of the same ventral prostate tumor. The tumor appears as a hypoechoic border surrounding a brighter central core with heterogeneous image texture. *D,* corresponding two-dimensional histology slide. H&E staining, ×4.

Wirtzfeld et al, Cancer Res 2005

Contrast-enhanced US (CE-US)

Microbubbles (Ultrasound contrast agents)

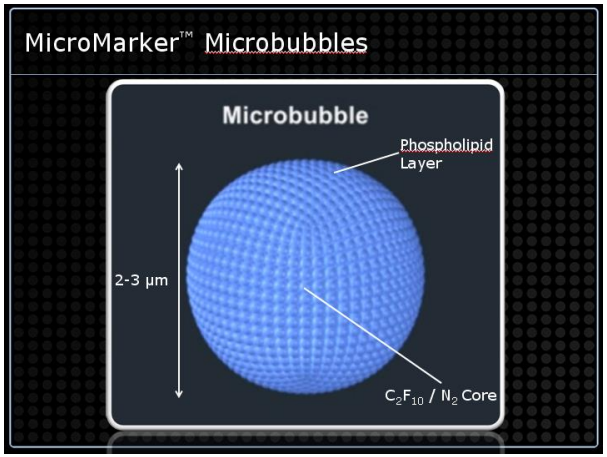

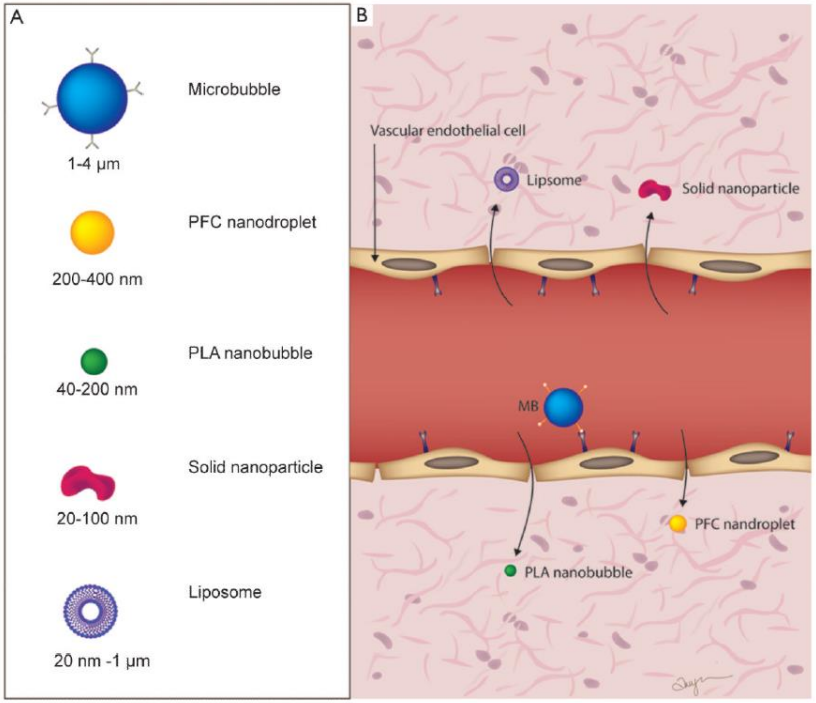

Lipid-shelled microspheres ~2.5 µm in diameter containing perfluoropentane gas.

Provide far greater contrast than RBC (imaging vasculature)

VisualSonics Corporation (FUJIFILM)

Kaneko and Willmann, 2011

CE-US

Non-linear contrast enhancement in the renal cortex and medulla

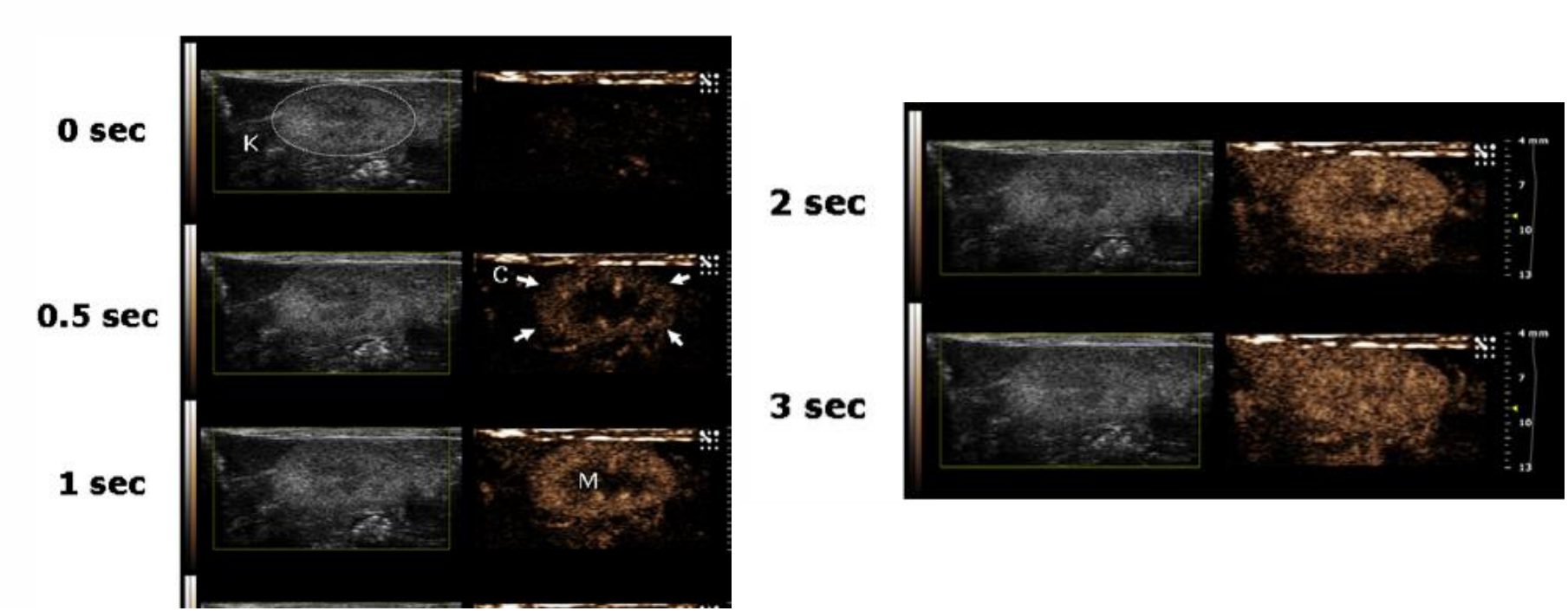

Needles et al., 2010

US imaging of Angiogenesis

VEGFR2 targeted microbubbles

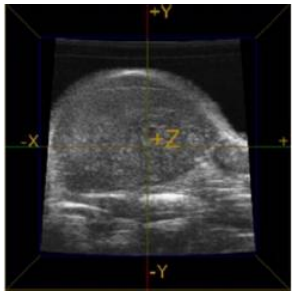

Zagorchev, EJR 2009

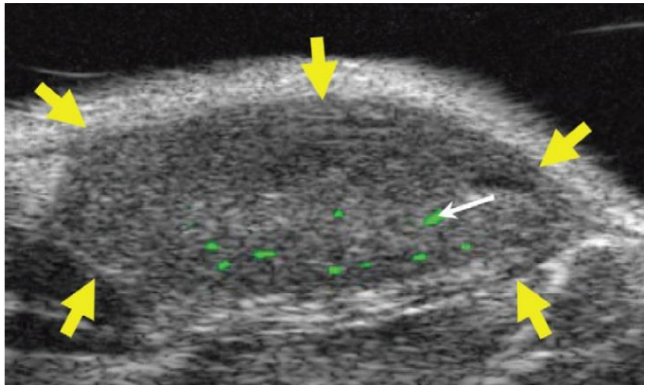

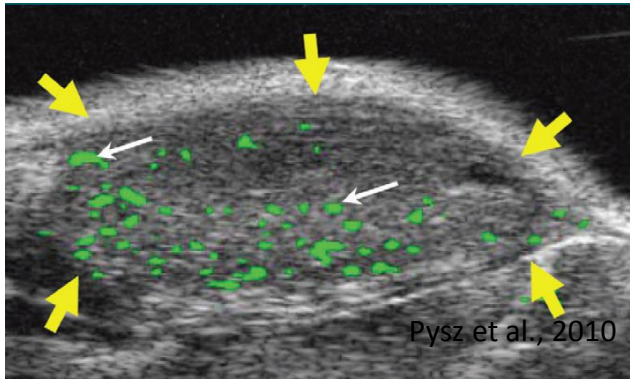

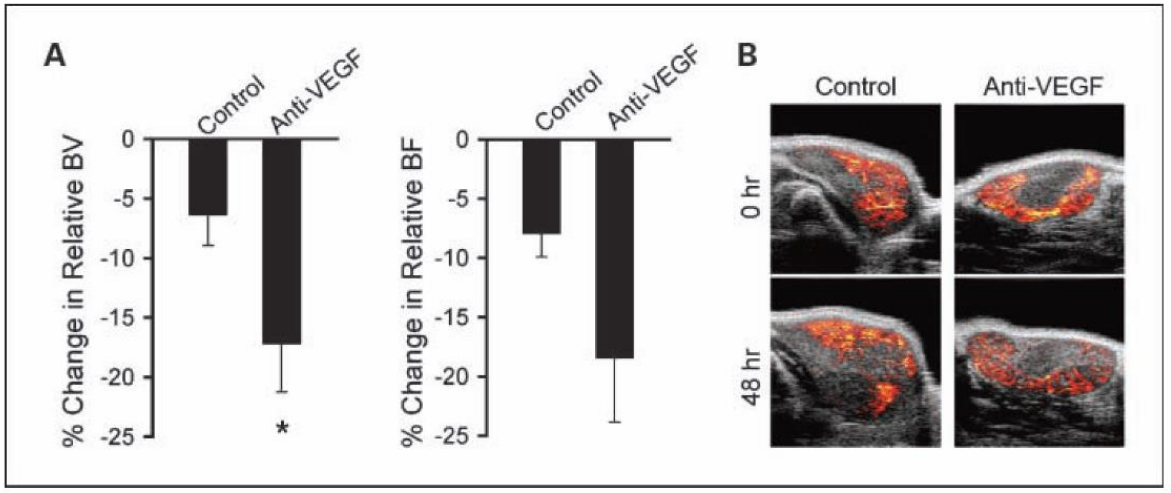

Fig. 2. *In vivo* evidence for reduction in rBV following G6-31. *A,* percentage change in rBV and rBF in control and treated groups after 48 h of anti-VEGF treatment. *B,* representative ultrasound perfusion blood volume maps for each treatment group pretreatment and at 48 h posttreatment.

Connor et al., CCR 2009

Parametric Imaging (CE-US)

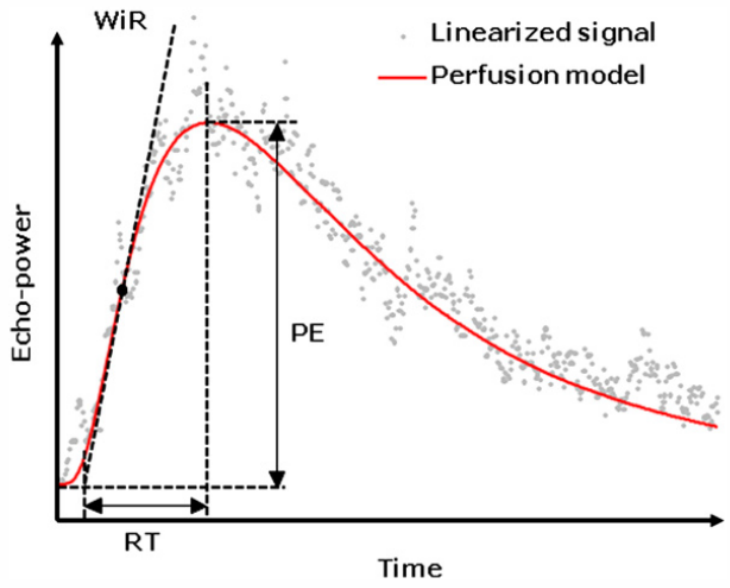

Fig. 3. Schematic representation of a bolus time-intensity curve (TIC). The linearized signal of echo-power is illustrated with grey dots, and the fitted perfusion model is shown in red. Parameters associated with the bolus model function include: peak enhancement (PE), wash-in rate (WiR) and rise time (RT).

Peak Enhancement (PE)
Difference between the maximum amplitude in the curve and the baseline (or level and is proportional to the concentration of the UCA dose (and thus indicative of relative blood volume as well).

Wash-in rate (WiR)
Maximum slope of the fitted bolus function and is proportional, for a given UCA dose, to local blood flow rate.

Rise time (RT)
Represents the time it takes to go from baseline to PE.

Needles et al., 2010

Parametric Imaging (CE-US)

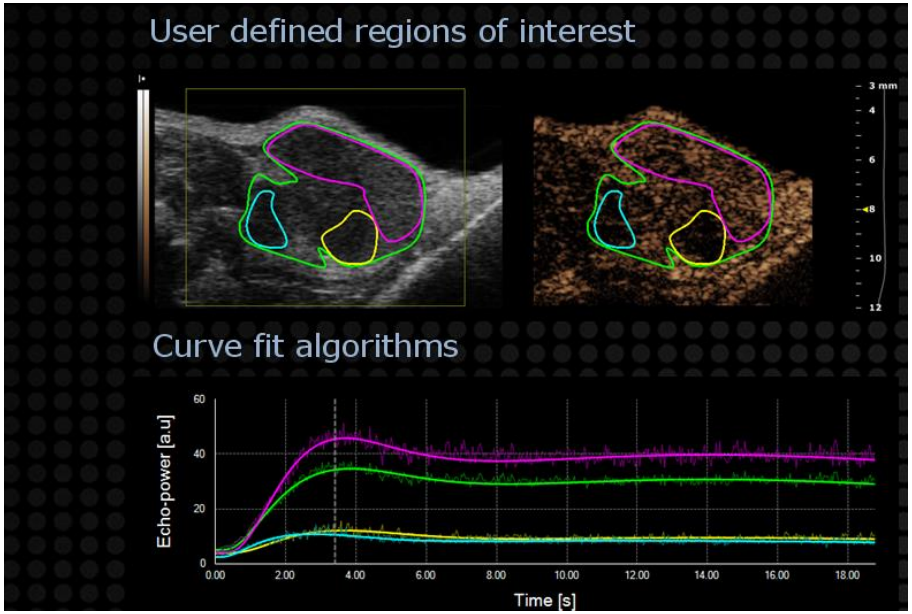

Parametric image gives the spatial distribution of a particular parameter

Sub-region analysis enables visualization of spatial heterogeneity in vascularity

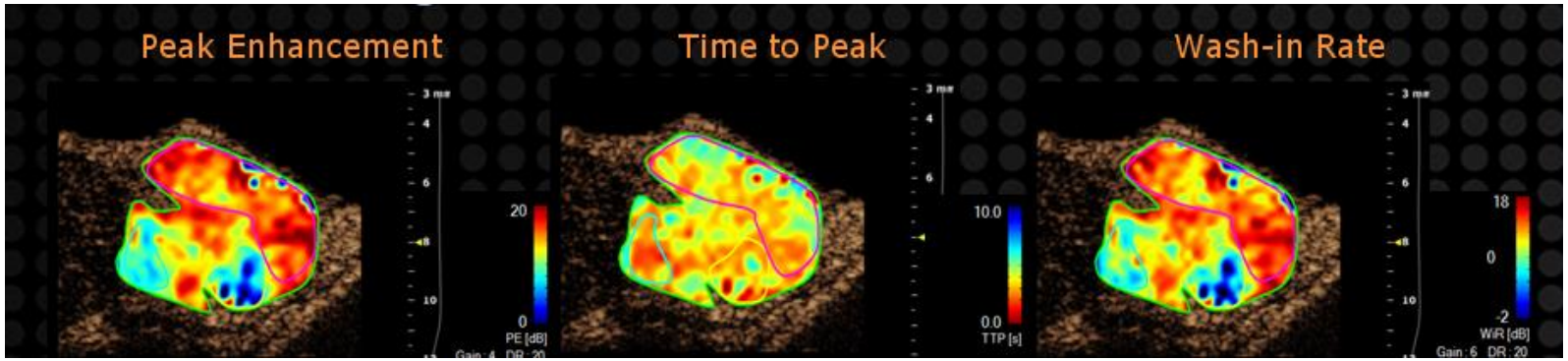

US Molecular Imaging of Breast Cancer

Earlier Detection of Breast Cancer with US Molecular Imaging

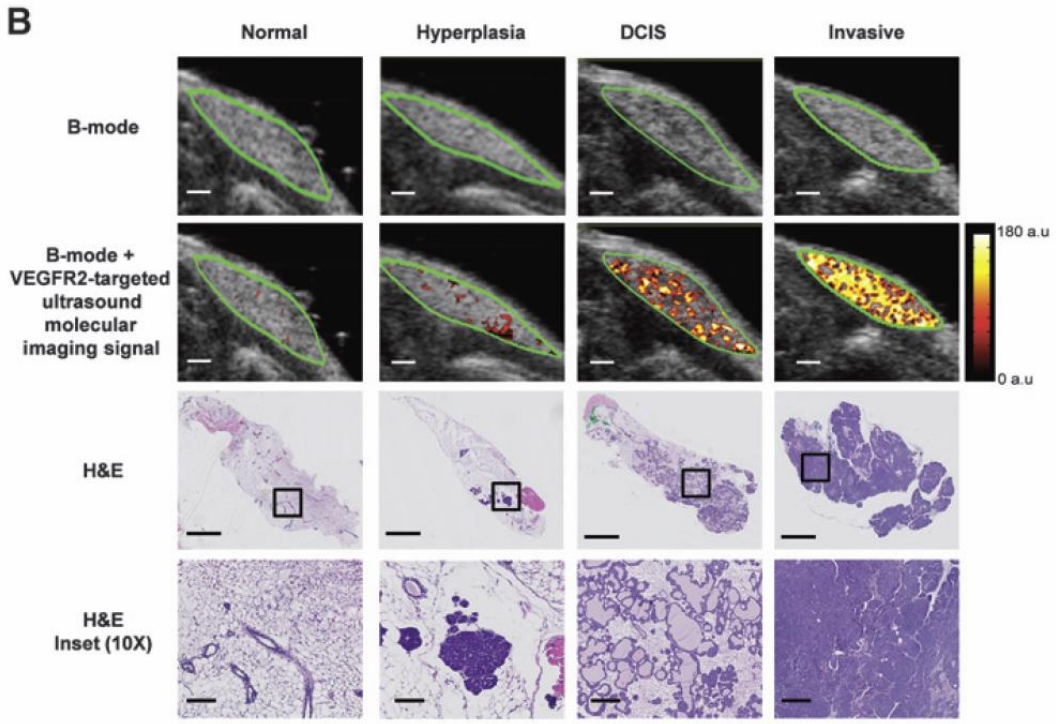

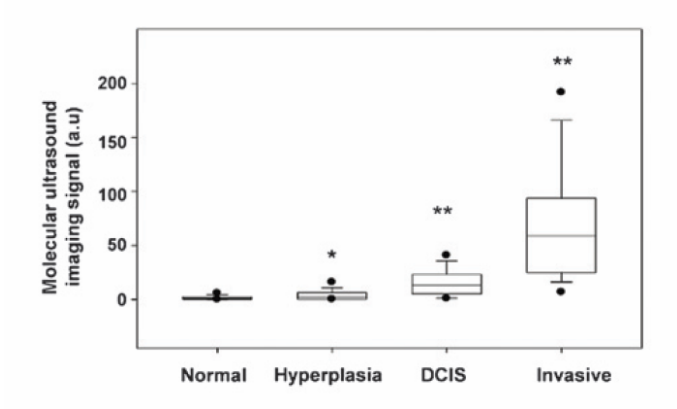

Table 2. Summary of 4 (cases A–D) of 63 cases with discrepancies between prospective ultrasound imaging diagnosis provided by two independent readers and histologic findings

Misdiagnosed cases	Histologic finding	Ultrasound signal measured by reader 1	Diagnosis by reader 1	Ultrasound signal measured by reader2	Diagnosis by reader 2
A	Benign (normal)	4.16	Benign	4.75	Malignant
B	Benign (normal)	4.96	Malignant	0.57	Benign
C	Benign (hyperplasia)	8.81	Malignant	4.67	Malignant
D	Benign (hyperplasia)	11.87	Malignant	8.48	Malignant

NOTE: Both readers independently misdiagnosed 3 of 63 cases compared with histology using the ultrasound imaging threshold value of 4.6 a.u., corresponding to an error rate of 4.8%. Two cases (C and D) were overcalled as malignant by both readers; there was discrepancy between the two readers in two cases (A and B).

Bachawal et al., 2011

Photoacoustic Imaging

Photoacoustic imaging is a hybrid imaging modality combining optical and ultrasound imaging

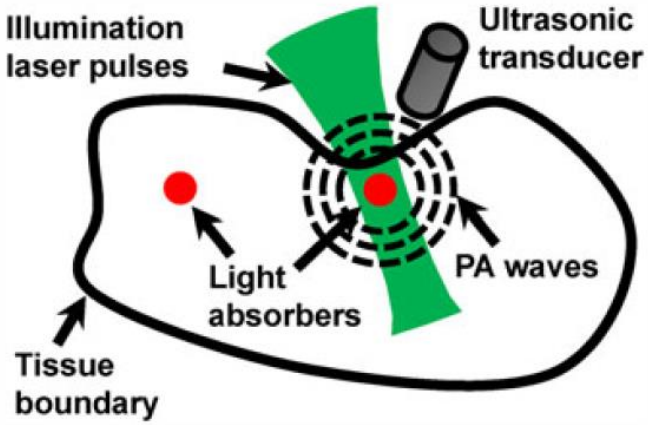

Figure 1. Illustration of the photoacoustic (PA) effect and PA imaging.

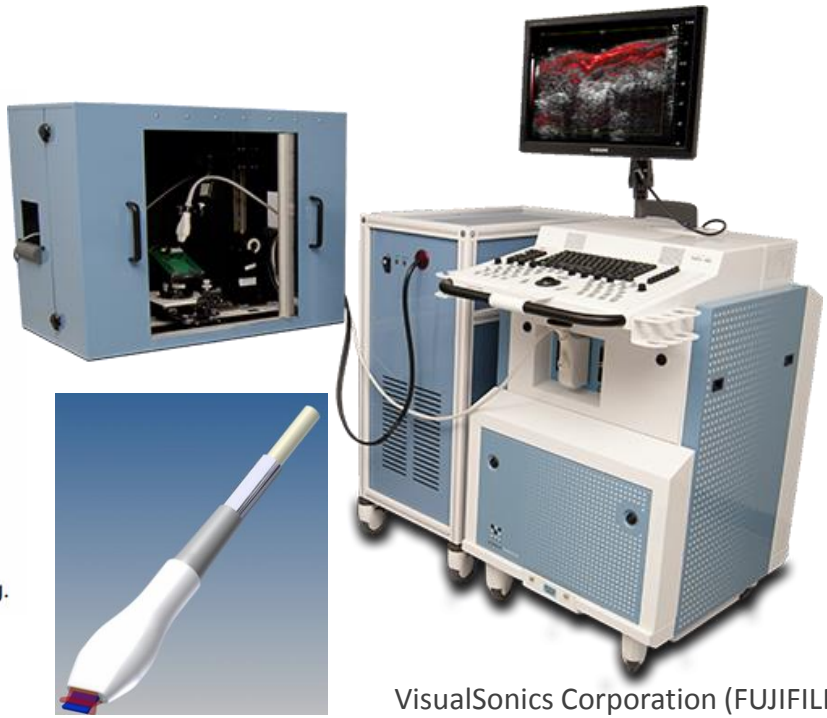

VisualSonics Corporation (FUJIFILM)

Signal is generated from absorption properties of chemical species within tissue to generate optical contrast at specific wavelengths

Yao and Wang, 2011

Yao and Wang, 2014

Photoacoustic Imaging

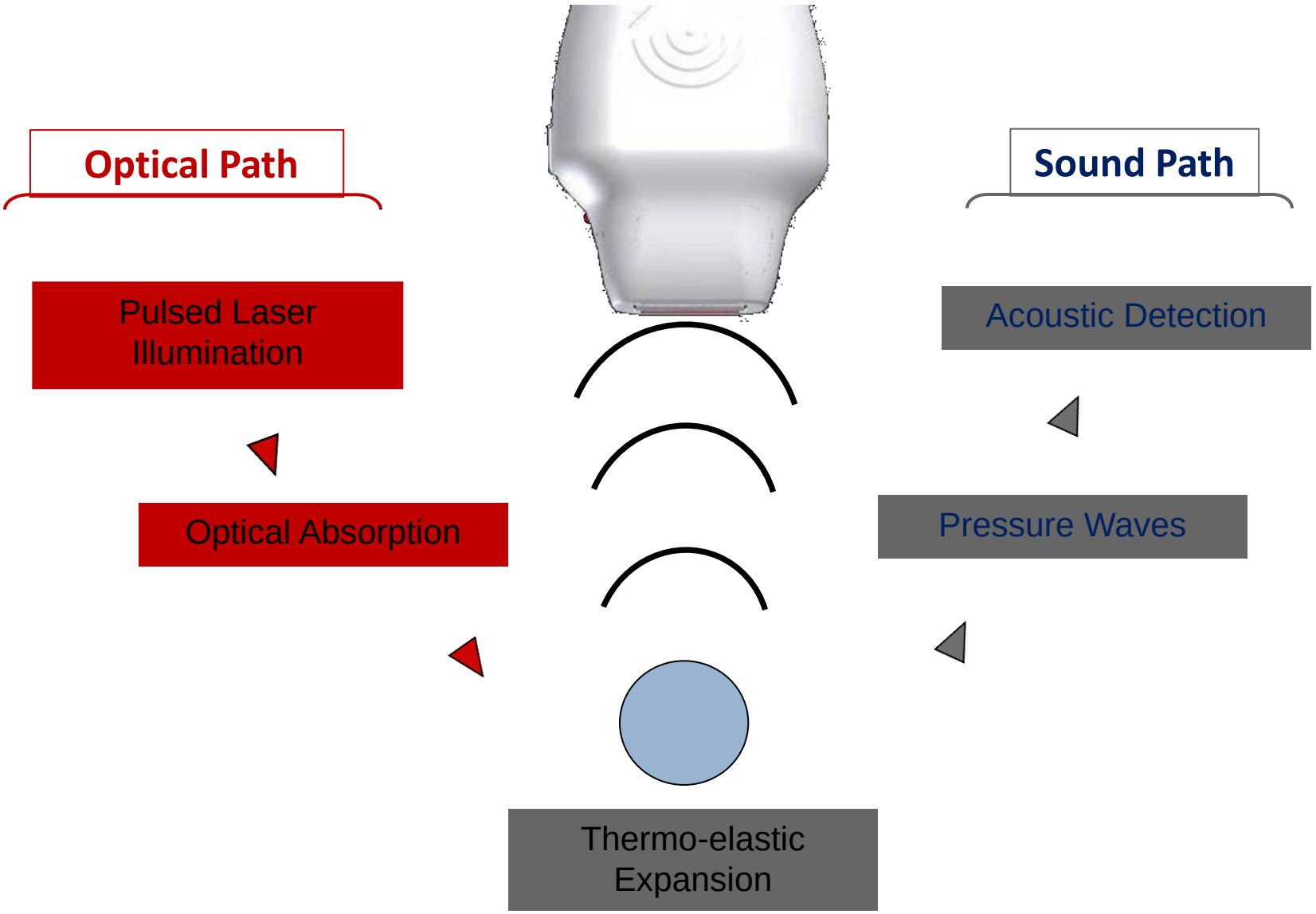

Principles of PAI

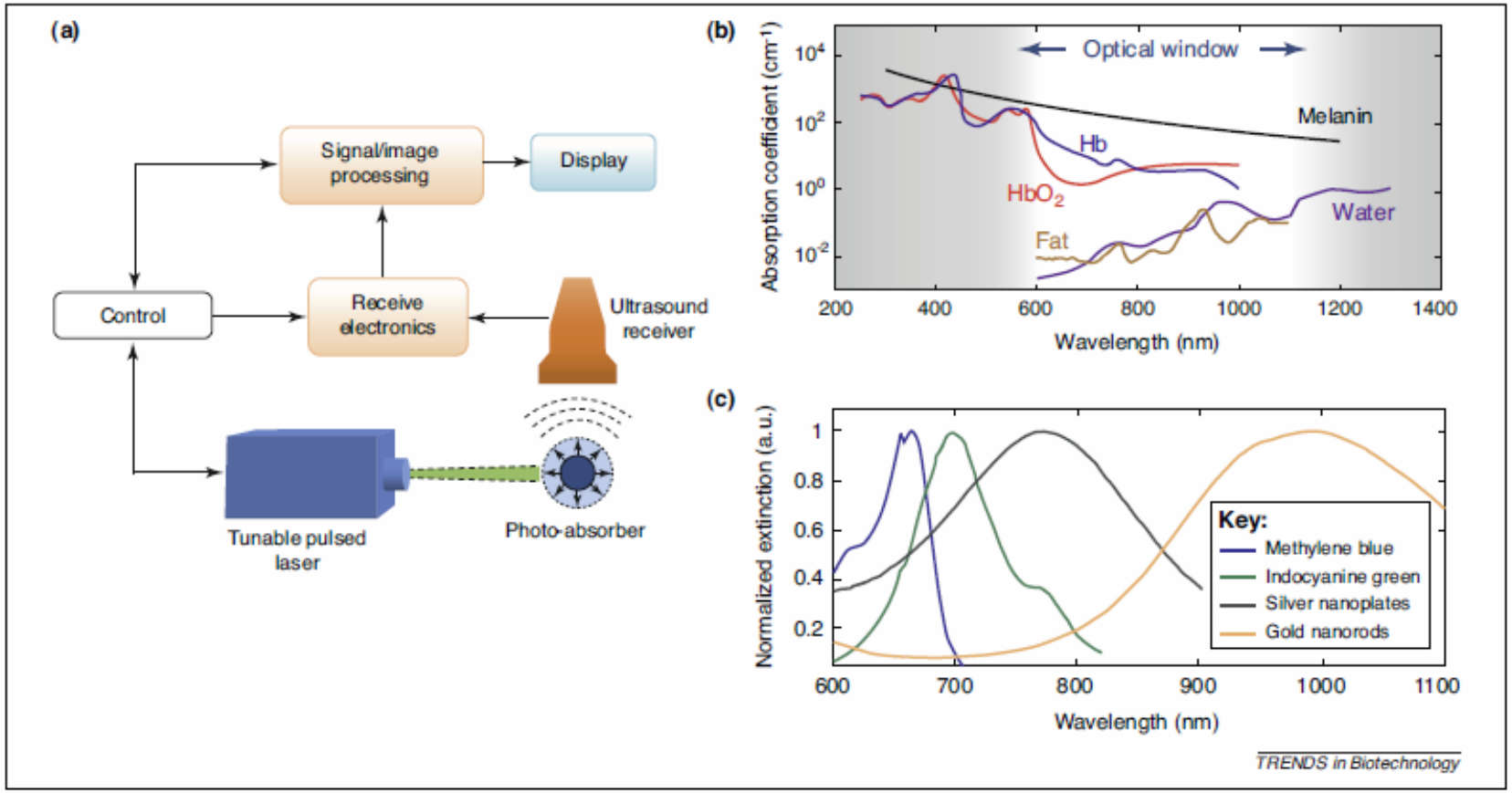

Figure 1. PAI principles **(a)** Block diagram of a typical PAI system. **(b)** Absorption spectra of endogenous chromophores in the body. The optical absorption of these endogenous chromophores is wavelength dependent; therefore, the PA signal intensity at different optical wavelengths can be used to characterize optical properties of tissue. Data for the absorption coefficient were obtained from http://omlc.ogi.edu/spectra/. The 'optical window' (600–1100 nm) is the wavelength range in which tissue absorption is at a minimum. **(c)** Extinction spectra of common exogenous contrast agents with peaks in the optical window.

Mallidi et al., 2011

PAI – Endogenous contrast

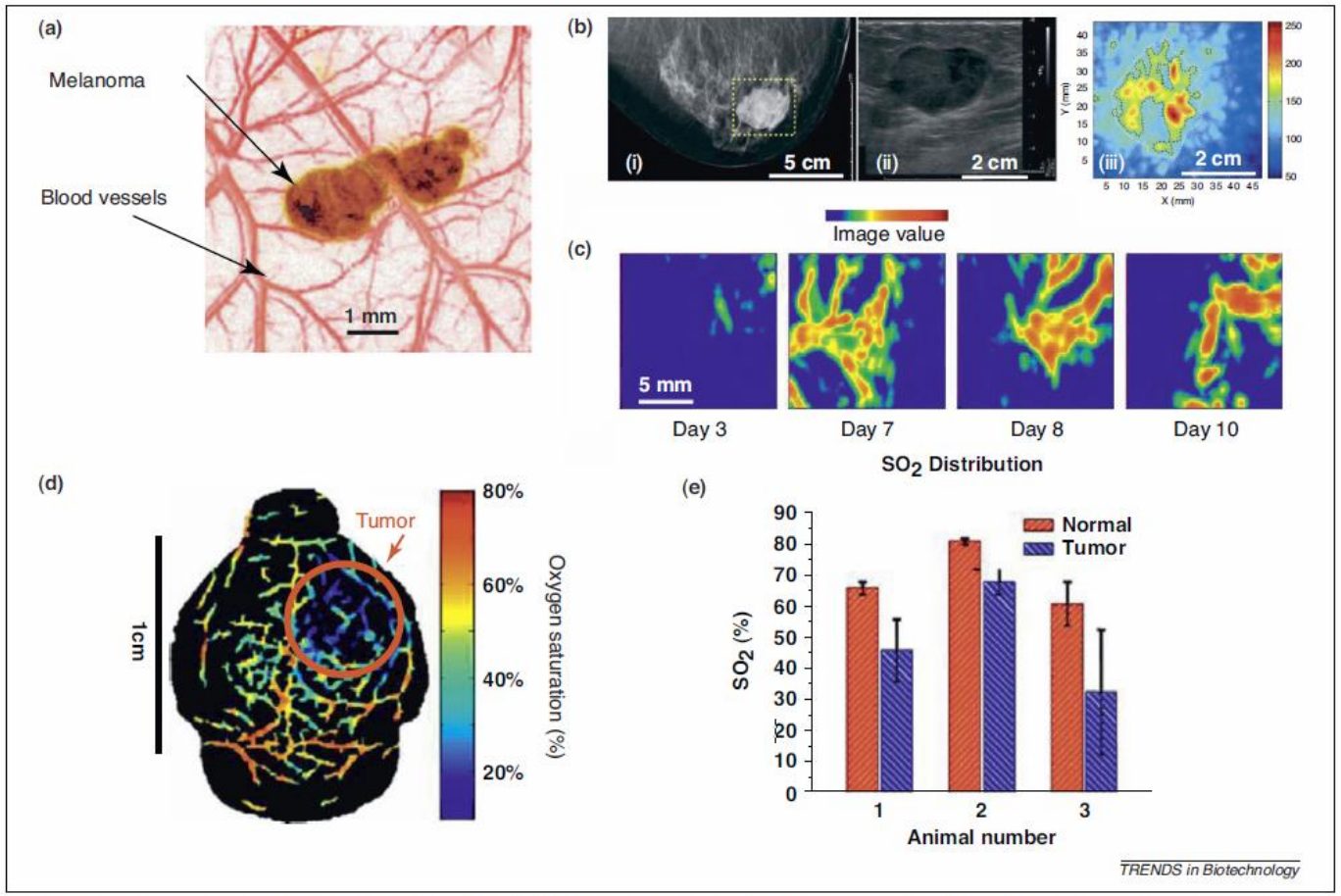

Figure 2. PAI of tumors using endogenous contrast **(a)** Overlaid maximum amplitude projections of PA images at 764 nm and 584 nm showing a tumor and its surrounding vasculature, respectively. The image clearly shows the vessel branching and structure around the tumor. **(b)** Images of the breast of a 57-year-old woman with invasive ductal carcinoma: **(i)** X-ray mammogram; **(ii)** sonogram; and **(iii)** PA image at 1064 nm. The X-ray mammogram and the sonogram depict the gross anatomical features of the tumor, but do not provide functional information. The high PA amplitude corresponds with abundant vasculature associated with malignant tumors. The PA image clearly depicts higher vascular densities in the tumor periphery, whereas the core of the tumor has minimum vasculature. **(c)** Pancreatic tumor cells were inoculated on a rat hind leg on day 1. PAI was used to monitor angiogenesis associated with the tumor growth.PA images obtained from the tumor region on days 3, 7, 8 and 10 are maximum intensity projections of the PA source strength in the xy-plane (i.e., top view on the tumor tissue). **(d)** *In vivo* functional imaging of a mouse brain with a glioblastoma xenograft obtained using PAI. Spectroscopic PAI (wavelengths from 764 nm to 824 nm) was used to detect hypoxia in a brain tumor. The heat map represents the percentage SO_2 in the blood vessels (blue = hypoxic; red = hyperoxic). The area indicated by the red arrow is the tumor. **(e)** A comparison of normal (red bars) and brain tumor (blue bars) vasculature SO_2in three mice. Three normal vessels and three tumor vessels were chosen from each SO_2 image that had been processed from spectroscopic PA images, such as the one shown in **(d)**. The results clearly indicate that the percentage SO_2 in tumors is lower than in the surrounding normal tissue, thus indicating hypoxia. Adapted with permission from [4] **(a)**, [15] **(b)**, [5] **(c)** and [22] **(d,e)**.

Mallidi et al., 2011

PAI – Endogenous contrast

Photoacoustic Imaging of Tumor Perfusion/Oxygenation

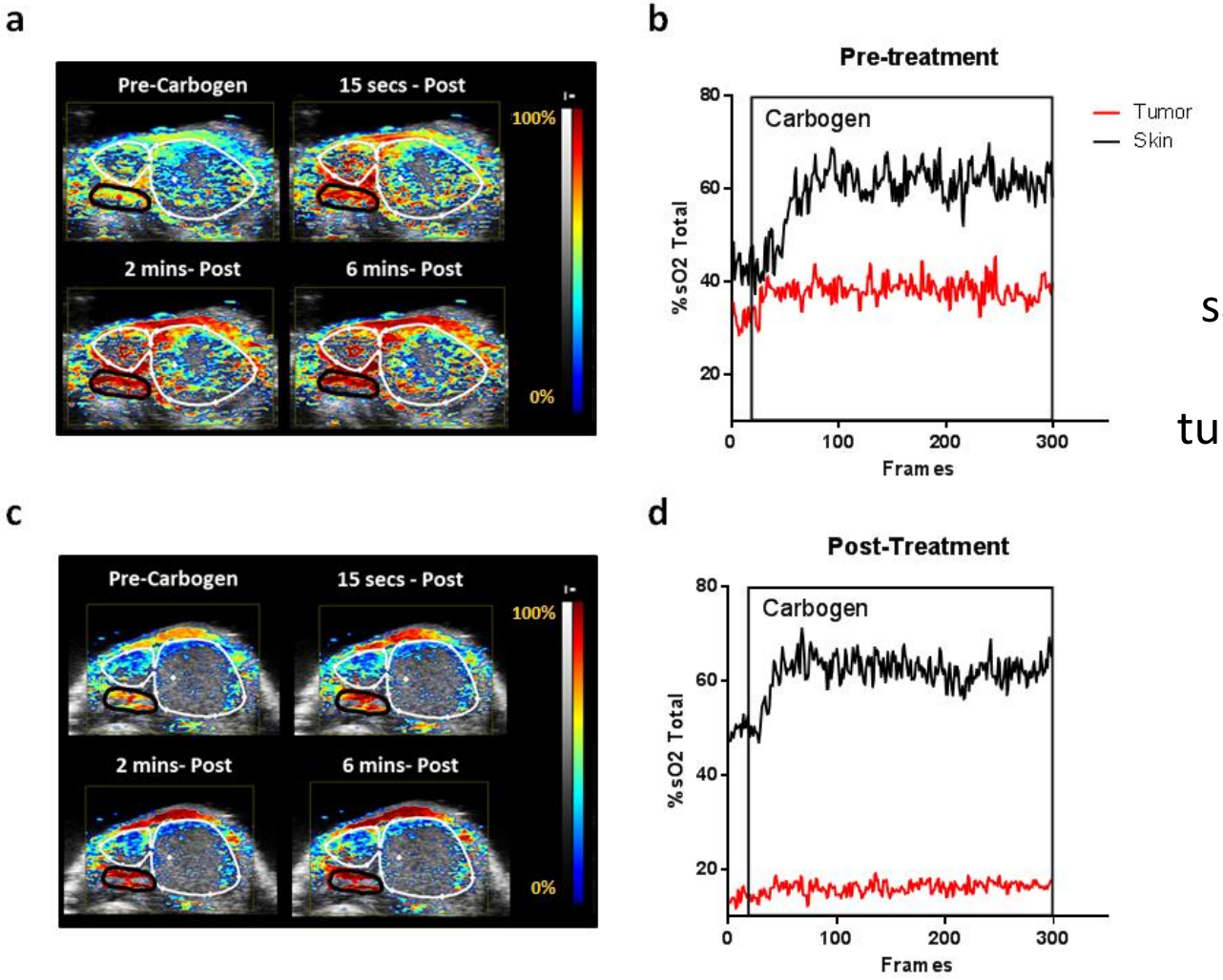

PA-based oxygen saturation maps (sO_2) of head and neck tumors before and after treatment with vascular-targeted therapy

Rich and Seshadri, 2015 Radiology

PAI – Endogenous contrast

3.3 Hemodynamics of salivary gland cancer

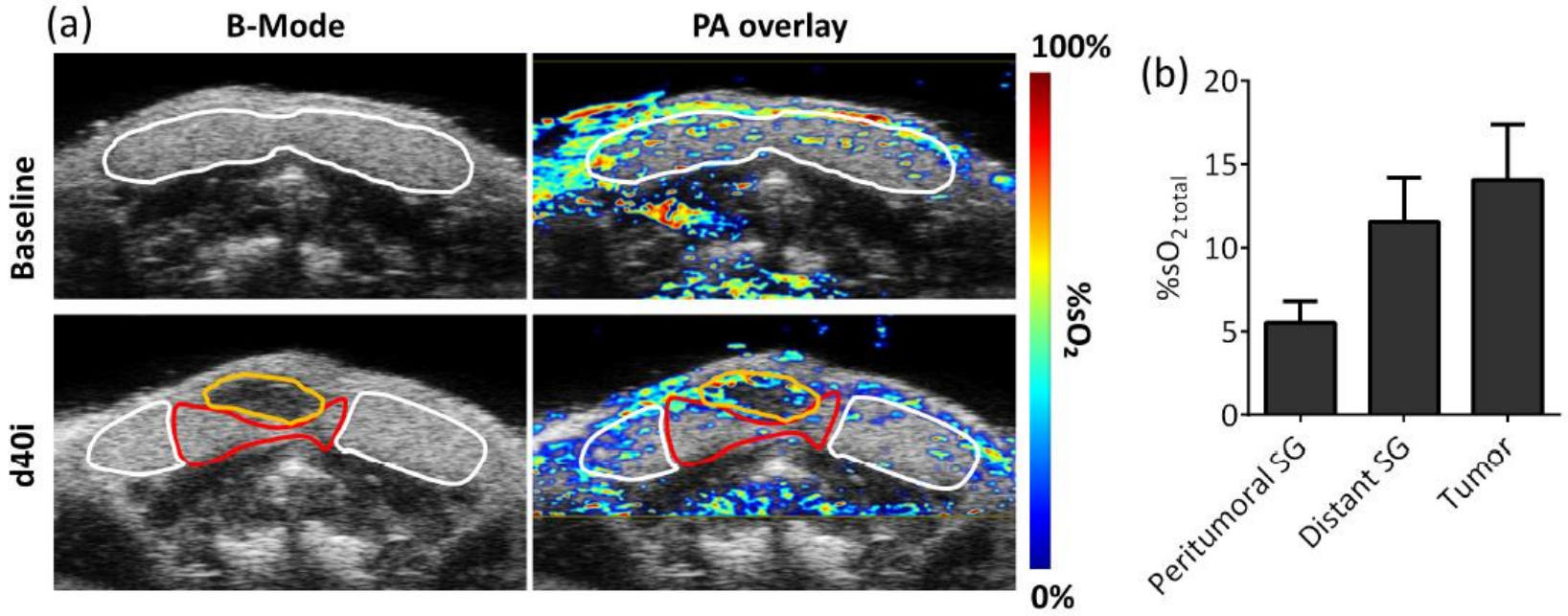

Fig. 4. Influence of focal salivary gland malignancy on hemodynamics. (a) B-mode ultrasound (left) and PA (right) images of mouse salivary gland prior to (baseline) and 40 days (d40i) following implantation of adenoid cystic carcinoma xenografts. At d40i the tumor was clearly visualized on B-mode ultrasound images (*outlined in yellow*). (b) Sub region analysis of the tumor bearing salivary gland into peritumoral (*outlined in red*) and distant salivary gland regions (*outlined in white*) showed lower $\%sO_2$ levels in the peritumoral region compared to distant salivary gland tissue and the tumor.

Rich and Seshadri, 2015 Biomed Opt Express

PAI – Endogenous contrast

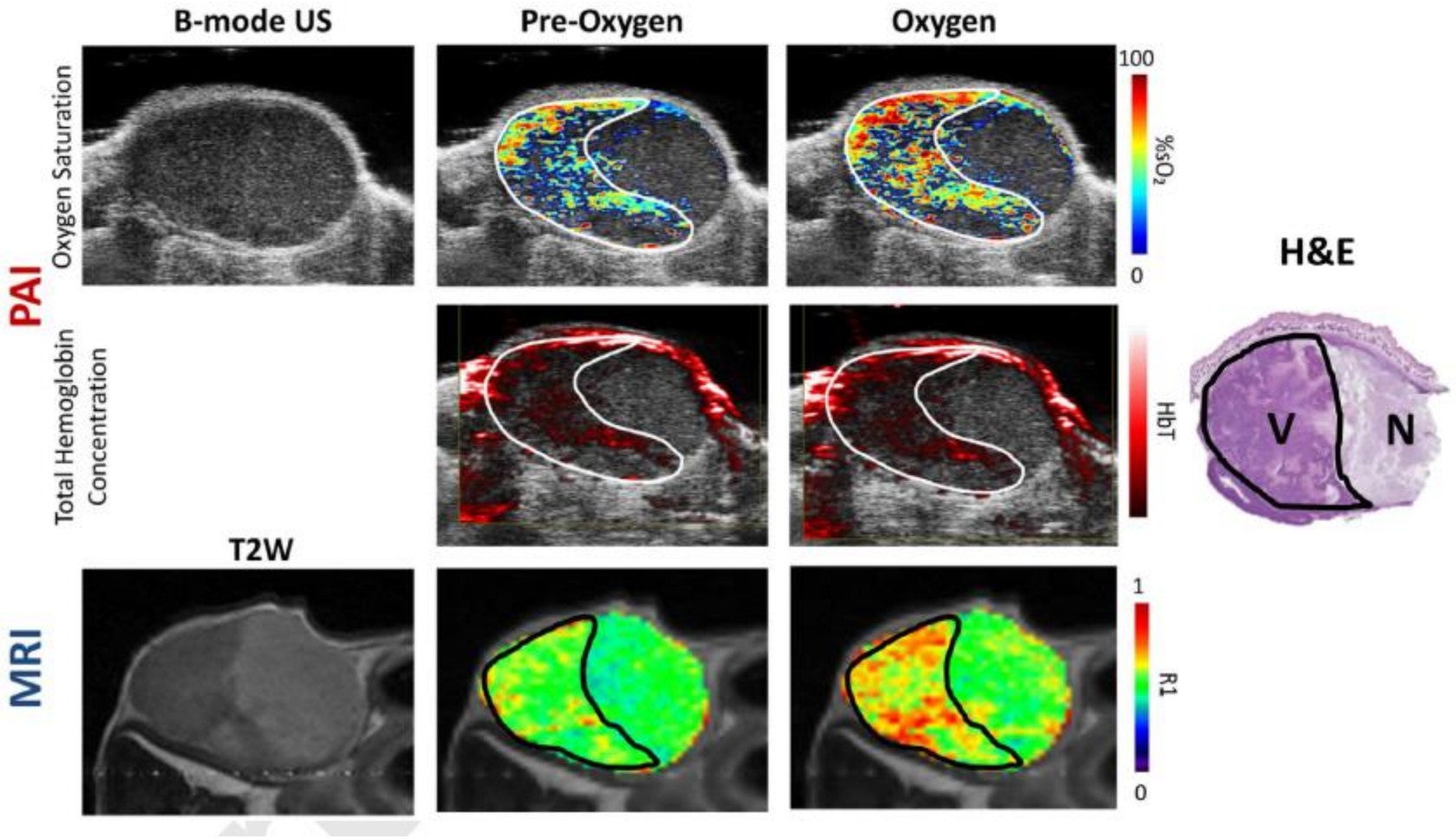

Rich and Seshadri, 2016 Scientific Reports. In press

PAI – Endogenous contrast

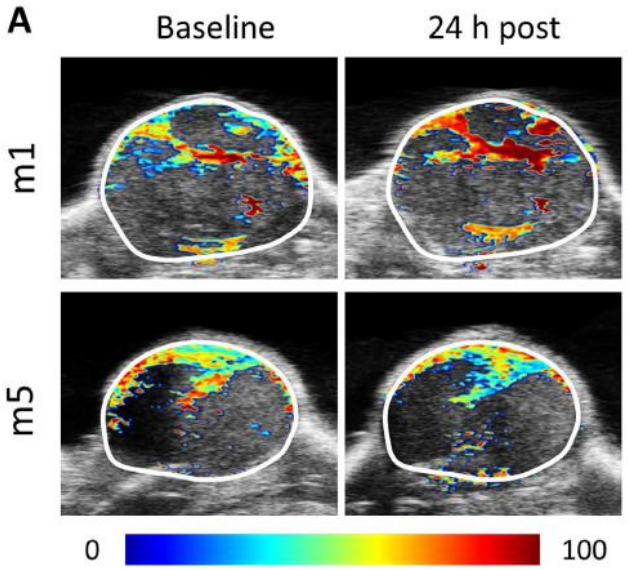

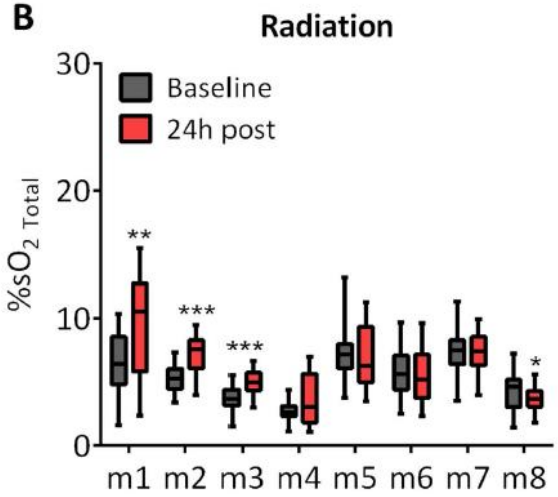

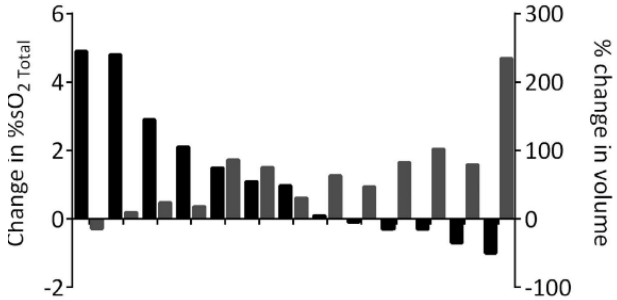

Utility of PAI in detecting tumor and normal tissue hemodynamic response to radiation in head and neck cancers.

Rich and Seshadri, Scientific Reports. 2016 In press

Exogenous contrast agents for PAI

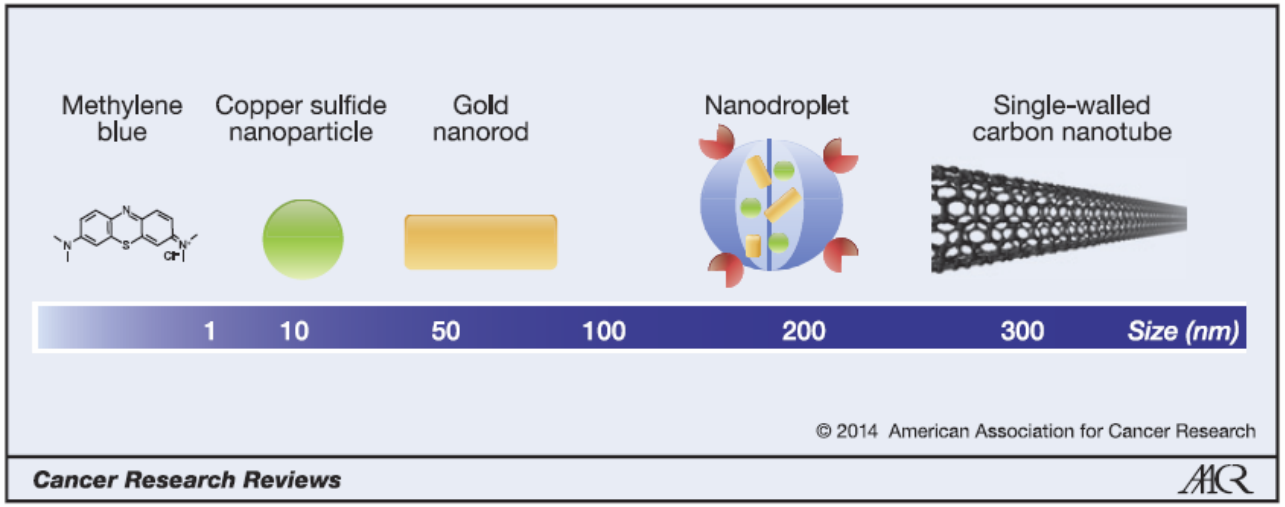

Figure 4. Illustration of several different types of PAI agents from small to large (left to right). See Table 1 for more detailed information on these imaging agents. The displayed imaging agents are nontargeted, however, they can all be functionalized by conjugation with specific targeting moieties.

Zackrisson and Gambhir, Cancer Res 2014

PAI – Nanoparticle based contrast agents

- Napthalocyanines (nanonaps)
  - Biocompatible nanoparticle formulation
  - Attractive spectral properties
  - Safe for in vivo application
  - Excellent contrast for PAI

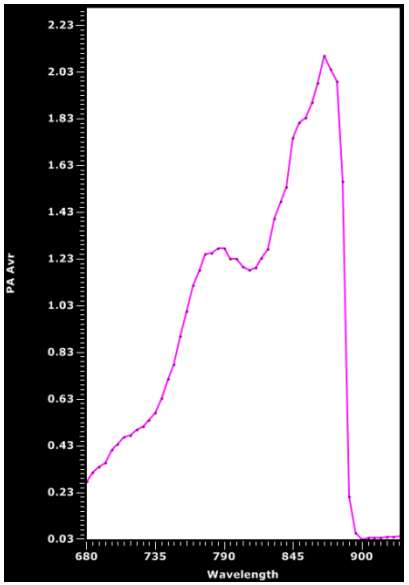

Peak absorption – 876 nm

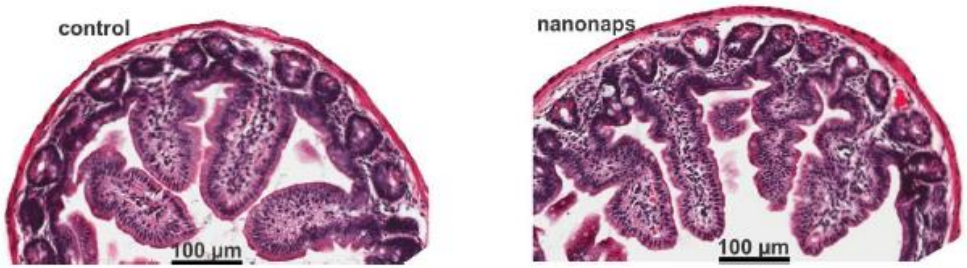

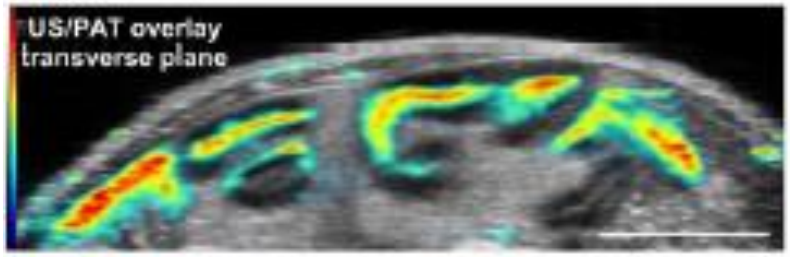

Zhang et al., Nat Nano 2014

PAI – Nanoparticle based contrast agents

In vivo imaging of primary head and neck cancer

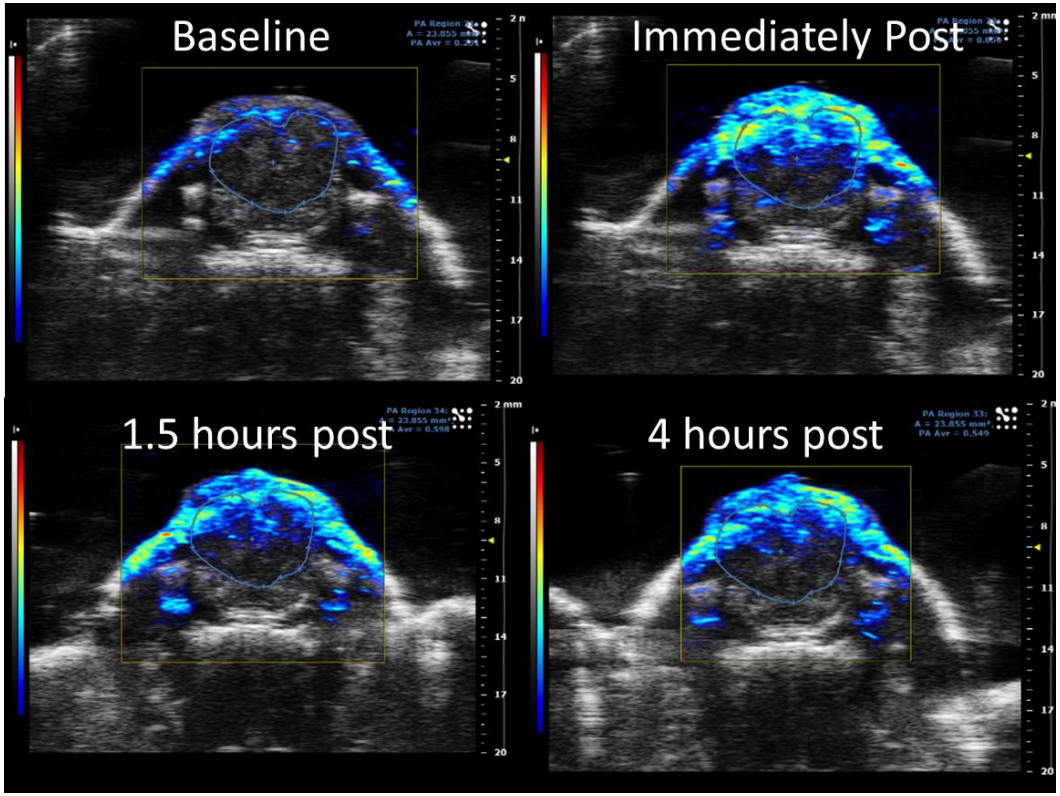

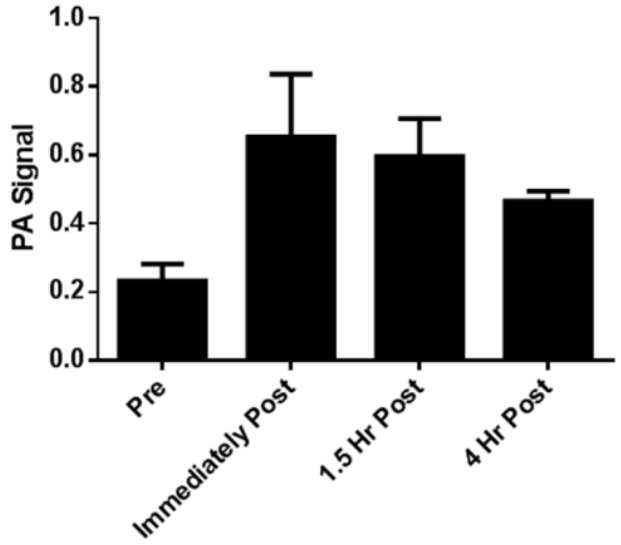

Persistent enhancement of PA signal was observed up to 4 hours post administration of Nanonaps

Seshadri lab, unpublished data

Clinical PAI

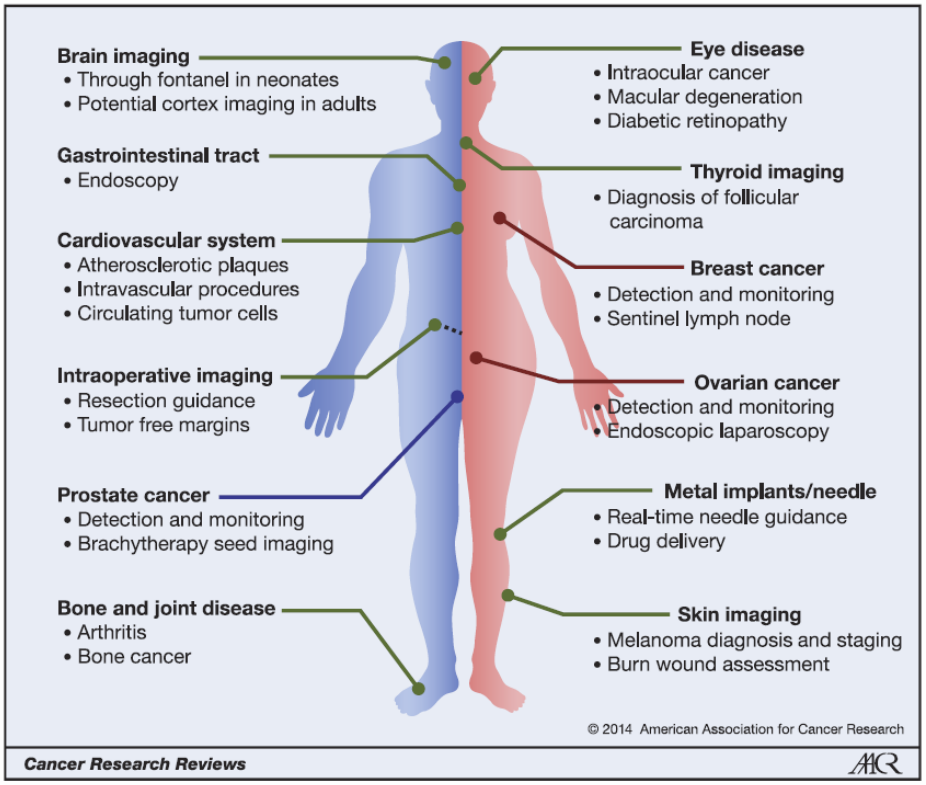

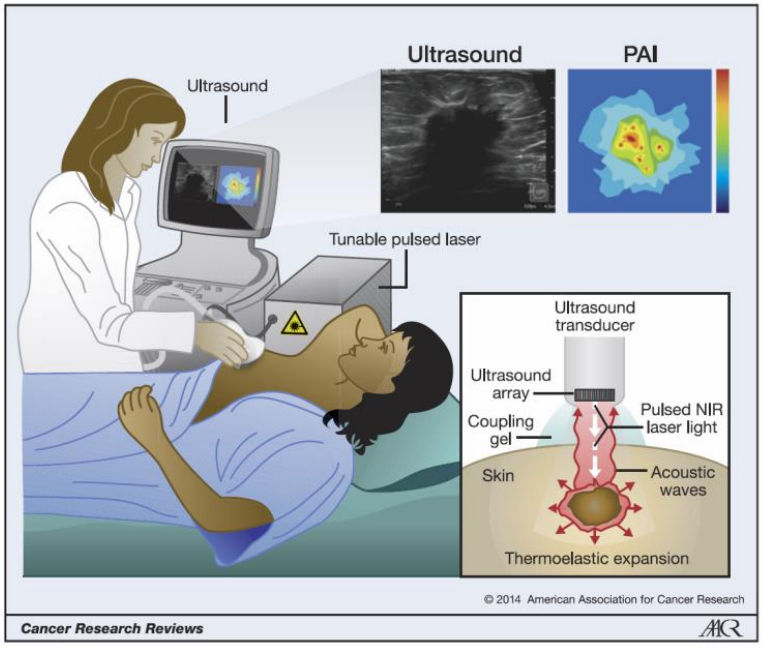

Zackrisson and Gambhir, Cancer Res 2014

Clinical PAI

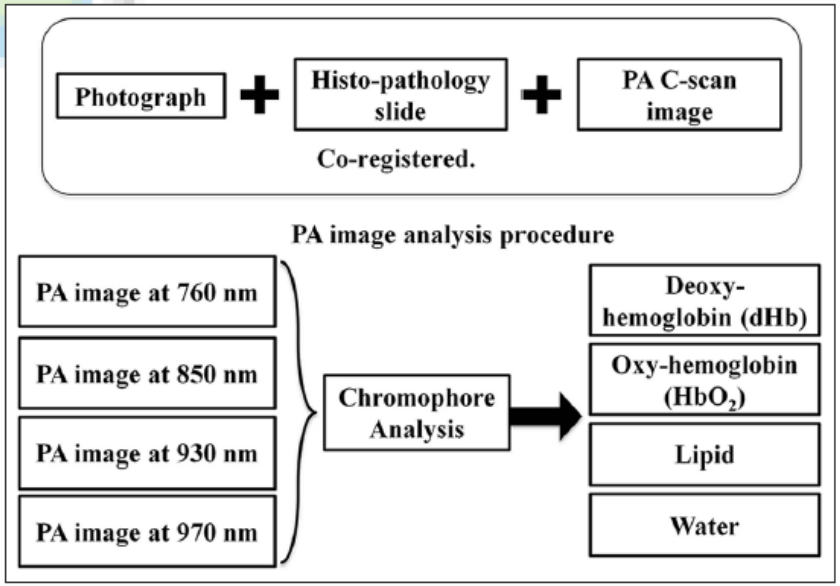

Figure 2: Photoacoustic (PA) image analysis procedure. Chromophore analysis was performed on the acquired multispectral composite PA images to extract individual optical absorption maps of dHb, HbO_2, lipid and water. Each PA image is co-registered with the photograph of gross prostate tissue and histopathology for further evaluation.

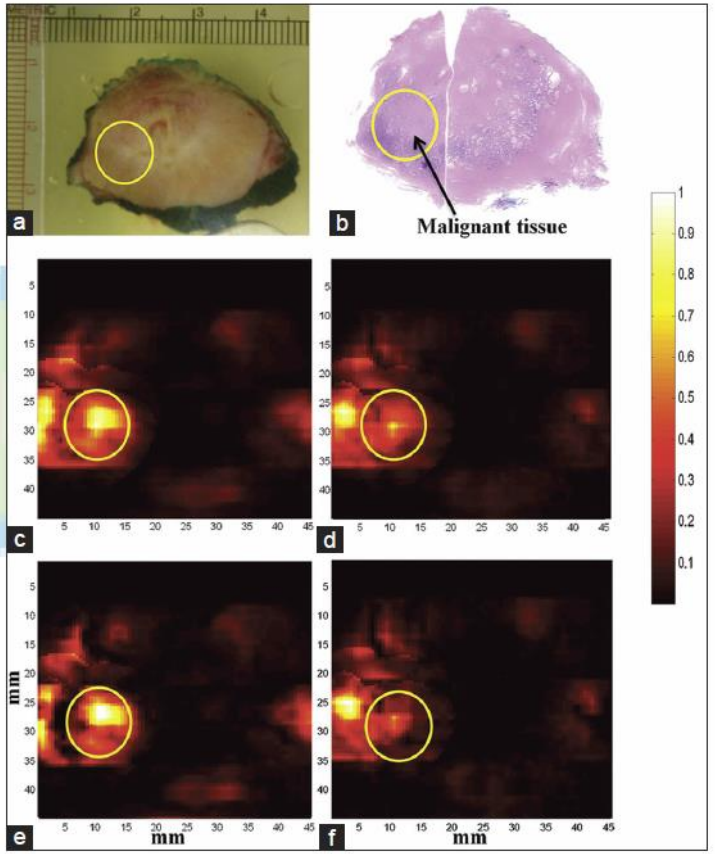

Figure 7: Multispectral photoacoustic (PA) imaging of prostate. PA images are acquired at multiple laser wavelengths. Each wavelength image is a composite image of all the tissue constituents such as deoxy-hemoglobin (dHb), oxy-hemoglobin (HbO_2), lipid and water. Chromophore analysis was performed to extract PA images showing absorption of individual constituents from the multi-wavelength images. All the PA images are co-registered with histopathology and photograph of the gross specimen. (a) Photograph of gross prostate specimen (b) Histopathology of prostate with malignant region encircled. (c) Composite PA image acquired at 760 nm wavelength (d) Composite PA image acquired at 850 nm wavelength (e) PA image showing absorption of dHb (f) PA image showing absorption of HbO_2. Higher absorption of dHb was seen in the region of interest corresponding to malignant prostate tissue compared to HbO_2.

Dogra et al., 2013

Do you recognize these images?

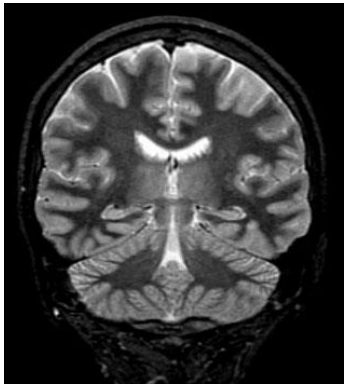

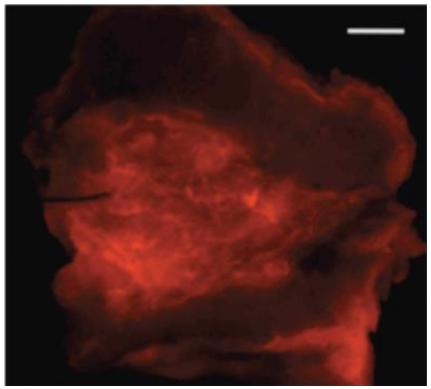

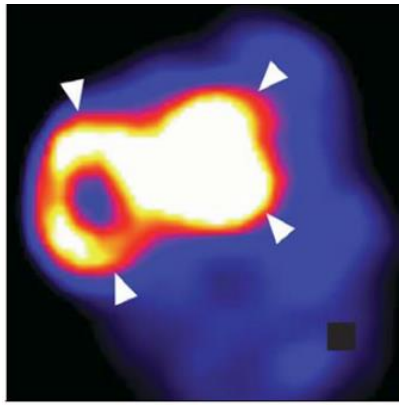

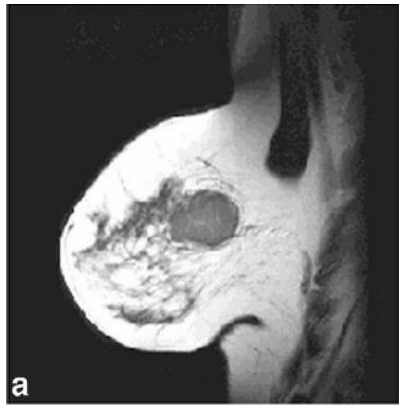

Concluding remarks

Table 1. Sensitivity, spatial resolution and clinical translation of molecular-functional imaging modalities

Imaging modality	Sensitivity of detection in MFI	Spatial resolution *in vivo*	Advantages	Disadvantages
CT	500 micromolar (Gd-DTPA)–low millimolar (Iodine) range	>10 μm	High spatial resolution	Patients are exposed to radiation
MRI	T_2-contrast, iron oxide nano-particles: nanomolar–micromolar range	4 μm (experimental MRI), 250 μm in plane (clinical MRI)	High spatial resolution	Particle size is often large, which restricts *in vivo* delivery
	T_1-contrast, multilabeled targeted Gd-DTPA macromolecules: >10 μM	4 μm (experimental MRI), 250 μm in plane (clinical MRI)	High spatial resolution	Particle size of contrast agent or reporters is relatively large
MRS	Millimolar range (^{1}H at 4.7–11 Tesla)	≥0.5 cm (3 Tesla), 0.7 cm (1.5 Tesla)	Detection of endogenous metabolites	Low sensitivity results in low spatial resolution
Optical	Nanomolar range: ≥50 cells (fluorescence); ≥1000 cells (bioluminescence)	>25 μm, intravital microscopy: 1–15 μm	High sensitivity, high spatial resolution	Restricted depth detection
PET	Picomolar range	≥1 mm (microPET), ~4–5 mm (clinical PET)	High sensitivity, short-lived isotopes	Low spatial resolution, cyclotron required for generating some isotopes
SPECT	Picomolar range	>1 mm (microSPECT), ≥3 mm (clinical SPECT)	High sensitivity	Low spatial resolution, long-lived isotopes
Ultrasound	>10^6 microbubbles per ml blood	>40 μm	High spatial resolution, cost effective	Few probes available

Glunde et al, Trends in Mol Medicine

The Future of Molecular Imaging